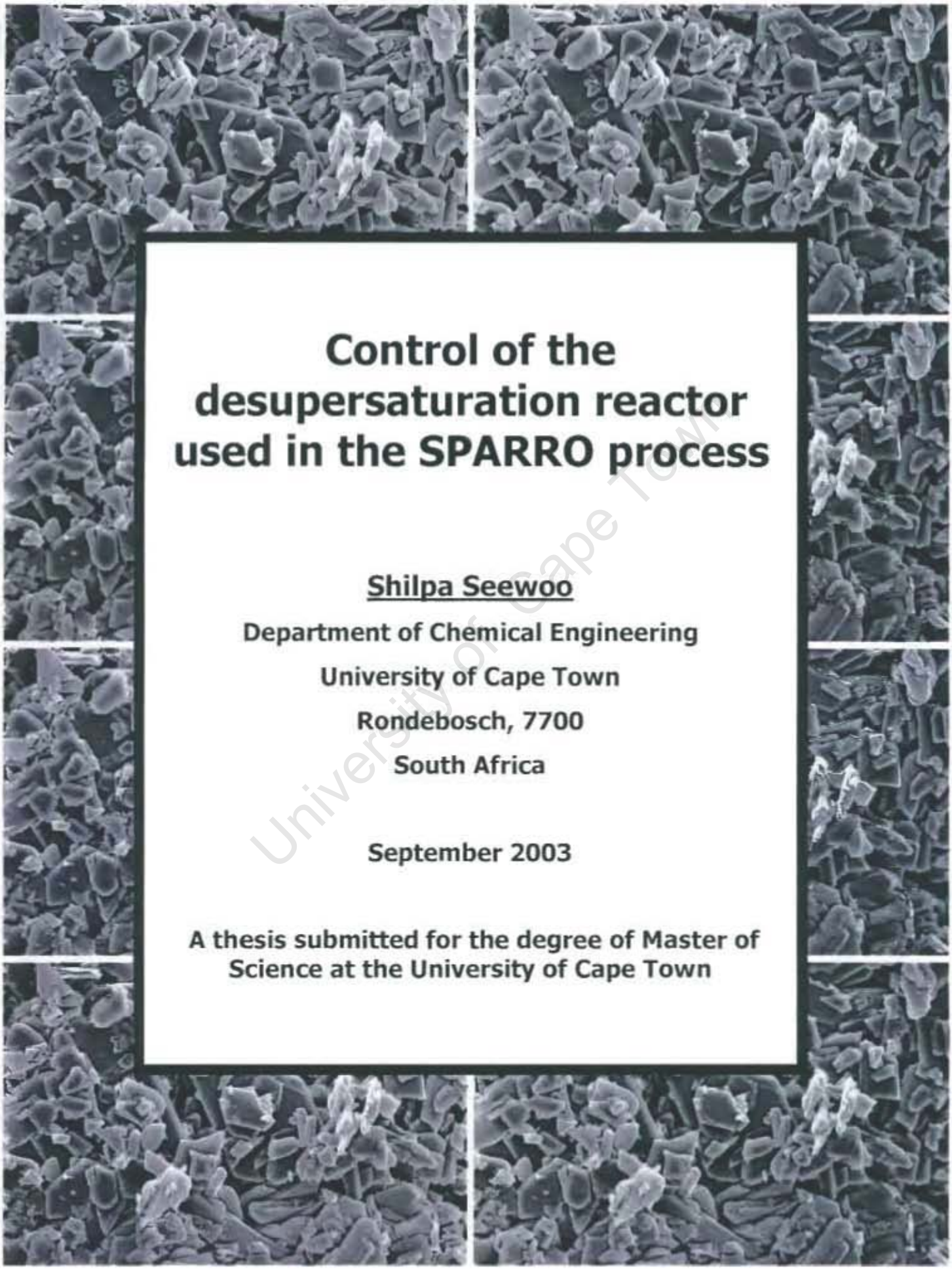

Control of the desupersaturation reactor used in the SPARRO process

Shilpa Seewoo

Department of Chemical Engineering

University of Cape Town

Rondebosch, 7700

South Africa

September 2003

A thesis submitted for the degree of Master of Science at the University of Cape Town

Acknowledgements

I want to thank Prof. A.E. Lewis for having given me the opportunity to carry out research in the precipitation and crystallisation research unit. Two years of my postgraduate studies have elapsed very fast. I had a lot of fun and it was a very enriching experience.

I want to thank Prof. A.E. Lewis and Dr. Rob van Hille for their time, support and supervision.

Many thanks also go to:

- Miranda Waldron from the Scanning Electron Microscope unit of the University of Cape Town,
- Prof. D. Chalton from the statistics department of the University of Cape Town,
- Doug Hatfield for having helped me with digital image processing,
- Fran Pocock, research assistant of the precipitation and crystallisation research unit,
- My family for their constant support,
- Jeeten, Kalpana, Ashton, Ochieng, Stella, Karen and Mandy for their friendship.

Above all, I would like to thank Jay who has been understanding, patient and a source of inspiration and motivation over the past years. Thank you, Jay, for all your love and support.

Synopsis

The work described in this thesis focuses on the Slurry Precipitation And Recycle Reverse Osmosis (SPARRO) process. The process was designed to treat calcium sulphate (gypsum) scaling mine waters by encouraging preferential crystal growth onto introduced seeds, rather than on the reverse osmosis membranes. The major problem faced by the SPARRO process was the short membrane life span, possibly due to damage caused by contact with gypsum crystals. Gypsum exists in two extreme morphologies, plate and needle-like crystals, which are formed from high (0.2 M) and low (0.04 M) concentration of $CaCl_2$ and Na_2SO_4 solutions respectively. This research reinvestigated the SPARRO process from a crystallisation perspective with the aims of:

- Increasing the level of understanding of fundamental aspects of the SPARRO process.
- Developing a technique to quantify the gypsum crystal morphology.
- Developing design specifications for a 5 L lab scale desupersaturation reactor.
- Developing and defining the critical parameters in controlling production of gypsum of a specified crystal size and morphology in the desupersaturation reactor.

The morphology of the crystals was defined using digital image processing. The edges of crystals in the digital images were detected. Needle-like crystals exhibited % edges detected below 6 and plate-like crystals exhibited % edges detected above 8.

Response surface methodology was used to investigate seeded precipitation. Experiments were carried out in a 5 L Perspex lab-scale reactor. The factors investigated were the seed morphology, seed quantity (SQ), pH, impeller speed (N) and sulphate to calcium molar ratio (SCR). The three responses measured were the time required for the solutions to reach equilibrium (T), the percentage growth of the crystals during the experiments (% Growth), and the crystal morphology (expressed by % edges detected). The second order models using plate-like seed crystals for the three responses were given by the following:

$$T = 333.6 - 47.4(SQ) - 39(SCR) - 8.8(pH) - 0.2(N) + 2.2(SQ)^2 + 2.4(SQ)(SCR) + 2.1(SCR)^2 + 0.7(SQ)(pH) + 0.4(pH)^2 + 0.003(SQ)(N) + 0.0002(N)^2$$

The model accounted for 97.4 % of the variation in time to reach equilibrium. A minimum occurred at seed quantity (SQ) of 6.33 % by volume, sulphate to calcium molar ratio of 5.68, pH of 5.54 and impeller speed (N) of 595 rpm (Reynolds number of 4.5×10^4).

$$\%\ \text{Growth} = 102.0 - 14.8(SQ) - 6.2(SCR) - 3.6(pH) - 0.04(N) + 0.6(SQ)^2 + 0.4(SQ)(SCR) + 0.4(SCR)^2 + 0.2(SQ)(pH) + 0.2(pH)^2 + 0.005(SQ)(N) + 0.000004\,(N)^2$$

The model accounted for 84.9 % of the variation in percentage crystal growth. A minimum occurred at seed quantity (SQ) of 8.06 % by volume, sulphate to calcium molar ratio of 4.54, pH of 5.39 and impeller speed (N) of 496 rpm (Reynolds number of 3.7×10^4).

$$\%\ \text{Edges} = 9.8 - 1.4(SQ) - 0.5(SCR) + 0.3(pH) - 0.0002(N) + 0.09(SQ)^2 + 0.17(SQ)(SCR) + 0.05(SCR)^2 + 0.002(SQ)(pH) - 0.02(pH)^2 + 0.001(SQ)(N) + 0.000003\,(N)^2$$

The model accounted for 89.06 % of the variation in the percentage edges detected. A ridge analysis showed that percentage edges detected as high as 22% could be achieved by using a seed quantity (SQ) of 9 % by volume, sulphate to calcium molar ratio of 8.23, pH of 5.5 and impeller speed (N) of 644 rpm (Reynolds number of 4.8×10^4).

The most significant factors were seed quantity and sulphate to calcium molar ratios. By keeping the least significant factors, pH and impeller speed constant at 7 and 500 rpm, the surface plots for the three responses were fitted and the respective contour plots were superimposed. The contours were used to locate the operating conditions of the desupersaturation reactor required to achieve the fastest gypsum precipitation kinetics, the minimum crystal growth and the highest percentage edges detected. The criteria to achieve a minimum time to reach equilibrium and percentage crystal growth were satisfied simultaneously. However, as it was beyond the scope of this project to investigate the size and morphology of the gypsum crystals that cause least damage to the reverse osmosis membranes used in the SPARRO process, it was not possible to define the exact operating conditions at which all three criteria of the desupersaturation reactor can be met. The ideal operating conditions for the reactor can be found to meet all the three criteria if the required percentage edges detected lies between 12 and 14 %. If the percentage edges required is above 16% or below 12%, a trade off between the three responses and the levels of the factors will have to be carried out.

At low supersaturation (0.03 M of Na_2SO_4 and $CaCl_2$ solutions) needle-like crystals formed in the absence of seed crystals after very long induction times. When plate-like seed crystals were used there were no needle-like crystals formed. An increase in the seed quantity decreased the growth per seed crystal. Precipitation kinetic data confirmed that gypsum precipitation is surface controlled. The growth of gypsum crystals was found to be a second order process. The initial seed morphology also influenced the gypsum precipitation kinetics. Equilibrium was reached much faster when plate-like seed crystals were used compared to when needle-like seed crystals were used.

Hydrodynamic studies were performed to determine the macromixing times. Macromixing time decreased when the Reynolds number increased from 2.2×10^4 to 6.7×10^4. Theoretically calculated micromixing time was significantly smaller than macromixing time. An increase in the Reynolds number caused a decrease in the percentage crystal growth and the time required to reach equilibrium. This phenomenon is consistent with the occurrence of primary nucleation. However, there is overwhelming evidence that crystal growth rather than nucleation occurred under the operating conditions of the reactor.

Table of Contents

List of Figures

List of Tables

Nomenclature

Roman symbols

Symbol	*Definition*	*Units*
a_i	Activity of species	-
A	Constant for turbulence	-
A'	Constant of proportionality	-
A_s	Crystal surface areas	m^2
c	Clearance of impeller off vessel bottoms	m
C	Concentration	M
C^*	Solubility limit	M
C_A	Concentration of reactant A	M
C_i	Solute concentration at crystal-solution interface	M
D	Impeller diameter	m
D_f	Diffusion coefficient	-
e	Error term	-
f	Response function	-
g	Gravitational acceleration	$m\ s^{-2}$
G	Gibbs energy	$J\ mol^{-1}$
G_x and G_y	Gradients in x and y directions	-
H	Height of liquid in reactor	m
J	Nucleation rate	$s^{-1}\ m^{-3}$
k	Growth rate constant	$L\ (mol\ s)^{-1}$
k_d	Coefficient of mass transfer by diffusion	$m\ s^{-1}$
K_r	Rate constant for surface reaction	$m\ s^{-1}$
L	Least squares estimates	-
m	Molality	$mol\ Kg^{-1}$
M	Molecular weight	$g\ gmol^{-1}$
n	Order of growth	-
n'	Number of impellers	-
N	Impeller speed	rpm
N_{crit}	Critical impeller speed	rpm
N_{FR}	Froude number	-

Symbol	Definition	Units
N_p	Power number	-
N_{RE}	Reynolds number	-
p'	Number of model parameters	-
P	Power	W
P'	Growth constant	cm(mS min^{-1})$^{-1}$
q_c	Pumping capacity of impeller	$m^3 s^{-1}$
Q_b	Reactant flow rate	$m^3 s^{-1}$
r	Number of seed crystals	-
R	Universal gas constant	J (mol K)$^{-1}$
R^2	Regression coefficient	-
S	Supersaturation ratio	-
S_{YY}	Total sum of squares	-
SS_R	Sum of squares due to model	-
SS_E	Sum of squares due to residuals	-
t	Time	s
t_0	t-test	-
t_R	Reaction time	s
T	Tank diameter	m
u	Fluid velocity	m s^{-1}
V	Volume of reactor contents	m^3
w	Weights in an array used in detection algorithms in DIP	-
W	Impeller width	m
x	System variable	
y	Real response	-
$\hat{y}$	Model response	-

Greek symbols

Symbol	Definition	Units
ρ	Fluid density	Kg m^{-3}
γ_i	Activity coefficient of species i	-
λ_k	Kolmogoroff velocity microscale	μm
λ_B	Batchelor concentration microscale	μm
μ	Fluid viscosity	Kg (m s)$^{-1}$

Symbol	Definition	Units
η	True regression	-
τ_c	Circulation time	s
τ_M	Macromixing time	s
τ_{meso}	Mesomixing time	s
τ_{micro}	Micromixing time	s
Λ	Macro scale turbulence	m
ε	Local energy dissipation rate	$m^2 s^{-3}$
γ	Kinematic viscosity	$m^2 s^{-1}$
σ	Relative supersaturation	-
σ^2	Variance	-
ξ	Input variable	-
β	Regression coefficient	-
κ	Conductivity of the total ions present in the solution at time t	mS cm^{-1}
κ^*	Conductivity of total ions present in solution at equilibrium	mS cm^{-1}
α	Level of significance	-

Abbreviations

Abbreviation	Definition
DIP	Digital Image Processing
eq	Equilibrium condition
MR	Mixed Reactor
PFR	Plug Flow Reactor
RO	Reverse Osmosis
RSM	Response Surface Methodology
SCR	Sulphate to calcium molar ion ratio
SEM	Scanning Electron Microscopy
SPARRO	Slurry Precipitation And Recycle Reverse Osmosis
SQ	Seed quantity
TDS	Total Dissolved Solids

1. Introduction

1.1 Background information

The mining, pulp and paper industries, the electricity generating companies together with the petroleum refineries in South Africa consume a significant amount of fresh water annually. These industries are under great pressure from the Government to reduce their fresh water intake by treating and re-using their waste water streams (Pulles *et al.*, 1992).

Treatment of effluent streams using conventional desalination techniques, including electrodyalisis and tubular reverse osmosis, are technically viable for non-scaling waters. Partially treated gold mine waters, in particular, have high levels of calcium and sulphate ions. Lime, which is used for neutralisation of mine waters, is the source of calcium ions and oxidation of pyrite ores present in gold bearings is the source of the sulphate ions (Juby and Schutte, 2000). When the solubility of calcium sulphate (commonly known as gypsum) is exceeded, precipitation of the salt is uncontrollable and scaling occurs. This renders the application of the conventional desalination technique difficult and inappropriate. Moreover, gypsum scales deposit on process equipment and this adds to technical, economical and environmental burdens.

The Chamber of Mines Research Organisation undertook research into the treatment of scaling waters. This started in the early 1980's and continued until 1993 in several phases, culminating in the patenting of the novel design of the SPARRO (Slurry Precipitation And Recycle Reverse Osmosis) process. The SPARRO process (Figure 1.1) is based on the Seeded Reverse Osmosis (Harries, 1985) process and involves the use of membrane technology. Seeds of gypsum are synthesised in a desupersaturation reactor and are fed to the membrane together with the scaling water to be treated. Seeds provide preferential sites for gypsum precipitation. The permeate is a stream of scale-free water that is separated by reverse osmosis in the membrane. The reject stream is a supersaturated solution of gypsum, which is recycled to the reactor. The reactor provides sufficient residence time for the supersaturated solution to reach equilibrium.

Several aspects of the SPARRO process have been investigated in detail and the latest achievement was the production of high quality water at water recoveries of around 95%

(Juby, 1994). However, further research was discontinued due to the short life span of the membrane in use, which resulted in high operating costs.

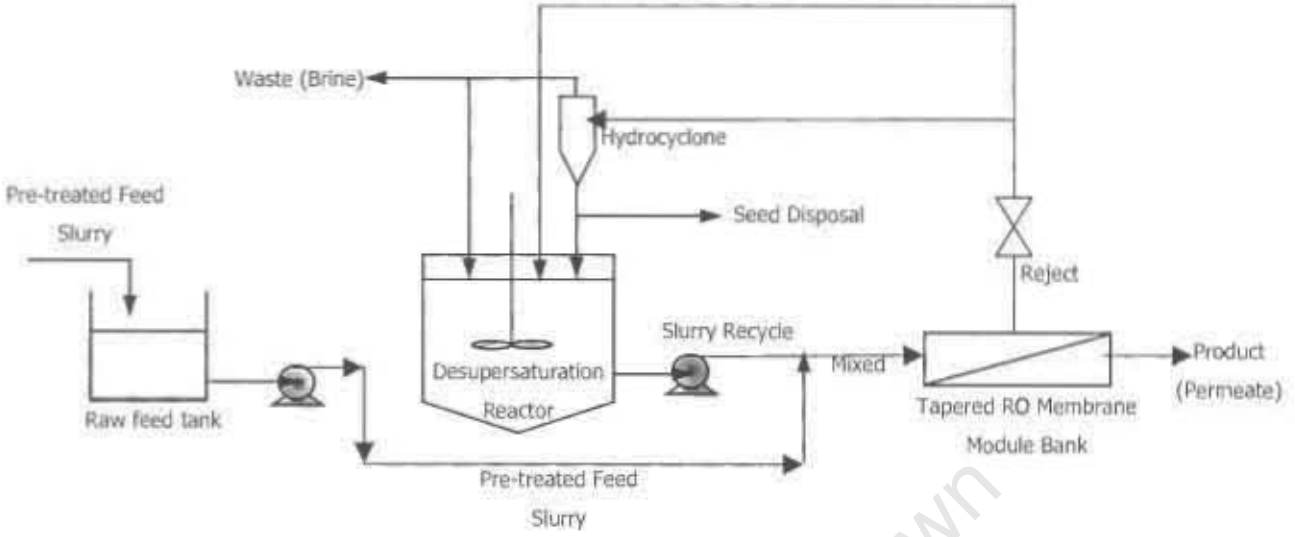

Figure 1.1: Schematic representation of the SPARRO process (Juby, 1994)

The collaboration between the University of Cape Town (UCT) and the Water Research Commission (WRC) rekindled the possibilities of exploring SPARRO project from a crystallisation perspective (hither to unexamined) and hence this project was initiated.

1.2 Problem statement

After previous research work on the development of the SPARRO process there is still a lack of fundamental and practical understanding of the SPARRO process. Problems regarding the short membrane lifetime have not yet been resolved and the cause of membrane damage has not been confirmed. The studies were not carried out from a crystallisation point of view. There is a possibility that gypsum is the major source of damage to the membranes. Information on which gypsum crystal size and morphology can be tolerated by the membranes is not available. The operation of the desupersaturation reactor used in the SPARRO process is not fully controlled with respect to particle size and morphology. This is as a result of lack of knowledge of appropriate crystal size required by the membranes.

1.3 Scope of study

Recent studies (Lewis *et al.*, 2002) show that gypsum occurs in two distinct morphologies, plate-like and needle-like, which form at high (above 0.1 M) and low (below 0.04 M) concentrations respectively as shown in Figures 1.2 and 1.3.

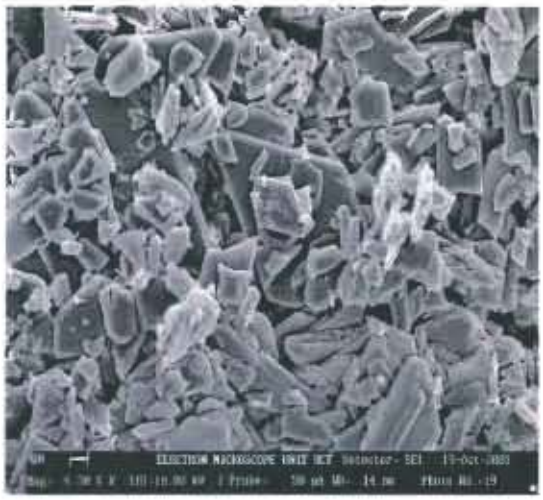

Figure 1.2: Plate-like crystals, scale-bar: 2 μm

Figure 1.3: Needle-like crystals, scale-bar: 10 μm

This research has been taken from a crystallisation perspective with the main aim of understanding the factors controlling the morphology of the gypsum crystals.

This thesis starts with chapter 2, a review of the most relevant literature available on the topic of gypsum precipitation and the SPARRO process. Chapter 3 deals with the principles and computations involved in response surface methodology. The lack of a technique to quantify the gypsum crystal morphology motivated the formulation of a strategy of using digital image processing. This strategy is presented in chapter 4. Chapter 5 covers the experimental part of this research. Results are presented and discussed in chapter 6. Chapter 7 includes the conclusions. Finally, chapter 8 presents some recommendations.

1.4 Aims and objectives

The aims and objectives of this project are to:

- Increase the level of understanding of the fundamental aspects of the SPARRO process.
- Develop a technique to quantify the gypsum crystal morphology.
- Develop design specifications for a 5 L lab scale desupersaturation reactor relating to the crystallisation parameters of the SPARRO process. This will include the setting of the dimension and type of reactor, the stirring type and the operating conditions.
- Develop and define the critical parameters in controlling production of gypsum of an appropriate crystal size and morphology in the desupersaturation reactor.

2. Literature review

The first section of this chapter describes precipitation theory. The second section of this chapter gives the relevant properties of gypsum and reviews previous research carried out involving gypsum. Section three outlines the consideration that should be taken into account in the design a reactor vessel. Section four reviews the fundamentals of reactor hydrodynamics. Section five deals with the South African mine water qualities and the issues surrounding scaling. The last section focuses on the technical aspects of the SPARRO process.

2.1 Precipitation Theory

Precipitation has been described as fast crystallisation. Precipitation processes are of great importance in the chemical and process industries (Sohnel and Garside, 1992).

Precipitation involves a number of processes including nucleation, crystal growth and other secondary processes such as ageing and agglomeration (Sohnel and Garside, 1992) and these are illustrated in Figure 2.1. The time scale during which precipitation takes place can vary greatly, from a few micro seconds to many days. The degree of supersaturation of a solution determines the rates of these different steps.

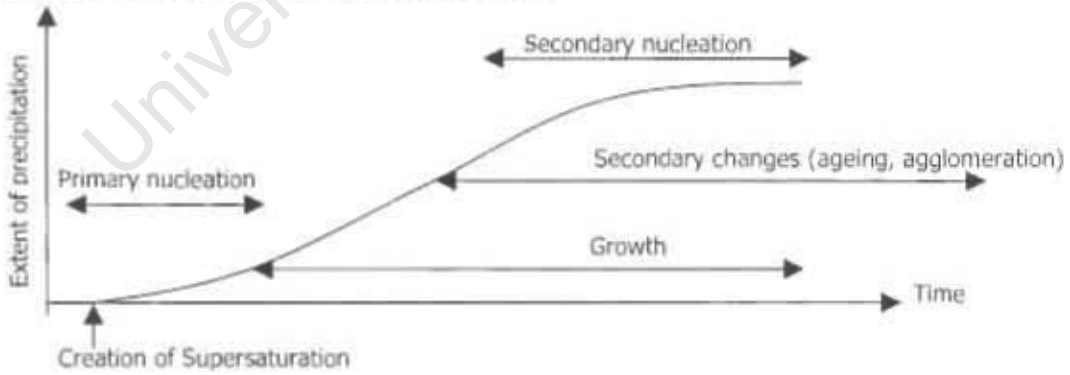

Figure 2.1: Steps involved in precipitation (Sohnel and Garside, 1992)

2.1.1 Supersaturation

Supersaturation is the thermodynamic driving force for any precipitating process and is the key variable in setting the rates of the steps involved in precipitation (Mullin, 2001). The driving force for precipitation can be expressed in concentration terms as in equation 2-1.

The supersaturation ratio, S, is given by equation 2-2. Relative supersaturation, σ, a dimensionless number, is given by equation 2-3 (Sohnel and Garside, 1992).

$$\Delta C = C - C^* \tag{2-1}$$

$$S = C/C^* \tag{2-2}$$

$$\sigma = \frac{\Delta C}{C^*} = S - 1 \tag{2-3}$$

where C: concentration of the solution [M]

C^*: solubility of the precipitating species [M]

From precipitation thermodynamics, a solid is formed when (Cairncross *et al.*, 1997):

$$\Delta G = -RT \ln\left(\frac{a}{a^{eq}}\right) < 0 \tag{2-4}$$

where Δ G: change in Gibbs Energy [J mol^{-1}]

R: universal gas constant [J mol^{-1} K^{-1}]

T: temperature [K]

a: activity of the solute in the solution

a^{eq}: activity of the saturated solution

For a reaction $A + B \rightarrow C$, supersaturation ratio, S can be defined as (Cairncross *et al.*, 1997):

$$S = \frac{a_A a_B}{a_A^{eq} a_B^{eq}} = \frac{\gamma_A m_a \gamma_B m_B}{\gamma_A^{eq} m_A \gamma_B^{eq} m_B} = \frac{\text{Ion Activity Product}}{\text{Solubility Product}} \tag{2-5}$$

where for component *i*,

a_i: activity

γ_i: activity coefficient

m_i: molality [mol kg^{-1}]

eq refers to equilibrium conditions

When S is greater than 1, 0 or less than 1, the solution is supersaturated, saturated or under saturated respectively.

2.1.2 Nucleation

The rate of nucleation, J, the number of nuclei formed per unit time per unit volume can be expressed as (Mullin, 2001):

$$J = A'\left(-\frac{16\Pi\sigma^3 M^2}{3R^3T^3\rho^2(\ln S)}\right) \tag{2-6}$$

where A': constant of proportionality

σ: interfacial tension [J m^{-2}]

M: molecular weight [g $gmol^{-1}$]

R: universal gas constant [J mol^{-1} K^{-1}]

T: temperature [K]

ρ: fluid density [kg m^{-3}]

S: supersaturation ratio

Equation 2-6 shows that the three main variables that govern the rate of nucleation are temperature, supersaturation and interfacial tension. The theoretical description of nucleation depends on the mechanism responsible for nucleus formation, which can be schematically represented as:

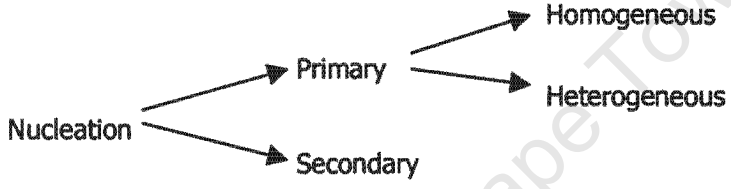

Figure 2.2: Schematic diagram showing different nucleation mechanisms (Mullin, 2001)

Primary nucleation is the formation of a new solid particle without the presence of an existing nucleus of the solid phase (Sohnel and Garside, 1992). The rate of primary nucleation increases strongly with supersaturation. Due to the high supersaturation in precipitation processes, primary nucleation is very fast and therefore a local process (Franke and Mersmann, 1995). Two possible mechanisms of primary nucleation can occur:

- Homogeneous nucleation

When a nucleus forms by itself, without the presence of any solid phase.

- Heterogeneous nucleation

When a nucleus is formed in the presence of a foreign solid phase (Sohnel and Garside, 1992).

In secondary nucleation, the presence of the crystallising material promotes the formation of a nucleus (Sohnel and Garside, 1992).

2.1.3 Crystal growth

Crystal growth is the enlargement of crystals caused by the deposition of solid material onto a nucleus (Sohnel and Garside, 1992). The mechanism and rate of crystal growth can be classified under adsorption-layer and diffusion theories (Mullin, 2001).

2.1.3.1 Adsorption-layer theory

The concept behind the adsorption layer theory is that atoms or molecules in the vicinity of a crystal face tend to attach themselves onto the surface in positions where the attractive forces are greatest. These molecules migrate towards positions where a maximum number of like elements are located. This step-wise build up continues until the whole plane surface is completed. Few crystals ever grow in the ideal layer-to-layer fashion without some imperfection occurring in the pattern. Dislocation consists of some geometrical irregularity in the crystal lattice. One type of crystal defect is the screw dislocation. During solute deposition a step may develop on the crystal face, extending over only part of the surface. Once a screw dislocation has been formed, the crystal face can grow in a spiral direction (Mullin, 2001).

2.1.3.2 Diffusion-reaction theories

Crystal growth rate can be defined as the rate of displacement of a given crystal face in the direction perpendicular to the face. Crystal growth can be limited by (Sohnel and Garside, 1992):

- Transport from solution to the crystal surface by volume diffusion or convection or by both of these mechanisms.
- Incorporation of material into the crystal lattice through a surface integration process, which is more commonly referred to as a surface reaction.

Figure 2.3 represents the concentration driving forces for diffusion and surface reaction. The solution that is in contact with a growing crystal face is supersaturated.

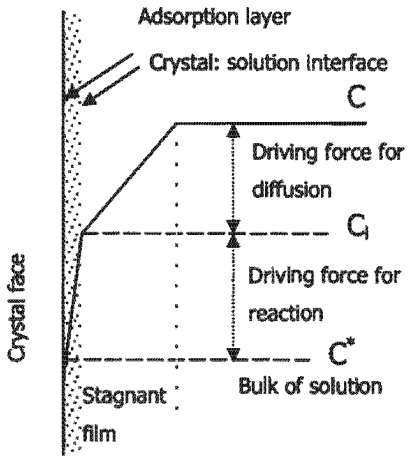

Figure 2.3: Concentration driving forces in crystallisation from solution according to the simple diffusion-reaction model (Mullin, 2001)

A diffusion process transports solute molecules to the solid surface from the bulk of the fluid phase, followed by a first order reaction when the solutes molecules arrange themselves into the crystal lattice. These two stages, occurring under the influence of different concentration driving forces can be represented by equations 2-7 and 2-8 (Mullin, 2001).

$$\frac{dm}{dt} = k_d A_S (C - C_i) \quad \text{(diffusion)} \tag{2-7}$$

$$\frac{dm}{dt} = k_r A_S (C_i - C^*) \quad \text{(reaction)} \tag{2-8}$$

where m: mass of solid deposited in time t seconds [kg]

A_S: surface area of the crystal [m^2]

C: solute concentration [M]

C_i: solute concentration in the solution at the crystal-solution interface [M]

C^*: solubility of the precipitating species [M]

k_d: coefficient of mass transfer by diffusion [m/s]

k_r: constant for the surface reaction [m/s]

2.1.4 Secondary processes

Ageing and aggregation can occur and cause further changes of the physical and chemical properties of the precipitated phase. Ageing, is a slow process and involves a change in the solid phase, changes of the crystal modification, habit, specific surface or chemical composition of the solid phase (Sohnel and Garside, 1992). Aggregation is the clustering of separate particles to form larger particles. This initial clustering can be the result of number of mechanisms and the particles may be held together by several different forces. Agglomeration is the clustering of the initial particles to form more or less strong secondary particles held together primarily by crystalline bridges or physical forces. Coagulation is a specific case of agglomeration occurring only with very small particles when clusters are bound solely by physical forces (Sohnel and Garside, 1992).

2.2 Calcium sulphate and its properties

Calcium sulphate exists in three different forms:

1. Anhydrite ($CaSO_4$)
2. Hemihydrite ($CaSO_4 . \frac{1}{2} H_2O$)
3. Dihydrate ($CaSO_4 . 2H_2O$)

Of these three forms, the dihydrate, also known as gypsum, is the compound that is of major interest as it is predominant at ambient conditions.

Gypsum is a white and lustrous compound. Crystals of gypsum are likely to be curved or even lenticular; in twins this sometimes produces arrowhead forms (Miers, 1929). The structure of gypsum consists of strongly bonded layers of SO_4^{2-} and Ca^{2+} with alternating layers of H_2O. Hydrogen bonding holds the H_2O molecules to the $CaSO_4$ layers and allows for cleavage (Nesse, 2000). The relevant properties of gypsum are highlighted in Table 2.1.

Table 2.1: Properties of gypsum (Othmer, 1995)

Molecular Weight [g/mol]	172.17
Transition point (to hemihydrate form) [°C]	128
Melting point [°C]	1450
Specific gravity	2.32

Christoffersen *et al.* (1982) experimentally determined the solubility of gypsum. Growth experiments were conducted in a closed system and continued until a constant concentration of calcium was measured by an EDTA titration method. The solubility limit obtained for gypsum was C_s=0.0151 ± 0.0001 M. This is in agreement with the solubility value of gypsum of 0.015 M obtained experimentally by Lash and Burns (1984).

2.2.1 Physical aspects of gypsum precipitation

2.2.1.1 Crystal morphology

The shape of the crystal is largely determined by crystal growth and aggregation. If surface reaction controlled growth takes place at lower supersaturation, crystals of compact shape such as cubes and octahedrals are formed. If the growth is largely anisotropic (where the precipitating molecules align in specific directions), elongated shapes such as needles, rods and plates are formed (Sohnel and Garside, 1992).

Franke and Mersmann (1995) studied gypsum precipitation in a batch reactor. The reagents, $CaNO_3$ and Na_2SO_4 solutions, were fed simultaneously into the reactor. The initial supersaturation ratio was varied between 15 and 30. Only needle-like crystals precipitated.

Lash and Burns (1984) prepared gypsum crystals using stock solutions of H_2SO_4 and $CaCl_2$. They found that at room temperature (23 °C), from solutions whose initial concentration

(where the stated concentration of the solutions always refers to the calculated molarity based on $CaSO_4$ at the moment of mixing, before any precipitation occurred) was greater than 0.4 M in $CaSO_4$, exothermic precipitation occurred. For solutions whose initial $CaSO_4$ concentration was less than 0.25 M the crystallisation was endothermic. Under microscopic examination the exothermically produced gypsum crystals appeared as very thin needles, while the endothermic crystals were platelets.

Christoffersen *et al.* (1982) studied gypsum morphologies and precipitation kinetics. One type of crystal was prepared by drop wise addition of stoichiometric amounts of Na_2SO_4 and $CaCl_2$ solutions, resulting in a 0.3 M gypsum solution. These crystals were needle-like and varied between 30 and 200 μm in length. Many small crystals were also attached in parallel or twinned positions to the larger ones. Other crystals formed by the addition of equal volumes of $CaCl_2$ and Na_2SO_4 solutions, resulting in a 0.725 M gypsum solution produced crystals with a much smoother surface and varied between 10 and 100 μm in length.

Liu and Nancollas (1970) studied the crystallisation of gypsum by the addition of seed crystals to supersaturated gypsum solutions at temperatures varying between 15 and 45 °C. The seed crystals were prepared by the drop wise addition of $CaCl_2$ to Na_2SO_4, resulting in a 0.1 M gypsum solution. Needle-like crystals, 80-120 μm in length were formed.

Çetin *et al.* (2001) produced gypsum crystals by the dissolution reaction of colemanite with sulphuric acid. The sulphate ion concentration was varied between 0.156 and 0.623 M. The colemanite compound was a mixture of B_2O_3 (37.71% by weight), CaO (20.79 % by weight), and a mixture of oxides of sodium, magnesium, aluminium, silicon, iron and titanium. Different amounts of colemanite were added to sulphuric acid, providing an initial concentration of B_2O_3 in the range of 0.194-0.777 M. The gypsum crystals formed were needle-like.

2.2.1.2 Particle Size Distribution

Nucleation, growth and ageing kinetics influence the particle size distribution (Sohnel and Garside, 1992).

Franke and Mersmann (1995) studied the continuous precipitation of gypsum using $CaNO_3$ and Na_2SO_4 solutions. They found that for precipitation processes the median crystal size

was predominantly affected by primary nucleation, which increased strongly with supersaturation and was a very rapid process.

Christoffersen *et al.* (1982) and Liu and Nancollas (1970) prepared gypsum seed crystals using Na_2SO_4 and $CaCl_2$ solutions. Both studies showed that high concentrations resulted in a large number of small (10-100 μm) particles while lower concentrations resulted in fewer particles but much larger (30-200 μm) in size.

2.2.1.3 Seeded Precipitation

Precipitation at low supersaturation levels is relatively slow and can be induced by seeding the solution. Kinetic relations for the growth of seed crystals from solution are fairly well established (Brandse *et al.*, 1977):

$$-\frac{dC_A}{dt} = kr\left(C_A - C^*\right)^n \qquad (2\text{-}9)$$

where k: constant ($L^{n-1}/(mol^{n-1}s)$)

r: number of seed crystals

(C_A-C^*): excess solute concentration (M),

n: order of growth.

The number of seed crystals affects the growth rate either through the:

- Total surface area for surface-reaction phenomena, or
- Number of surface-active sites as with screw dislocations

Desupersaturation is a decrease from influent concentration to a lower effluent concentration and can be achieved in a desupersaturation unit using seed crystals (Bremere *et al.*, 1999). Once the supersaturated solution is introduced into the unit, sparingly soluble salts precipitate on active centres of the crystal lattice and create new active surface area. Supersaturation dictates the rate of crystal growth, the surface area and reactivity of the seeds. The amount of seed crystals added alters the surface area available for precipitation. Reactivity of crystals depends on key growth sites on the surface, i.e. flat terraces, and kink sites formed from incomplete regions on steps. Rough surfaces lead to faster growth rates. Adsorption of impurities, antiscalants and organic matter, even at low concentrations, can inhibit crystal growth kinetics.

Seeds can be either from the same material as the precipitate or from a foreign material (Verdoes and Hanemaaijer, 1996). When seeds are from the same precipitate material, then

precipitation occurs mainly by growth of the seed crystals. One disadvantage is that precipitation happens only on the active growth sites of the seeds and thus the active surface area available for precipitation is relatively small. When foreign seeds are used, precipitation is dominated by heterogeneous nucleation. The energy barrier for this process at low to intermediate supersaturation is lower than for homogeneous nucleation, which becomes dominant at higher supersaturation. Foreign seed precipitation has the advantage of the ability to control the active surface area available for precipitation by means of the particle size and the surface roughness of the seeds. Verdoes and Hanemaaijer (1996) studied the effect of seed size on crystallisation kinetics for the precipitation of calcium carbonate. They found that precipitation on smaller seeds was measurably faster than on larger ones, confirming the accelerating effect of the larger surface area available.

Liu and Nancollas (1970, 1973) found that the seeded crystal growth of gypsum from supersaturated solutions was 2nd order in relative supersaturation. The growth rate was found to be directly proportional to the quantity of seed crystals added. Gypsum growth was found to be surface controlled (Liu and Nancollas, 1970). The effects of potential scale inhibitors including methyl enephosphoric acid and methylene phosphoric acid on the seeded growth of gypsum from supersaturated solutions were also studied (Liu and Nancollas, 1975). It was found that, in the presence of trace amounts of these additives, complete inhibition of growth for a certain period was achieved, thereafter the precipitation rate followed a second order law.

Seeded precipitation of gypsum from supersaturated solutions, with and without the presence of sodium chloride, was studied by Brandse *et al.* (1977). They utilised 10% by volume of seed crystals and plotted the mean linear growth rate, R against the relative supersaturation, σ. For σ values between 0.15 and 0.35 a parabolic law was obtained and for σ values above 0.4, growth rate was related to supersaturation ratio, S, by orders higher than two. They also found that the presence of sodium chloride in the precipitating system greatly increased the precipitation rate.

Seed preparation is an important step in seeded precipitation. Christoffersen *et al.* (1982) experimented with seeded gypsum precipitation using six batches of gypsum seed crystals. These seed crystals were prepared differently and had distinct specific surface areas and sizes. Their results showed that the rate of growth varied for the different preparations of the gypsum seed crystals. The overall rate of growth decreased with increasing mass of the

crystals. It was found that growth of the gypsum crystals was screw dislocation controlled in the supersaturation ratios range of 1.03 and 1.15. For this supersaturation ratio range, transport and surface nucleation processes were unimportant.

The growth of gypsum crystals from supersaturated solutions obtained by dissolving colemanite in sulphuric acid was found to be a second order process. The reaction was mass transfer limited (Çetin *et al.*, 2001).

Nancollas *et al.* (1973) investigated seeded gypsum precipitation at elevated temperatures varying between 60 and 150 °C. The rate of crystal growth was proportional to the square of the relative supersaturation.

2.2.1.4 Effect of pH

pH can influence the precipitation kinetics and the shape and size of crystals formed if the equilibrium solubility limit is pH dependent (Sohnel and Garside, 1992).

Liu and Nancollas (1970) found that changing pH between 7.6 and 11.6 did not have any effect on the growth of gypsum crystals.

Hina *et al.* (2001) studied the kinetics of gypsum crystal growth on calcium hydrogen phosphate dihydrate (DCPD) surfaces in supersaturated gypsum solutions. The initial growth rate increased when the pH was raised from 4.8 to 5.5. This was related to the increase in the zeta-potential of DCPD as the pH increased.

2.2.1.5 Effect of ion levels on precipitation product

In any precipitation process, it is very unlikely that there will be a uniform stoichiometric distribution of the specific anions and cations responsible for product formation. The level and ratio of the ion concentration determine the crystallisation mechanism and different precipitation products can be expected (Gosele and Kind, 1991) as shown in Figure 2.4.

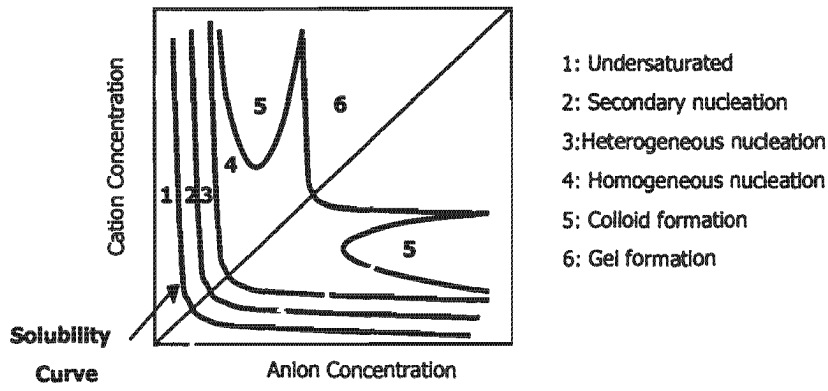

Figure 2.4: Speciation of the solid formation as a function of the anion and cation concentration in the solution at a constant temperature (Gosele and Kind, 1991).

Liu and Nancollas (1970) found that for a given supersaturation, the presence of excess sulphate ion favoured gypsum crystal growth. Higher sulphate to calcium ion molar ratios resulted in faster precipitation kinetics.

Alimi *et al.* (2003) investigated the influence of varying the calcium to sulphate ion molar ratio on the spontaneous gypsum precipitation from gypsum solutions of supersaturation ratios of 4.5 and 8.1. It was observed that the ion molar ratios of the solution had a strong effect of induction period (time for nucleation to start). The degree of effect on the induction period increased with increasing supersaturation, and was more important for the higher calcium to sulphate ratios. The lowest nucleation period was obtained for calcium to sulphate molar ion ratio of one.

2.3 Design of reactor vessel

Mixing is used to reduce nonuniformalities or gradients in compositions, properties or temperature of a material in the bulk. Hydrodynamics and mixing have a critical role to play in precipitation as they affect the local supersaturation and thus the characteristics of the precipitate. Both nucleation and growth kinetics are often greatly influenced by the hydrodynamic conditions prevailing (Sohnel and Garside, 1992). Physical aspects of the reactor such as impeller type and tank geometry can enhance mixing and solid-liquid suspension.

2.3.1 Impeller Type

Axial-flow impellers are best for most effective solid suspension and induce high fluid flow rate with lower shear rate (Oldshue, 1983). Lower impeller speed is required to drag the particles off the bottom of the reactor for suspension when axial impellers are used. The fluid flows in either a top-to-bottom pattern for down-pumping impellers or bottom-to-top pattern for up-pumping impellers. Multiple impellers should be used when liquid height is larger than the tank diameter, to maintain a full top-to-bottom flow pattern, thus utilising the full depth of liquid. Axial flow impellers require the least power input compared to the other impeller types (Harnby and Nienow, 1992). For a maximum flow to shear ratio, the impeller diameter and the clearance from the bottom to the impeller should be (Oldshue, 1983):

$$D = T/3 \tag{2- 10}$$

$$c = H/3 \tag{2- 11}$$

$$H = n'T \tag{2- 12}$$

where D: impeller diameter [m]
T: tank diameter [m]
c: off-bottom clearance [m]
H: height of liquid in the reactor [m]
n': number of impellers

2.3.2 Tank geometry

Turbulence is important to achieve good mixing. Various geometric improvements of the internals of the vessel help to break up circulatory flow to produce turbulence and reduce the formation of vortices. The following are the relevant parameters:

- Baffles. These interrupt the flow circulation and create turbulence in the fluid. Baffles of widths 1/10-1/12 of the tank diameter are usually enough to generate top-to-bottom mixing to reduce vortexing and swirling (Doran, 1995). The vertical circulatory flow in a baffled tank is four times as large as that in an unbaffled tank (Nagata, 1975).
- Draft tubes. These improve axial flow movement from the impeller (Uhl and Gray, 1966). Draft tubes ensure top-to-bottom flow for all tanks with height of liquid larger than tank diameter, and also decrease the tendency of solid deposition by sweeping the solids away from the draft tube (Oldshue, 1983). Care should be taken with the position and size of the draft tube (Harnby and Nienow, 1992). Ideally, the flow area in the core, in the annulus, between the bottom of the tube and the base and between the top and the liquid surface should all be equal.

- Bottom geometry. For flat-bottomed vessels, with down pumping impellers, it has been seen that solids form dead zones in the corners of the vessel. To eliminate these dead zones formation, rounded edges are employed or the vessel fitted with a dished bottom (Nagata, 1975).

2.4 Reactor hydrodynamics and dimensional analysis

2.4.1 Relevance of dimensionless analysis

Scale-up involves the translation of data on a small scale to production size equipment. The differences between the physical, mass transfer and mixing parameters of small and large-scale reactors are significant. The use of dimensionless analysis is a basic tool in a reactor scale-up practice (Ulbrecht and Patterson, 1985). The three most relevant dimensionless numbers are Reynolds (N_{RE}), Froude (N_{FR}) and Power (N_P) numbers given by equations 2-13, 2-14 and 2-15 respectively.

$$N_{RE} = \frac{D^2 N \rho}{\mu} \quad (2\text{-}13)$$

$$N_{FR} = \frac{DN^2}{g} \quad (2\text{-}14)$$

$$N_P = \frac{Pg}{\rho N^3 D^5} \quad (2\text{-}15)$$

where D: impeller diameter [m]

ρ: fluid density [kg/m^3]

μ: fluid viscosity [kg/ms]

P: power draw [W]

N: impeller rotational speed [rps]

g: gravitational acceleration [m/s^2]

The Reynolds number, N_{RE}, represents the ratio of inertial forces to viscous forces. This ratio determines whether conditions of the flow are turbulent or laminar and is thus a critical group in the correlating power. If the Reynolds number is lower than 10^4 the flow is considered to be laminar and greater than 10^4, turbulent (Uhl and Gray, 1966).

The Froude number, N_{FR}, represents the ratio of inertial to gravitational forces. This term can be unimportant in flow problems, but in the case of unbaffled tanks where vortexing occurs, the shape of the vortex represents a balancing of gravitational to inertial forces (Uhl and Gray, 1966).

The Power number, N_P, represents the ratio of pressure differences producing flow to inertial forces (Uhl and Gray, 1966).

2.4.2 Mixing time scale analysis

In the complex process of turbulent mixing three simpler stages of mixing can be distinguished, i.e. macromixing, mesomixing and micromixing (Baldyga and Bourne, 1999).

2.4.2.1 Macromixing

Macromixing is termed as the process of mixing that takes place on the scale of the whole vessel. Mixing at macro level decreases the scale of the concentration inhomogeneities from sizes of the order of the vessel diameter to that of the Kolmogoroff velocity microscale, λ_K. This microscale is a measure of the turbulent eddy size and is given by (Sohnel and Garside, 1992):

$$\lambda_K = \left[\frac{\left(\mu/\rho\right)^3}{\varepsilon}\right]^{1/4} \qquad (2\text{-}16)$$

where ρ: fluid density [kg/m^3]

μ: fluid viscosity [kg/ms]

ε : energy dissipation rate [W/kg]

For $\left(\mu/\rho\right) = 10^{-6}$ m^{2}s^{-1} and an energy dissipation rate of 1 W/kg, $\lambda_K \approx 30$ μm. These large-scale concentration variations reflecting the macromixing can be described by the fluid residence time distribution.

It has been experimentally found that for a well-baffled tank and fully developed turbulence the macromixing time, τ_M, is between 3 and 5 times the circulation time, τ_c (Baldyga and Bourne, 1999).

$$\tau_M = 4\tau_C \qquad (2\text{-}17)$$

For a vessel using an impeller with four pitched blades the circulation time, τ_c, can be expressed as follows (Roelands *et al.*, 2003):

$$\tau_C = \frac{V}{q_C} \qquad (2\text{-}18)$$

where V: vessel contents [m^3]

q_c: pumping capacity of the impeller [m^3/s]

The pumping capacity of impeller with four pitched blades is given by (Roelands *et al.*, 2003):

$$q_C = 1.5ND^3 \tag{2- 19}$$

where N: impeller speed [rps]
D: impeller diameter [m]

2.4.2.2 Mesomixing

When a reagent, A, is introduced in a reactor containing reagent, B, a plume of fresh feed of A is formed at the feed point of A in the reactor. This plume is coarse-scale relative to the micromixing scales and is of fine-scale compared to the scale of the system. Mesomixing at this intermediate scale characterises the inertial-convective mixing of a fresh feed stream (Baldyga and Bourne, 1999). The mesomixing time is defined as (Torbacke and Rasmuson, 2001):

$$\tau_{meso} = A\left(\frac{\Lambda^2}{\varepsilon}\right)^{1/3} \tag{2- 20}$$

where A: constant (given as 2 for turbulence (Baldyga *et al.*, 1997)),
Λ : macroscale turbulence [m]
ε : average energy dissipation rate [m^2/s^3]

The macroscale turbulence is estimated (Torbacke and Rasmuson, 2001) as:

$$\Lambda = \sqrt{\frac{Q_b}{\pi u}} \tag{2- 21}$$

where Q_b: reactant flow rate [m^3/s]
u: fluid velocity [m/s]

The average energy dissipation rate is given by (Torbacke and Rasmuson, 2001):

$$\varepsilon = A\frac{N_P N^3 D^5}{V} \tag{2- 22}$$

where A: constant (given as 2 for turbulence (Baldyga *et al.*, 1997)),
N_p: power number (taken as 1.5 for a pitched blade (Uhl and Gray, 1966)),
N: impeller speed [rps]
D: impeller diameter [m]
V: reactor contents [m^3]

2.4.2.3 Micromixing

Micromixing is defined as mixing that takes place at the molecular level. Micromixing thus directly affects chemical reaction, nucleation and crystal growth, which are essentially molecular-level processes (Baldyga and Bourne, 1999). Micromixing by molecular diffusion occurs to such an extent that segregated areas of uniform but mutually different composition disappear and the mixture attains complete homogeneity on the molecular level (Sohnel and Garside, 1992).

Micromixing takes place through two mechanisms:

- Laminar stretching

During laminar stretching the overall volume of the segregated regions remain the same but their size becomes narrower, resulting in an increase in their area of contact.

- Turbulent erosion

In turbulent erosion, the volume of the segregated regions is continually decreased by forces within the fluid and by mass exchange between the regions (Sohnel and Garside, 1992).

In both mechanisms the final mixing process is by laminar convection and molecular diffusion over lengths of scale smaller than the Kolmogoroff velocity microscale, λ_K. These mechanisms are very rapid at the scales of the order of the Batchelor concentration microscale, λ_B (Sohnel and Garside, 1992):

$$\lambda_B = \left[\frac{\left(\mu/\rho\right)^3 D_f}{\varepsilon}\right]^{1/4} \qquad (2\text{-}23)$$

where ρ: fluid density [kg/m^3]

μ: fluid viscosity [kg/ms]

ε : average energy dissipation rate [W/kg]

D_f: diffusion coefficient

For $\left(\mu/\rho\right) = 10^{-6}$ m^{2}s^{-1}, $D_f = 10^{-9}$ and an energy dissipation rate of 1 W/kg, $\lambda_B \approx 1$ μm.

The micro mixing time is determined as (Baldyga and Bourne, 1989):

$$\tau_{micro} = 17.24\sqrt{\frac{\gamma}{\varepsilon}} \qquad (2\text{-}24)$$

where γ: kinematic viscosity [m^2/s]

ε : average energy dissipation rate [m^2/s^3]

2.4.3 Turbulent mixing and chemical reactions

Chemical reactions depend directly on the molecular scale mixing of the reagents, a process which in turn can be influenced by mixing on coarser scales (Baldyga and Bourne, 1999).

Sohnel and Garside (1992) identified three regimes that can be identified by comparing the reaction time, t_R, with the micromixing time, τ_{micro}:

- $\tau_{micro} \ll t_R$: slow regime, the reaction kinetics control the process, the vessel is basically homogeneous and the reaction takes place throughout the vessel
- $\tau_{micro} \approx t_R$: fast regime, the rate is influenced by both physical and chemical factors and the reaction takes place in a narrow zone on either side of the diffusion plane
- $\tau_{micro} \gg t_R$: instantaneous regime, the rate is limited by the rate of mixing by diffusion and the reaction takes place in the diffusion plane.

Chen *et al.* (1996) studied the effect of stirrer speed on the mean particle size of barium sulphate. A critical impeller speed, N_{crit}, was found at which the mean size was minimum. For impeller speeds higher than N_{crit}, the mean particle size increased when the stirrer speed was increased. For impeller speeds lower than N_{crit}, the mean particle size decreased with an increase in impeller speed.

Chen *et al.* (1996) and Baldyga and Pohorecki (1988) proposed a model to predict the influence of mixing on particle size distribution. The model hypothesises that two zones exist in a reactor. One is the segregated zone around the feed jet and the other is the bulk well-mixed zone comprising the remainder of the vessel. Micromixing creates a region of higher supersaturation in the first zone, and thus more nuclei form in this zone. In the second zone of the reactor low supersaturation prevails. Regions described by the second zone dilute any supersaturation in the bulk regions of the reactor and as a result, crystals growth overtakes nucleation. The reactor can be viewed as comprised of two sub-reactors, a plug flow reactor (PFR) and a mixed reactor (MR), corresponding to the segregated zone and the bulk, well-mixed, zone respectively. The volumes of the two zones are determined by macromixing and micromixing. If macromixing is faster than micromixing, the volume of the PFR becomes smaller and the reaction proceeds slowly due to slower micromixing. The reaction extends to the MR where the nucleation process is negligible, fewer nuclei will be formed and larger mean particle size will be obtained. The reverse will happen is stirrer speed is increased. If the stirrer speed is raised to N_{crit}, the whole reaction zone will shift into the PFR and the

particle size decrease to a minimum. When the stirrer speed is increased beyond N_{crit}, the volume of PFR will get larger. But the total yield of the product will remain constant because the reaction has already taken place. So fewer nuclei and larger particles will be formed. For stirring speeds lower than N_{crit}, the process is controlled by macromixing. For stirring speeds greater than N_{crit}, the controlling step is micromixing.

2.5 South African mine waters and scaling

Most South African mine service waters have high calcium and sulphate concentrations. Oxidation of pyrite present in gold bearing ores is the source of the sulphate ions. The presence of calcium is as a result of addition of lime to mine waters for neutralisation purposes (Juby *et al.*, 1985). Typical compositions and quality of mine waters are given in Table 2.2.

Table 2.2: Quality of mine service water from different mines (Juby, 1994)

Determinant	Units	Free State Mine	West Rand Mine
TDS (total dissolved solids)	mg/l	3800	2200
PH		6.5	6.0
Sodium	mg Na/l	1000	170
Calcium	mg Ca/l	330	400
Sulphate	mg SO_4/l	1050	1400
Chloride	mg Cl/l	1400	60
Magnesium	mg Mg/l	30	50

Mine waters are dominated by the presence of calcium, sulphate and sodium. The degree of calcium sulphate saturation may have severe implications in desalination because of scaling (Juby, 1994). There is scaling potential whenever the solubility of sparingly soluble salts, such as calcium sulphate, is exceeded (Juby and Schutte, 2000). Scale formation is a serious problem to industries, since it brings about problems such as decline in volume capacity of equipment, blockages of pipes, corrosion, fatigue of metal parts, reduction in heat transfer rates (Sohnel and Garside, 1992). Calcium sulphate scaling poses technical problems to industry and constitutes a large load of pollution to the environment (Juby and Schutte, 2000).

2.6 SPARRO process review

The block flow diagram of the SPARRO process is shown in Figure 2.5. The first step in the SPARRO process is feed water pre-treatment. Pre-treatment is a requirement of all membrane systems, with the aim to remove any material/constituents from the water that may cause fouling or degradation of the membranes. The feed water is chemically treated with caustic soda, polyelectrolyte and potassium permanganate. The water is then sent to a clarifier where settled sludge is removed. The water is then passed through dual media anthracite/sand filters. Conditioning of the water via regulation of pH and temperature is also required so that it is suitable for the particular type of membrane used in the process.

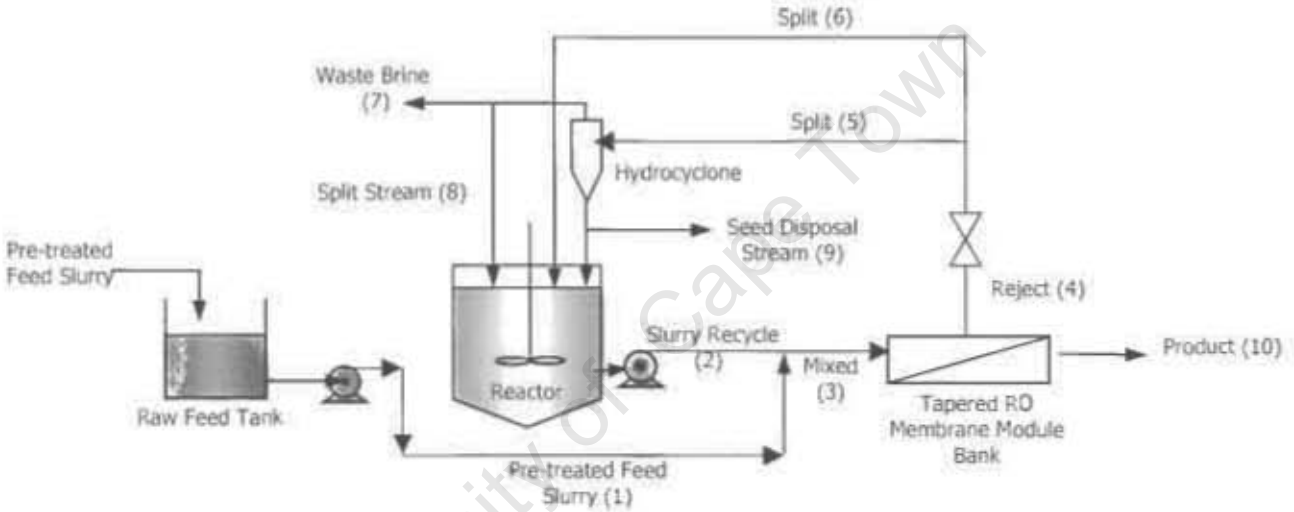

Figure 2.5: Block Flow Diagram of the SPARRO process (Juby, 1994)

The pre-treated and conditioned feed water is stored in a feed water tank and pumped to a gauge pressure of 4000 kPa. This pressurised raw feed water (stream 1) mixes with the gypsum slurry recycle (stream 2) at a specified mixing ratio. The recycle slurry stream contains approximately 41 g/L of gypsum crystals in suspension and the mixed stream (stream 3) contains approximately 18 g/L of gypsum crystals in suspension. Stream 3 is passed through the tapered membrane modules at a gauge pressure of 4000 kPa and a total dissolved solids (TDS) concentration of 7500 mg/L.

The SPARRO process is based on Seeded Reverse Osmosis (SRO), which involves circulating the slurry of seed crystals within the Reverse Osmosis (RO) system. As the solubility product is exceeded because of the concentration effect, precipitation of the $CaSO_4$ starts to take place. Instead of the $CaSO_4$ forming scale on the membrane, the seed crystals provide preferential growth sites for the $CaSO_4$ to grow, thus minimising the problems associated

with membrane scaling. The membrane splits stream 3 into a purified effluent stream (permeate product) and a reject stream, which is more concentrated in solute and contains the crystals that do not pass through the membrane pores. The product (stream 10) is the permeate from the membrane module and has a TDS of 900 mg/L

The reject of the membrane (stream 4) is delivered at a pressure of 2500 kPa and has a TDS of 15000 mg/L and 36.5 g/L gypsum crystals in suspension. Concentration effects within the membranes are the cause of increase in the TDS. The pressure of the stream 4 is reduced to 510 kPa by passing it through a pressure reducing orifice plate. The stream is then split into a controlled volume (stream 5), which is sent to the hydrocyclone, and the remainder (stream 6) is sent to the reactor.

A controlled volume (stream 8) of the overflow from the hydrocyclone is returned to the reactor. The remaining waste brine (stream 7) is disposed of. Seed blowdown (stream 9) is removed from the underflow while the bulk of the underflow of the hydrocyclone is sent to the reactor. Stream 9 maintains the required suspended solids concentration in the system.

In the reactor, mechanical stirring ensures complete mixing during the time required for desupersaturation of the supersaturated solutions, which return to the reactor from the membrane module.

2.6.1 The desupersaturation reactor used in the SPARRO process

The desupersaturation reactor acts as a storage buffer for the seed crystals that are required in the feed stream to the membranes. It provides sufficient residence time to allow the supersaturated brine solution that exits the membrane stack to return to equilibrium conditions. This is achieved by allowing the excess $CaSO_4$ to precipitate on the seed crystals present in the slurry.

Reverse osmosis (Figure 2.6) processes operate at elevated pressures. Thermodynamically, for solutions on either side of a membrane to be in osmotic equilibrium, their chemical potentials must be equal. Pure water has a higher chemical potential than a solution, indicating that a system consisting of pure water on one side of a membrane and a solution on the other will result in the transport of the pure water through the membrane into the solution i.e. in the direction of lower chemical potential. Increasing the pressure on the solution side would increase its chemical potential and restore the osmotic potential whilst at

higher pressures, it would force the water to flow through the membrane. This process is called reverse osmosis (Seader and Henley, 1998).

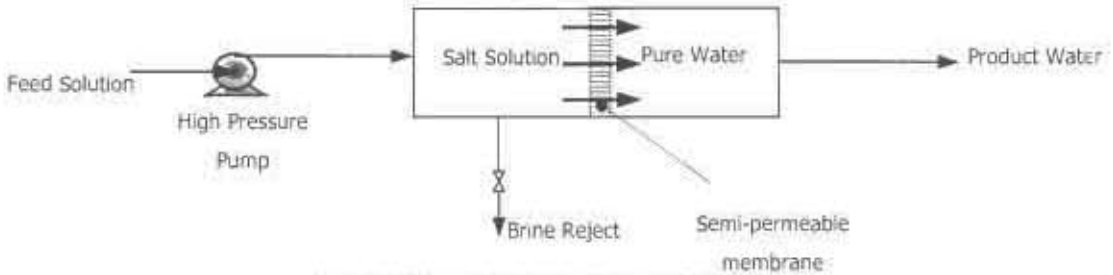

Figure 2.6: Principles of Reverse Osmosis

The minimum exit pressure from the membrane is 2000 kPa. The reactor can be operated at 2000 kPa and by doing so the cost of energy required to pump the feed solution from atmospheric pressure to the reactor operating pressure can be saved. At the same time, the savings in the pumping costs would not offset the capital costs associated with the pressurised reactor system. In his research, Juby (1994) chose to use atmospheric pressure for the operation of the reactor. For smooth operation of the SPARRO process the settling of gypsum crystals has to be avoided. Juby (1994) used a single mixed reactor for his pilot plant.

Juby (1994) designed the reactor used for his research based on the results obtained from an investigation into the kinetics of gypsum precipitation carried out by Maree *et al.* (1988). The SPARRO process was designed for treating 0.82 L/s of mine water. The specifications of the reactor designed by Juby (1994) are given in Table 2.3.

Table 2.3: Reactor Design specifications (Juby, 1994)

Description	Value
Maximum capacity [m^3]	4.5
Design capacity [m^3]	3.5
Diameter [m]	1.5
Height [m]	2.5
Power [kW]	0.75
Speed [rpm]	290
Hydraulic residence time [h] (at design)	1

The reactor contents and the outlet stream have a solid suspension of 41 g/L. This means that the quantity of solids (gypsum) in solution amounts to 1.76% by volume (Appendix A).

3. Response surface methodology (RSM)

Response surface methodology was utilised in the experimental part of this research. This chapter is thus devoted to the basic principles and computations involved in RSM.

3.1 Introduction to response surface methodology.

Response surface methodology is a collection of statistical and mathematical techniques useful for developing, improving and optimising processes (Myers and Montgomery, 1995). In a process there can be several controllable input variables that may influence some performance measure of the product or the process itself. The performance measure or quality characteristic is called a response and measured on a continuous scale. There can be more than one response. The relationship between a response, y and input variables ξ_1, ξ_2,..., ξ_k is:

$$y = f(\xi_1, \xi_2, \ldots, \xi_k) + e \qquad (3\text{-}1)$$

Where, f is the unknown form of the true response function

e is a term representing sources of variability not accounted for in f (e.g. background noise or measurement errors)

e can be treated as a statistical error, having a normal distribution with mean zero and variance σ^2. Then,

$$E(y) = \eta = E[f(\xi_1, \xi_2, \ldots, \xi_k)] + E(e) \qquad (3\text{-}2)$$

$$\eta = f(\xi_1, \xi_2, \ldots, \xi_k) \qquad (3\text{-}3)$$

The variables ξ_1, ξ_2,..., ξ_k are called the natural variables and are expressed in the units of measurement (e.g. g/L, °C, or kg). In RSM natural variables are coded to variables, x_1, x_2,..., x_k that are dimensionless with mean zero and the same standard deviation. The true regression is then written as:

$$\eta = f(x_1, x_2, \ldots, x_k) \qquad (3\text{-}4)$$

The unknown function f has to be approximated and it can be a first, second or higher order model. For the case of two independent variables, the first order model in terms of the coded variables is:

$$\eta = \beta_0 + \beta_1 x_1 + \beta_2 x_2 \qquad (3\text{-}5)$$

In 3-d, the response surface is a plane lying above x_1, x_2 space.

There can be often curvature in the true response and then a first order model is inadequate. A second order model may be required in that case. For two variables, the full second order model is:

$$\eta = \beta_0 + \beta_1 x_1 + \beta_2 x_2 + \beta_{11} x_1^2 + \beta_{22} x_2^2 + \beta_{12} x_1 x_2 \qquad (3\text{-}6)$$

An example of a second order model is $z = 50 + 8x_1 + 3x_2 - 7x_1^2 - 3x_2^2 - 4x_1x_2$. The corresponding response surface is shown in Figure 3.1.

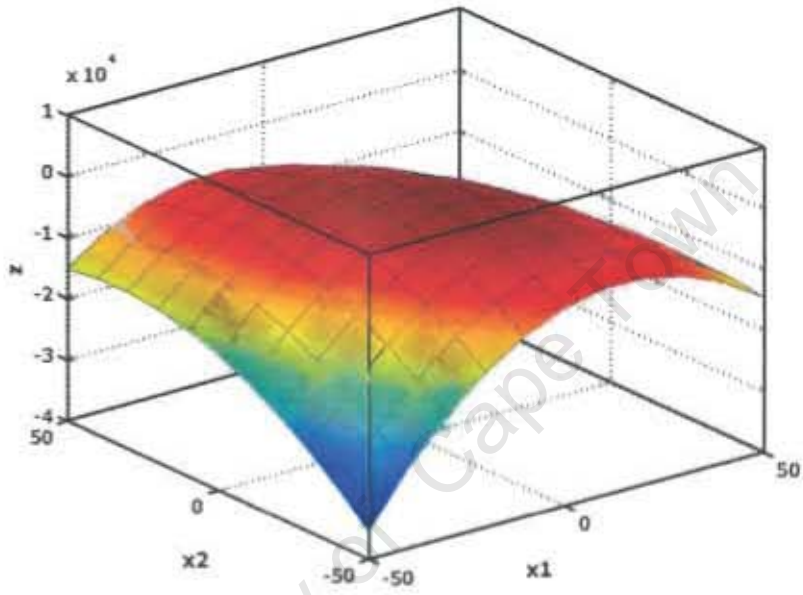

Figure 3.1: 3-d surface plot of $z = 50 + 8x_1 + 3x_2 - 7x_1^2 - 3x_2^2 - 4x_1x_2$

In general for k variables a first order model is given by:

$$\eta = \beta_0 + \beta_1 x_1 + \beta_2 x_2 + \ldots + \beta_k x_k \qquad (3\text{-}7)$$

A second order model is given by:

$$\eta = \beta_0 + \sum_{j=1}^{k} \beta_j x_j + \sum_{j=1}^{k} \beta_{jj} x_j^2 + \sum\sum_{i<j} \beta_{ij} x_i x_j \qquad (3\text{-}8)$$

The β's are a set of unknown parameters and can be estimated by analysing data collected from the system using linear regression (Myers and Montgomery, 1995).

3.2 Response surface methodology sequence.

Most applications of RSM are sequential in nature (Myers and Montgomery, 1995):

- Initially ideas concerning which factors in a process are likely to be important in the RSM study are generated.

- Screening studies are carried out to investigate the extent to which the factors affect the system, and the insignificant factors are then eliminated.
- A response surface design is generated and experiments are conducted.
- Data collected from the experiments is analysed using linear regression. A first order model can be fitted initially. If there is evidence of curvilinearity in the data then further data can be collected to fit a second order model. If there is no evidence of curvilinearity in the data then the experimental region should be changed in the direction of the steepest ascent or descent. The experiments are repeated until the region of the minimum or maximum is reached.

3.3 Building empirical models.

3.3.1 Estimating the parameters in the empirical models

A model used to approximate the observed response is called an empirical model. If the number of variables is smaller than the number of experimental runs then the response y may be related to the k regressor variables as:

$$y_i = \beta_0 + \sum_{j=1}^{k} \beta_j x_{ij} + e_i \quad i=1, 2,..., n \tag{3- 9}$$

$\beta_1, \beta_2,..., \beta_k$ are called the regression coefficients.

In a multiple regression technique it is simpler to solve for the regression coefficients in matrix notation (Myers and Montgomery, 1995). Then equation 3-9 can be written in matrix notation as:

$$\mathbf{y} = \mathbf{X}\boldsymbol{\beta} + \mathbf{e} \tag{3- 10}$$

where,
$$y = \begin{bmatrix} y_1 \\ y_2 \\ . \\ . \\ y_n \end{bmatrix}, \quad X = \begin{bmatrix} 1 & x_{11} & x_{12} & . & . & x_{1k} \\ 1 & x_{21} & x_{22} & . & . & x_{2k} \\ . & . & . & & & . \\ . & . & . & & & . \\ 1 & x_{n1} & x_{n2} & . & . & x_{nk} \end{bmatrix}, \quad \beta = \begin{bmatrix} \beta_0 \\ \beta_1 \\ . \\ . \\ \beta_k \end{bmatrix}, \quad e = \begin{bmatrix} e_1 \\ e_2 \\ . \\ . \\ e_n \end{bmatrix}$$

To find the vectors of least squares estimates, the following should be minimized:

$$L = \sum_{i=1}^{n} e_i^2 \tag{3- 11}$$

With some simplifications the least square estimate of β is:

$$\mathbf{b} = (\mathbf{X}'\mathbf{X})^{-1}\mathbf{X}'\mathbf{y} \tag{3- 12}$$

The fitted regression model is

$$\hat{\mathbf{y}} = \mathbf{Xb} \tag{3- 13}$$

In scalar notion, the fitted model is:

$$\hat{y}_i = b_0 + \sum_{j=1}^{k} b_j x_{ij} \quad i=1, 2,..., n \tag{3- 14}$$

The difference between the observation y_i and the fitted value $\hat{y}_i$ is a residual, say $e_i = y_i - \hat{y}_i$ and in vector notation:

$$\mathbf{e} = \mathbf{y} - \hat{\mathbf{y}} \tag{3- 15}$$

Equation 3.14 can be converted back to an equation in terms of natural variables $\xi_1, \xi_2,..., \xi_k$ using the conversion:

$$x_{i1} = \frac{\xi_{i1} - \left[\max(\xi_{i1}) + \min(\xi_{i1})/2\right]}{\left[\max(\xi_{i1}) - \min(\xi_{i1})\right]/2} \tag{3- 16}$$

3.3.2 Estimating the variance σ^2

The sum of squares, of the residuals, SS_E is given by:

$$SS_E = \sum_{i=1}^{n} (y_i - \hat{y}_i)^2 = \sum_{i=1}^{n} e_i^2 \tag{3- 17}$$

An unbiased estimator of σ^2 is given by:

$$\sigma^2 = \frac{SS_E}{n - p'} \tag{3- 18}$$

where p' is the number of model parameters (Myers and Montgomery, 1995).

3.3.3 Test for significance of regression

The total sum of squares S_{yy} is given by:

$$S_{yy} = \sum_{i=1}^{n} y_i^2 - \frac{\left(\sum_{i=1}^{n} y_i\right)^2}{n} \tag{3- 19}$$

S_{yy} can be split into a sum of squares due to the model (SS_R) and a sum of squares due to residuals (SS_E):

$$S_{yy} = SS_R + SS_E \tag{3- 20}$$

The sum of squares due to the model can be calculated as:

$$SS_R = b'X'y - \frac{\left(\sum_{i=1}^{n} y_i\right)^2}{n} \tag{3- 21}$$

The test for significance of regression is a test to determine if there is a linear relationship between the response variable y and a subset of the regressor variables (Myers and Montgomery, 1995). The appropriate hypotheses are:

$$H_0 : \quad \beta_1 = \beta_2 = \ldots = \beta_k = 0 \tag{3-22}$$

$$H_1 : \quad \beta_j \neq 0 \quad \text{for at least one } j \tag{3-23}$$

Rejection of H_0 means that at least one of the regressor variables $x_1, x_2, \ldots, x_k$ contributes significantly to the model. The test procedure would be to calculate F_0:

$$F_0 = \frac{SS_R / k}{SS_E / (n-k-1)} = \frac{MS_R}{MS_E} \tag{3-24}$$

H_0 can be rejected if the P-value for the statistic of F_0 is less than α. One could make an error by rejecting H_0, when in fact H_0 is true. The probability of such an error occurring is called the level of significance and is denoted by α (Walpole and Myers, 1995). The test procedure is called analysis of variance and is summarised as in Table 3.1:

Table 3.1: Analysis of variance for significance of regression in multiple regressions.

Source of variation	Sum of squares	Degrees of freedom	Mean Square	F_0
Regression	SS_R	k	MS_R	MS_R/MS_E
Residual	SS_E	n-k-1	MS_E	
Total	S_{yy}	n-1		

R^2 is the coefficient of multiple determination given by:

$$R^2 = \frac{SS_R}{S_{yy}} \quad \text{where} \quad 0 \leq R^2 \leq 1 \tag{3-25}$$

R^2 is the measure of the amount of variability of y accounted for by the regressor variables $x_1, x_2, \ldots, x_k$ in the model. R^2 basically gives an idea of the goodness of fit of the regression model for a given number of regressors.

3.3.4 Test on individual regression coefficients

Testing hypotheses on the individual regression coefficients is important as they determine the value of each of the regression variables in the model. The hypotheses for testing the significance of the regression coefficients, β_j are:

$$H_0 : \quad \beta_j = 0 \tag{3-26}$$

$$H_1 : \quad \beta_j \neq 0 \tag{3-27}$$

If H_0 is not rejected this indicates that x_i can be deleted from the model. The t-test statistics for this hypothesis is:

$$t_0 = \frac{b_j}{\sqrt{\hat{\sigma}^2 C_{jj}}} \quad (3\text{-}28)$$

Where, C_{jj} is the diagonal element of $(X'X)^{-1}$ corresponding to b_j. The P-value corresponding to the t-test and a level of significance, α, will show that for P-value < α, the regression coefficient contributes significantly to the model (Myers and Montgomery, 1995).

3.3.5 Fitting a second order model.

To fit a second order model like:

$$\hat{y} = \beta_0 + \beta_1 x_1 + \beta_2 x_2 + \beta_{11} x_1^2 + \beta_{22} x_2^2 + \beta_{12} x_1 x_2 \quad (3\text{-}29)$$

The same approach of linear regression outlined in section 3.3.1 can be used to solve for the regression coefficients. In this case x_1^2, x_2^2 and x_1x_2 will be treated as new variables (Myers and Montgomery, 1995). The test of significance of regression and the individual regression coefficients can also be done by the same approach outlined in sections 3.3.3 and 3.3.4.

3.3.6 Experimental designs

When investigating the joint effects of k factors on a response, 2^k factorial designs are widely used. The simplest case is the 2^2 factorial design for a process with two variables. The levels of the factors that are varied are called high (+) or low (-). Table 3.2 summarises the experiments required for 2^2 factorial design, varying factors, A and B, for example.

Table 3.2: The 2^2 factorial design

	Factor A	Factor B
Experiment 1	-	-
Experiment 2	-	+
Experiment 3	+	-
Experiment 4	+	+

3.3.6.1 The 2^3 factorial design

If three factors, A, B and C each at two levels (high and low) are of interest, then a 2^3 factorial design should be used. The eight treatment combinations can be displayed graphically in Figure 3.2. The high level of any factor at a point in the design is denoted by the corresponding lowercase letter and that the low level of a factor is denoted by the absence of the corresponding letter. Thus, as shown in Figure 3.2, (a) represents the point

in the design where factor A is to be set at the high level and the factors B and C set to low levels. The point abc would denote the point in the design where all three factors, A, B and C will be set at the high values. By convention, (1) is used to denote the experiment at which all the factors are set at the low levels (Myers and Montgomery, 1995).

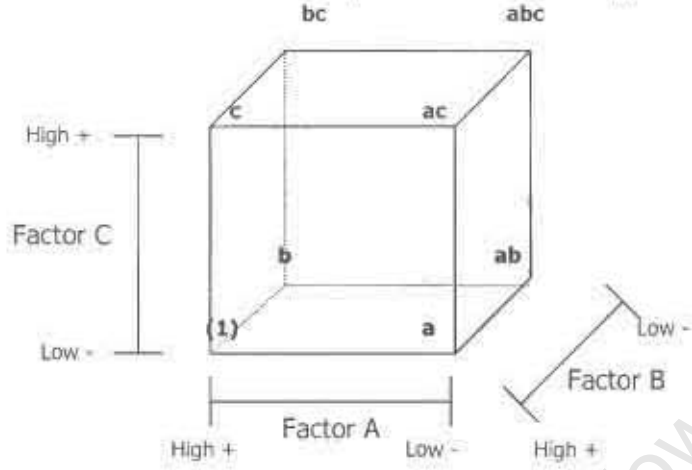

Figure 3.2: The 2^3 factorial design

Table 3.3 summarises the levels of factors for a 2^3 factorial design.

Table 3.3: The 2^3 factorial design

	Factor A	Factor B	Factor C	Treatment combination
Experiment 1	-	-	-	(1)
Experiment 2	+	-	-	a
Experiment 3	-	+	-	b
Experiment 4	-	-	+	c
Experiment 5	+	+	-	ab
Experiment 6	+	-	+	ac
Experiment 7	-	+	+	bc
Experiment 8	+	+	+	abc

3.3.6.2 The general 2^k factorial and one-half factorial design

In single replicate 2^k designs, there is no repetition of experiments to calculate experimental errors. In this case it is important to carry out experiments at centre points that would allow finding an estimate of the error. As the number of factors increases, the number of experiments increase and often time constraints are present. To reduce the number of experiments one can adopt the one-half factorial design whereby the number of experiments is halved and the new design is called the 2^{k-1} design (Myers and Montgomery, 1995). In the

case of three factors being varied, A, B and C, Figure 3.3 illustrates graphically a half-replicate design that would be relevant.

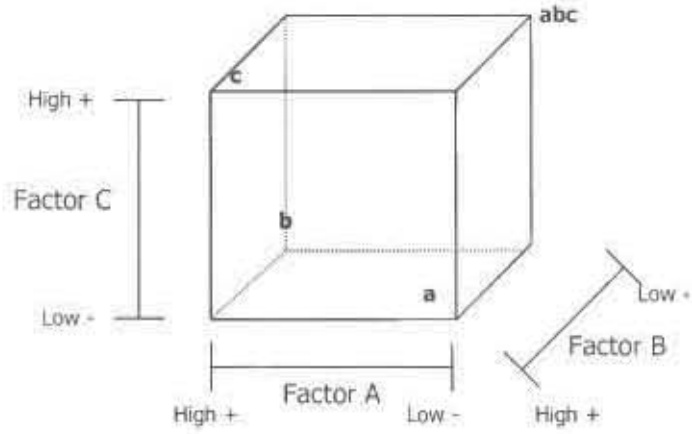

Figure 3.3: A half fraction of the 2^3 factorial design

3.3.6.3 Central composite design

To fit a second order model, the ideal experimental design would be the central composite design which consists of a full replicate design and further experiments at axial points (whereby one factor is changed and the rest of all the factors kept at zero-level). For example, for a system with two variables, A and B the axial points experiments will be as in Table 3.4.

Table 3.4: Axial point experiments for a system with two factors

	Factor A	Factor B
Experiment 1	+2	0
Experiment 2	-2	0
Experiment 3	0	+2
Experiment 4	0	-2

3.3.6.4 The ridge analysis

If a critical point is outside the experimental area investigated, then a ridge analysis can be used to determine the nature of the system inside or on the perimeter of the experimental region (Myers and Montgomery, 1995). The ridge analysis produces a locus of points, each of which is a point of maximum response with a constraint that the point lies on a sphere of a certain radius. The output of this analysis is the set of coordinates of the maxima (or minima) along with the predicted response, $\hat{y}$, at each computed point on the path.

4. Application of Digital Image Processing (DIP) in quantifying crystal morphology

As crystal morphology is an important response of a process, it is crucial to quantify it and relate it to the process conditions. Various techniques have been and are being developed to quantify crystal morphology. A classic example would be a fractal dimension, used by Lewis and Roberts (2003) in an attempt to quantify the morphology of nickel crystals. The fractal dimension technique is feasible for rugged surfaces. Since gypsum has non-rugged, defined surfaces, fractal dimension is inappropriate for quantifying the morphology of gypsum crystals. Width to length ratios can be used to quantify the gypsum crystals, however this manual procedure can be tedious, as well as prone to significant errors. Based on these considerations, it was decided to use DIP for quantification of the morphology of gypsum crystals. Digital images of the crystals can be generated by scanning electron microscopy. This chapter gives background information on digital image processing and identifies the Sobel edge operator as the most appropriate technique to quantify the gypsum crystal morphology.

4.1 Introduction to Digital Image Processing (DIP)

DIP is a powerful technique for the following reasons (Green, 1983):

- Digital imaging systems are capable of acquiring imagery that has a wider dynamic range than the human eye. The human eye can detect fewer than 100 shades of gray, while digital imaging can represent several thousand shades of gray.
- A single digital image contains a very large amount of information in a compact and easily interpreted form. DIP technology can process and manipulate imagery using methods including a variety of transformations that are impossible optically.

4.2 Basic definitions in digital imagery

A digital image acquisition system is a device that generates a sampled digital representation of a scene. The scanning electron microscope is a classic example of a digital image acquisition system whereby the output is represented as a two-dimensional matrix of numbers, called a digital image. Figure 4.1 illustrates the basic terms used in a digital image.

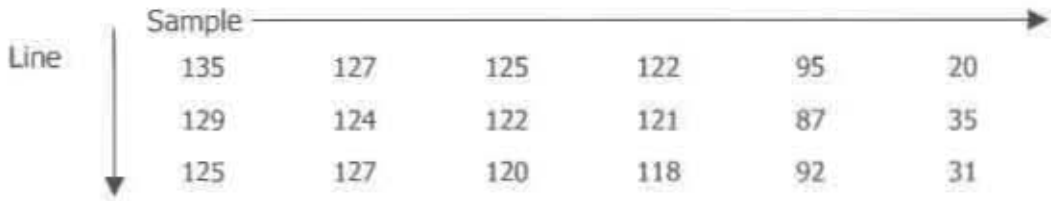

Figure 4.1: A digital representation of an image

The rows of the matrix are called lines and the columns are referred to as samples. The individual component elements within the digital image are referred to as picture elements (pixels). The digital value of each pixel that represents intensity is referred to as digital intensity. Using this notation, the digital intensity of the pixel at line 2 and sample 2, as shown in Figure 4.1, is 124. Digital intensity values can range from 0 to 255, with zero representing black and 255 representing white (Green, 1983).

4.3 Digital image processing

Digital image processing techniques fall into two categories (Green, 1983):

- Subjective image processing techniques, which are designed to improve human visual interpretation of an image.
- Quantitative image processing techniques, which are based on predefined mathematical algorithms (e.g. the computation of a 2-d Fourier transform of an image).

4.3.1 Quantitative image processing

Segmentation is one of the various quantitative image processing techniques and it consists of dividing an image into meaningful regions. The mathematical formulation for scene segmentation is called clustering. Clustering is defined as finding "natural grouping" in a set of measurements $\{\mathbf{x}\}$, where the vector $\mathbf{x}=(x_1, x_2,\ldots,x_n)'$ represents properties of some underlying set of patterns. Segmentation may also be considered as a special type of clustering in which some of the measurement components may correspond to spatial locations. The remaining components may correspond to point properties such as gray level of spectral coordinates, or to regional properties such as edge measurements (Hall, 1979).

4.4 Edge detection approach

Template matching is widely used in segmentation. A template (mask) is an array designed to detect some regional property. There can be a number of templates including those that detect a point, a tilted edge, a horizontal edge, a line or even a region. Of these the most

straightforward would be point detection. If $w_1, w_2, \ldots, w_N$ represent the weights in an N=nxn mask, and $x_1, x_2, \ldots, x_N$ are the gray levels of the pixels inside the mask, template matching can be taken as the inner product of the vectors

$$w = \begin{bmatrix} w_1 \\ w_2 \\ . \\ . \\ w_N \end{bmatrix} \quad \text{and} \quad x = \begin{bmatrix} x_1 \\ x_2 \\ . \\ . \\ x_N \end{bmatrix} \tag{4-1}$$

Where the first n elements of **w** are the elements in the first row of the template, the next n elements are from the second row and so on. The inner product of **w** and **x** is

$$w'x = w_1x_1 + w_2x_2 + \ldots + w_Nx_N \tag{4-2}$$

An edge is detected by the template **w** if $w'x > T$, where T is a specified threshold. The development of templates for edge detection follows the same reasoning with the interest of detecting transitions between regions. One approach often used for determining such transitions is to implement some form of two-dimensional derivative function. The Sobel edge operator is a local edge detection procedure, which is linear with a 3x3 template or mask. The gradient concept is employed (Hall, 1979).

4.4.1 The Sobel Edge detector

The Sobel operator performs a 2-D spatial gradient measurement on an image and so emphasizes regions of high spatial gradient that corresponds to edges. It is used to find the absolute gradient magnitude at each point in an image. The templates used in the Sobel edge are 3x3 arrays. G_x and G_y are the discrete gradients in the x and y directions, respectively. The gradient at point p is then defined as

$$G = \left[G_x^2 + G_y^2\right]^{1/2} \tag{4-3}$$

Edge detection can be expressed in vector form. Thus if **x** represents the image region in question (Hall, 1979), then:

$$G_X = w_1'x \tag{4-4}$$

$$G_y = w_2'y \tag{4-5}$$

where w_1 and w_2 are the two masks used as shown in Figure 4.2.

1	2	1
0	0	0
-1	-2	-1

1	0	-1
2	0	-2
1	0	-1

Figure 4.2: w_1 and w_2, the gradient templates used in the Sobel edge operator (Hall, 1979)

5. Experimental and methodology

Chapter 5 identifies the factors worth investigating. The design and specifications of the 5 L lab-scale reactor used in the experiments are presented. The statistical experimental designs adopted are listed followed by the detailed experimental procedures used for the batch and hydrodynamic study experiments. Figure 5.1 summarises the experiments and methodology adopted in the research.

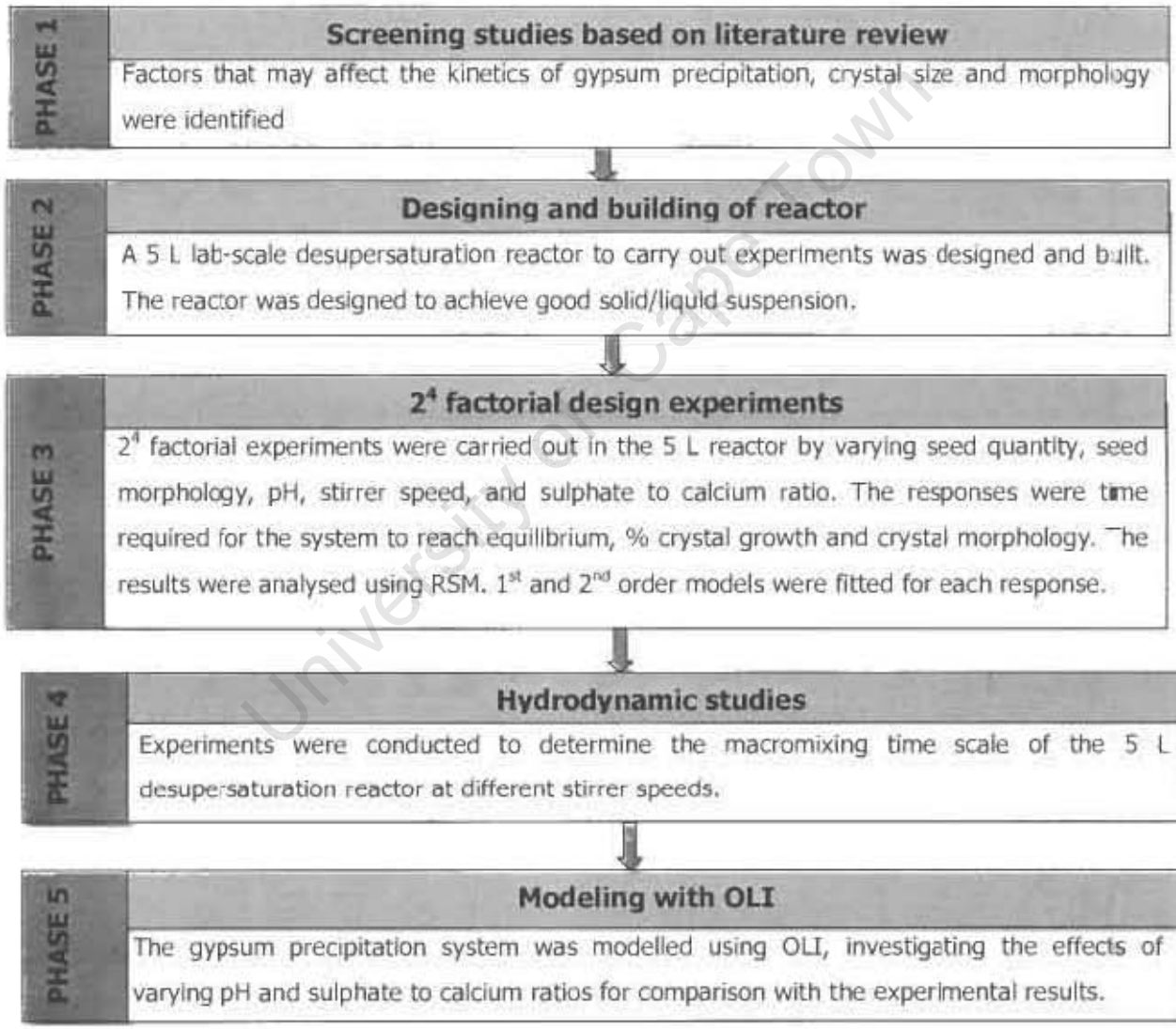

Figure 5.1: The research structure

5.1 Identification of factors for investigation

Screening studies identified factors affecting the kinetics and physical aspects of gypsum precipitation. Table 5.1 justifies why the various factors were worthy of investigation.

Table 5.1: Factors investigated in thesis

Factor	Justification of choice
Seed morphology	As one of the aims of the project was to control the morphology of the gypsum crystals to a certain size and morphology, it was decided to keep plate-like and needle-like crystals as two different factors.
Seed quantity	As presented in the literature review, seed quantity affects the kinetics of precipitation. The SPARRO process used only about 1.7% by volume of seed crystals (Juby, 1994) and thus it was important to investigate the influence of varying this factor.
pH	Acidic reactants can affect the morphology of the gypsum crystals. Also, reverse osmosis membranes can be pH sensitive.
Stirrer speed	The particle size distribution of gypsum crystals can be affected by the agitation speed. In SPARRO process a good solid/liquid suspension is required.
Sulphate to calcium molar ratio	This factor can affect supersatutation, the product size and morphology as presented in the literature review. Different mine waters have different sulphate to calcium levels.

5.2 Reactor design

5.2.1 Tank dimensions and geometry

The 5 L lab-scale desupersaturation reactor was designed based on the literature review with the aim of achieving good solid-liquid suspension. Figure 5.2 shows the schematic and Table 5.2 gives the specifications of the tank. The tank diameter could not be set to the height of the liquid as per equation 2-12. This was a design constraint due to availability of Perspex only in standard diameters. The highest possible ratio of liquid height to tank diameter of 0.773 was used.

Table 5.2: Tank geometry specification

Number of baffles	4, 90° to each other
Tank diameter, T [m]	0.22
Baffle width	$0.1\,T$
Draft tube diameter	$0.5\,T$
Draft tube height	$0.5\,T$
Tank bottom geometry	Rounded bottom
Height of liquid	$0.773\,T$
Material of construction	Perspex

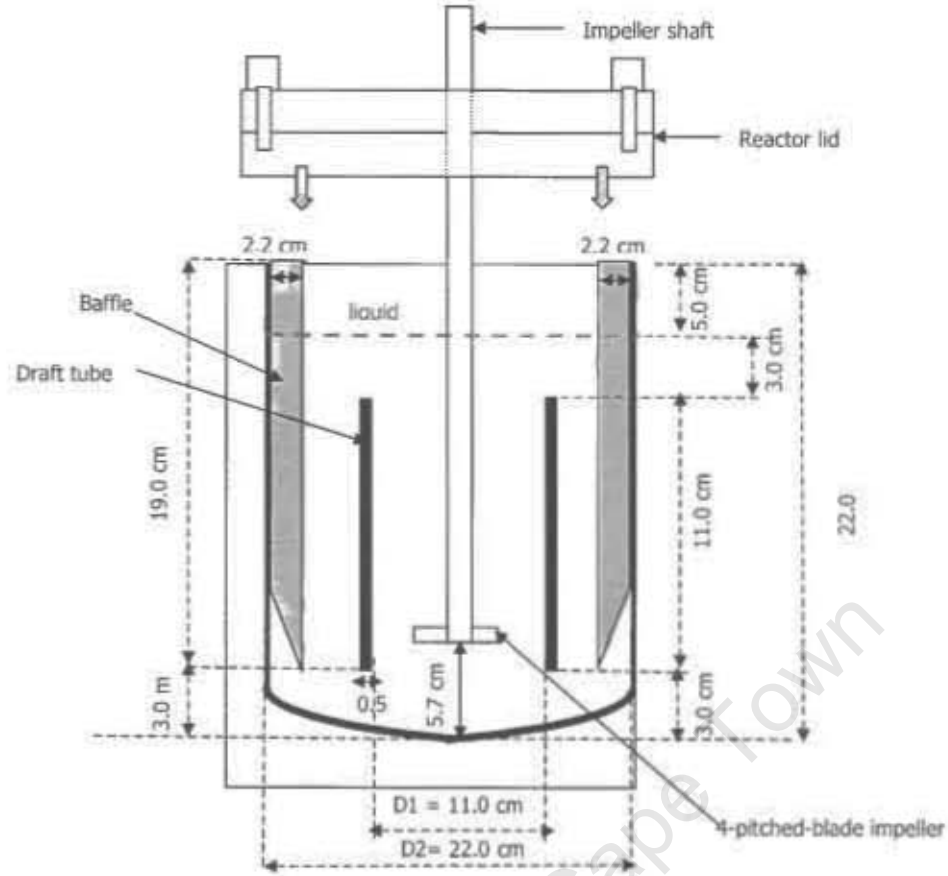

Figure 5.2: 5L lab-scale desupersaturation reactor design

5.2.2 *Impeller design*

Figure 5.3 illustrates the impeller that was designed for the experiments and Table 5.3 gives its specifications.

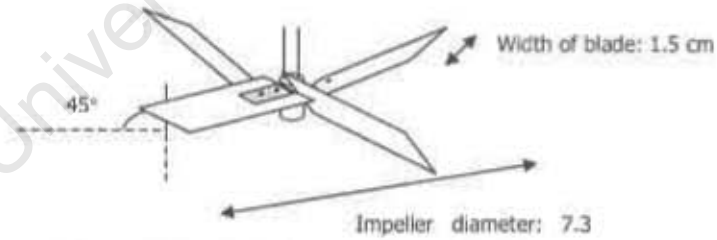

Figure 5.3: 4-pitched-blade impeller used in the experiments

Table 5.3: Specification of 4-pitched-blade impeller

Impeller type	Axial, 4-pitched-blades
Pitch	45°
Impeller diameter, D	$0.33\,T$
Blade width	$0.2\,D$
Impeller clearance	$0.33\,H$
Material of construction	Stainless steel

5.3 Experiments

5.3.1 Experimental designs

Experiments aimed at fitting 1st and 2nd order models were carried out using a half-replicate 2^4 factorial design and axial point experiments respectively. Seed quantity, pH, stirrer speed and sulphate to calcium ratio were varied as continuous factors. Seed crystal morphology was kept as a discrete factor to compare the effects of using different seed morphologies. Thus two half-replicates of 2^4 factorial design experiments were carried out for needle and plate-like crystals. The continuous factors were varied at levels given in Table 5.4.

Table 5.4: Levels of factors varied in experiments

Factor\Level	-2	-1	0	1	+2
SQ, Seed quantity [% by volume]	N/A	1	4	7	10
pH	1	4	7	10	N/A
N, Impeller speed [rpm]	N/A	300	500	700	900
SCR, Sulphate to calcium molar ratio	N/A	1	4	7	10

Some levels were not feasible due to negative values (e.g. –2 % by volume of seed crystals is impossible for –2 level) or because of physical constraints (e.g. impeller speed could not be set at 100 rpm for level –2, the minimum speed of the motor being 300 rpm). In these cases +1 or –1 level were used. Table 5.5 lists the levels of the factors in the experiments carried out for the half-factorial 2^4 designs each for the needle and plate-like seed crystals.

Table 5.5: Half-replicate of 2^4 factorial design for needle and plate-like seed crystals

Experiment for needle	Experiment for plate	SQ	pH	N	SCR
A1	**B1**	1	1	1	1
A2	**B2**	-1	1	-1	1
A3	**B3**	0	0	0	0
A4	**B4**	-1	-1	1	1
A5	**B5**	0	0	0	0
A6	**B6**	-1	1	1	-1
A7	**B7**	0	0	0	0
A8	**B8**	1	1	-1	-1
A9	**B9**	1	-1	-1	1
A10	**B10**	0	0	0	0
A11	**B11**	-1	-1	-1	-1
A12	**B12**	1	-1	1	-1

To fit the second order model, axial point experiments were carried out. The levels at which the factors were varied in the experimental runs are given in Table 5.6.

Table 5.6: Axial point experimental runs for plate-like seed crystals

Experiment number	SQ	pH	N	SCR
C1	-1	0	0	0
C2	+2	0	0	0
C3	0	-2	0	0
C4	0	+1	0	0
C5	0	0	-1	0
C6	0	0	+2	0
C7	0	0	0	-1
C8	0	0	0	+2

To analyse the kinetics of the gypsum precipitating system, control experiments D1-D3 were carried out at the levels given in Table 5.7.

Table 5.7 Control experimental runs for plate-like seed crystals

Experiment number	SQ	pH	N	SCR
D1	-1	0	0	-1
D2	0	0	0	-1
D3	+1	0	0	-1

5.3.2 Experimental procedure

Figure 5.4 shows the experimental set-up used to carry out experiments A1-A12, B1-B12, C1-C8 and D1-D3. The experiments were carried out in batch mode to investigate the effects of the factors independently without having a continuous stream coming into the reactor from the membrane module. The initial concentration of calcium ions was 0.03 M, a concentration that would normally occur in mine water.

The reactor was initially filled with 2.5 L of 0.06 M calcium chloride solution (prepared by dissolving high-purity anhydrous calcium chloride (Merck) in distilled water).

Needle-like or plate-like crystals were synthesised as in section 5.3.3. The particle size distribution of the seed crystals was determined using a mastersizer (Malvern mastersizer, model MAM 5002). A small sample of the seeds was filtered through a Millipore 0.45μm filter using a vacuum pump. These crystals were dried for scanning electron microscopy.

Preset quantities of seed crystals were transferred into the reactor. The impeller was set at the desired speed, reactor lid closed and the impeller was switched on.

The pH of the system was controlled by a pH controller (UCT custom-made), which was connected to an acid and base pump (UCT custom-made). pH readings were obtained and measured through a pH probe inserted in the reactor through an inlet provided on the reactor lid (Figure 5.5).

Figure 5.4: Experimental set-up

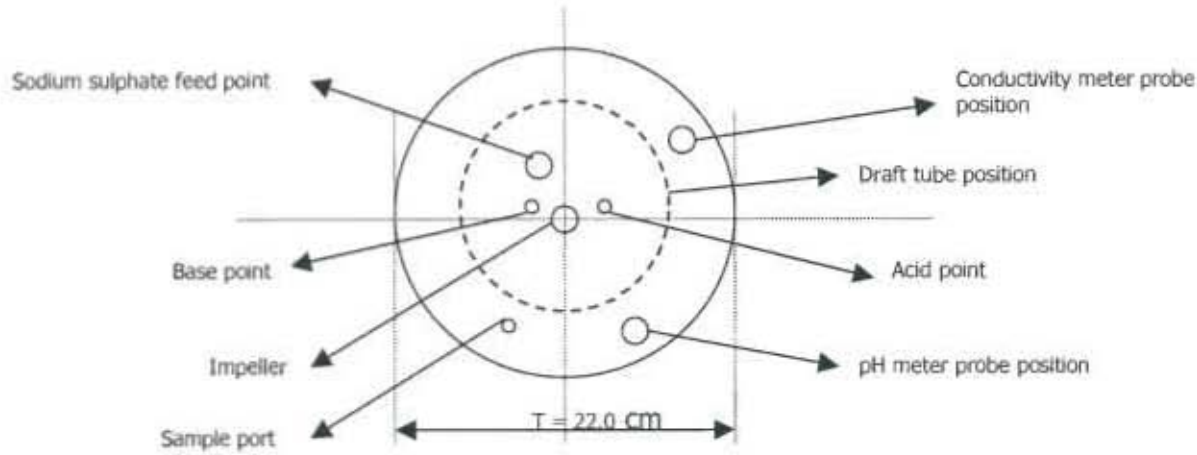

Figure 5.5: Schematic of top section of reactor lid

The position of the probe was outside the draft tube, in the annular region of the vessel. The probe was thus far from the acid and base inlet. The higher set point of the pH controller was 0.5 above the pH required while the lower set point was 0.5 below the pH required. 0.05 M NaOH and 0.05 M HCl solutions were used to raise and lower the pH of the system. These solutions were prepared using analytical grade chemicals (Merck) and distilled water. The pH control unit is as shown in Figure 5.6. The base and acid feed inlet in the reactor were located close to the impeller to ensure rapid dispersion.

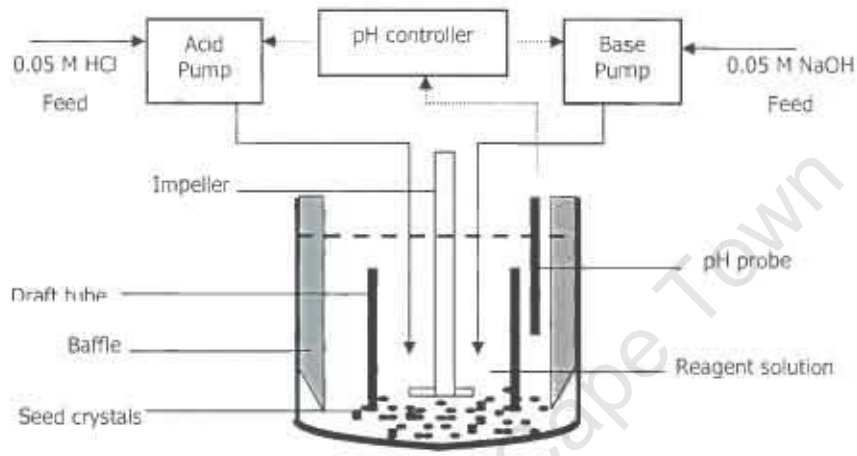

Figure 5.6: Schematic of pH control mechanism

The experiment was initiated by pumping (Masterflex peristaltic pump, model 7521-47) 2.5 L of sodium sulphate solution into the reactor at 9.5 ml/s. The feed point of sodium sulphate was kept close to the impeller to ensure good dispersion. The pH controller was activated and readings from a conductivity meter (Radiometer analytical, Ion check 30) were taken at 1-minute intervals. The conductivity probe was inserted in the reactor lid (Figure 5.5) at a position far from the sodium sulphate feed point.

When the readings from the conductivity meter stabilised, samples were withdrawn from the sample port using a syringe. For all the experiments, the samples were taken from the same position in the reactor. The particle size distribution of the sample was measured using a mastersizer (Malvern mastersizer, model MAM 5002). Samples of crystals were filtered through a Millipore 0.45μm filter using a vacuum pump and left to dry for 96 hours for scanning electron microscopy.

5.3.3 Seed preparation

5.3.3.1 Preparation of needle-like seed crystals

Needle-like seed crystals were prepared by pumping (Masterflex peristaltic pump, model 7521-47) 0.08 M sodium sulphate solution at 9.5 ml/s into 0.08 M calcium chloride solution. Analytical grade chemicals (Merck) and distilled water were used to prepare these reagents, which resulted in a weakly supersaturated solution (0.04 M, supersaturation ratio of 2.27) of calcium and sulphate ions. Therefore, a long induction time and large volumes of reagents were required to produce a small amount of seed crystals. A 15 L tank was used as the reacting vessel and a 4-pitched blade impeller, identical to that used in the desupersaturation reactor, was used to agitate the reagents at 500 rpm. Each batch of the 15 L preparation was left for 24 hours and yielded 200 ml of crystals (4% by volume in the 5L desupersaturation reactor). These crystals were filtered for use in the batch desupersaturation experiments.

5.3.3.2 Preparation of plate-like seed crystals

Plate-like seed crystals were prepared by direct addition of 0.4 M sodium sulphate solution to 0.4 M calcium chloride solution. These reagents resulted in a highly supersaturated solution (0.2 M, supersaturation ratio of 10.86) of calcium and sulphate ions. Therefore, a short induction time and small volumes of reagents had to be used to produce a large amount of seed crystals. A 250 ml beaker was used as the reacting vessel and a magnetic stirrer at 500 rpm was used for mixing the reactants. Each batch of the 250 ml preparation was agitated for 1 minute and yielded 25 ml of crystals (0.5% by volume in the 5L desupersaturation reactor). These crystals were filtered and used in the desupersaturation reactor.

Dry samples of the seed crystals were ground and analysed by powder X-Ray Diffraction (Philips, model PW1050).

5.3.4 Responses and methods of analysis

The three responses that were measured were the time to reach equilibrium, % growth in the crystal size, and the crystal morphology.

5.3.4.1 Time to reach equilibrium

The conductivity meter provided an accurate and online measurement of the conductivity of the solution. When the conductivity meter readings were fully stabilised, the system reached equilibrium. Reaction between the calcium and sulphate ions to form solid gypsum caused a

decrease in the conductivity of the solution due to reduced ion concentration. The system volume and performance are affected when there is constant withdrawal of samples from the reactor. With online measurements the removal of samples is avoided.

5.3.4.2 Percentage crystal growth

The mean particle size of the initial seed crystals, denoted by $D[4,3]_{seeds}$ and the mean particle size of crystals withdrawn from the equilibrium solution, denoted by $D[4,3]_{crystals\ at\ equilibrium}$, were used to calculate the percentage crystal growth:

$$\%\ crystal\ growth = \frac{(D[4,3])_{crystals\ at\ equilibrium} - (D[4,3])_{seedcrystal}}{(D[4,3])_{seedcrystal}} * (100) \qquad (5\text{-}1)$$

An average of three readings taken from the Malvern mastersizer for each crystal sample was used for the mean particle size. Crystal samples were placed in an ultrasonic bath (EIA, model CP823) for 3-5 minutes at 25 °C at 90% power prior to size measurement to prevent particle agglomeration. Propanol was used as the medium as it acts as a good dispersant for gypsum particles. To minimise the amount of propanol, the 100 ml dispenser unit of the Malvern mastersizer was used.

5.3.4.3 Percentage edges detection

The crystal morphology was expressed as the % edges detected over the digital image of the crystal sample. A scanning electron microscope (analytical, model S4440) was used to acquire these digital images. Dry samples of the crystals were mounted on stubs with carbon glue and coated with gold palladium alloy. The images were taken at a magnification of 1000x. The digital images acquired were the input of the following script, which was executed on Matlab 6.5 with Image Processing Toolbox.

```
clear all
warning on
mix_raw = imread('c:|chrystal morphology|shilpa|14a_01.tif');
rows = 700;
cols = 1000;
picture1 = mix_raw(1:rows,1:cols);
edgepic = edge(picture1,'sobel',0.1);
figure(1), imshow(picture1)
figure(2), imshow(edgepic)
percentage_edge = sum(sum(edgepic))./(rows*cols).*100
```

The algorithm generated digital images of the edges detected in addition to the percentage edges detected. To record the error in measurement, 10 pictures of each sample were acquired and analysed by the image analysis and an average taken.

5.3.5 Hydrodynamic experiments

It was important to isolate mixing and reaction phenomena to determine the macromixing time scale of the 5L desupersaturation reactor. The reactor was initially filled with 5L of distilled water and the reactor lid was closed. The impeller was switched on at the required speed. 5 ml of 10 M sodium hydroxide solution was injected into the reactor at the sodium sulphate feed point location using a syringe and pH meter readings were taken every 10 seconds. The macromixing time was taken as the time at which the pH became steady. This procedure was repeated three times for different impeller speeds as listed in Table 5.8.

Table 5.8: Experiments for hydrodynamic studies

Experiment number	Impeller speed (rpm)
E1	300
E2	500
E3	700
E4	900
E5	1100

5.3.6 Modeling with OLI 1.2

OLI Systems Inc. (Stream Analyser 1.2) was used to model the gypsum precipitating system and investigate the effect of varying pH and sulphate to calcium ratios on the solubility of gypsum and for supersaturation ratio calculations.

6. Results and discussion

6.1 Seed material

6.1.1 Seed crystal size and morphology

Figures 6.1 and 6.2 show the images of needle-like and plate-like seed crystals obtained from scanning electron microscopy at a magnification of 1000x.

Figure 6.1: Needle-like seed crystals (scale-bar: 10 μm)

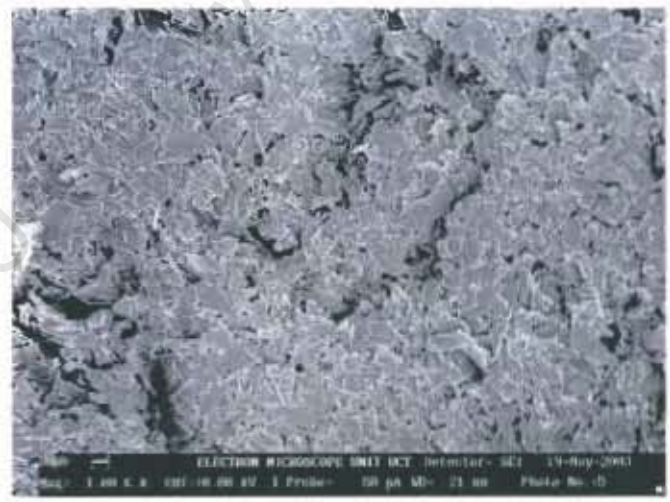

Figure 6.2: Plate-like seed crystals (scale-bar: 10 μm)

The needle-like seed crystals are significantly larger in size and have sharper edges when compared to the plate-like seed crystals. The average particle size of the needle-like seed crystals is above 100 μm while that of the plate-like seed crystals is approximately 25 μm. As the plate-like seed crystals are small, they can provide a large surface area to volume ratio for gypsum precipitation to take place. A closer inspection of the plate-like crystals at a

magnification of 2500x (Figure 6.3) reveals that the plate-like seed crystals have smoother edges.

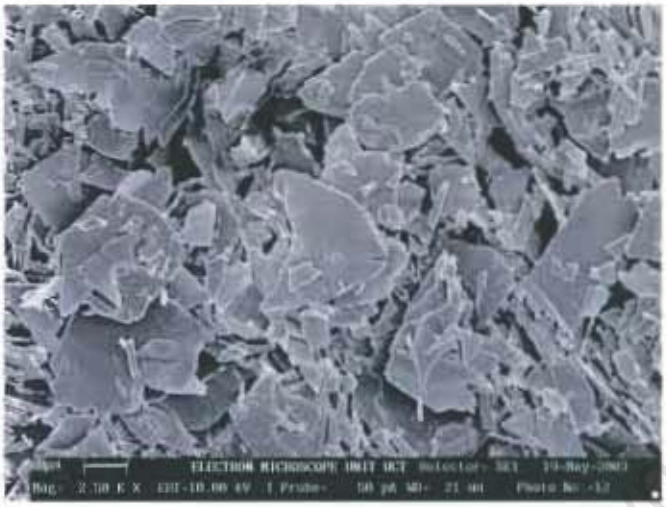

Figure 6.3: Plate-like seed crystals (scale-bar: 10 μm)

6.1.2 Quantifying gypsum crystal morphology

Figures 6.4 and 6.5 are the corresponding images of the edges detected for the Figures 6.1 and 6.2 using the edge detection technique (section 5.3.4.3). There are significantly more edges detected from the picture of the plate-like seed crystals as compared to that of the needle-like seed crystals. 30 pictures of needle-like and plate-like seed crystals were analysed using digital image processing and Figure 6.6 shows the corresponding percentage edges detected.

Figure 6.4: Edges detected for needle-like seed crystal image.

Figure 6.5: Edges detected for plate-like seed crystal image.

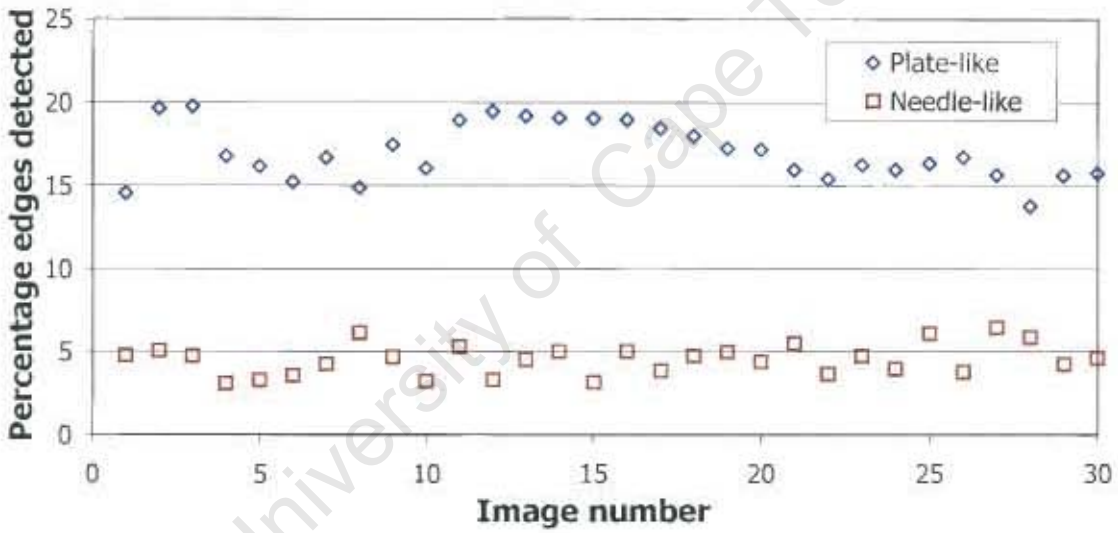

Figure 6.6: Graph of percentage edge detected for batches of seed crystals

From the numerical analysis, plate-like seed crystals yield a higher percentage of edges detected than the needle-like seed crystals. As it is desired to control the morphology of gypsum crystals to the plate-like crystals, the implication is that the number of edges should be maximised in the experiments B1-B12 and C1-C12. The average percentage edges detected for the 30 images of plate and needle-like crystals are 16.99 ± 1.68 and 4.53 ± 0.94 respectively. The percentage edges detected for the plate-like and needle-like crystals do not overlap and thus the two distinct morphologies have been classified and quantified appropriately.

The use of the edge detection technique has led to the following possibilities:

- A fast, relatively easy and automated technique to quantify gypsum crystal morphology
- A number of images can be analysed and errors associated with the quantifying technique can be easily obtained
- A reliable technique to classify and quantify the crystal morphology, which is an important response in this project. This gives way to the opportunity to relate this important response to the operating conditions of the reactor in a quantitative as opposed to a purely qualitative manner.

There has not been any precedent research, in literature, which involved the use of DIP in an attempt to quantify gypsum crystal morphology. The edge detection technique using the Sobel Edge operator thus provides a novel technique in this research.

6.1.3 XRD results

Figure 6.7 shows the result obtained from XRD powder analysis of the plate-like and needle-like crystals. These patterns match exactly that displayed by pure gypsum, confirming the composition of the needle and plate-like crystals.

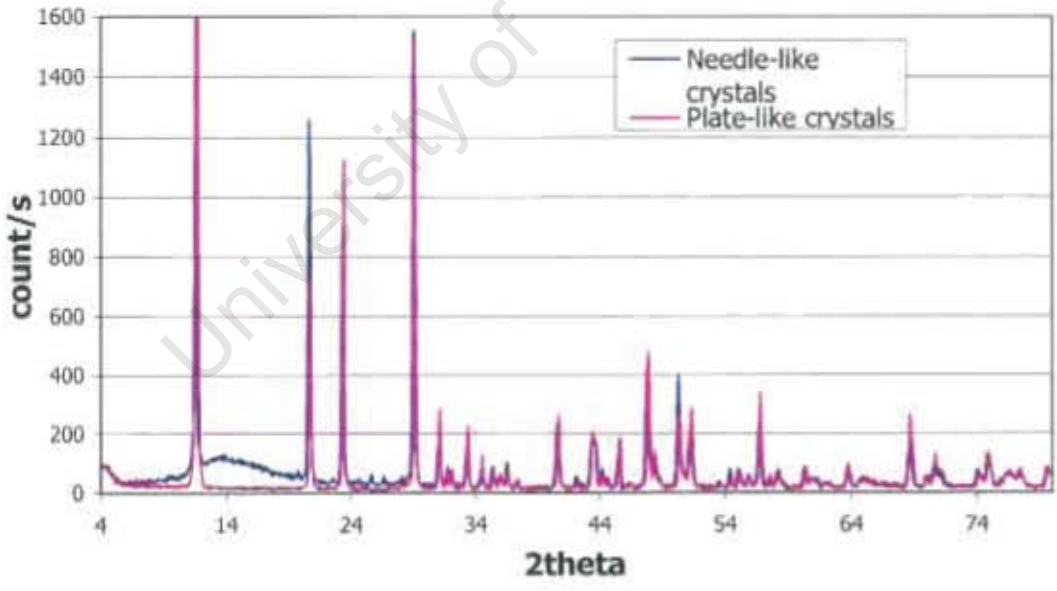

Figure 6.7: XRD results

6.2 Results database

The conductivity meter readings, the % crystal growth values, the SEM photos of gypsum crystals and the % edge detected for experiments A1-A12, B1-B12, C1-C8, and D1-D3 can

be found in appendices B, C and D and E respectively. Since the results are extensive, a few examples have been referenced in the following sections to highlight the key aspects of the results.

6.2.1 Conductivity meter readings

Figure 6.8 shows the graph of the conductivity meter readings obtained from experiment A6 in which the sulphate to calcium molar ratio was 1. When the sulphate and calcium ions react to form solid gypsum, the conductivity of the solution decreases. When the solubility limit of gypsum is reached, no more ions react and equilibrium is reached. For the experiment A6, the conductivity meter reading stabilised to a steady value of 9.86 mS/cm in 215 minutes.

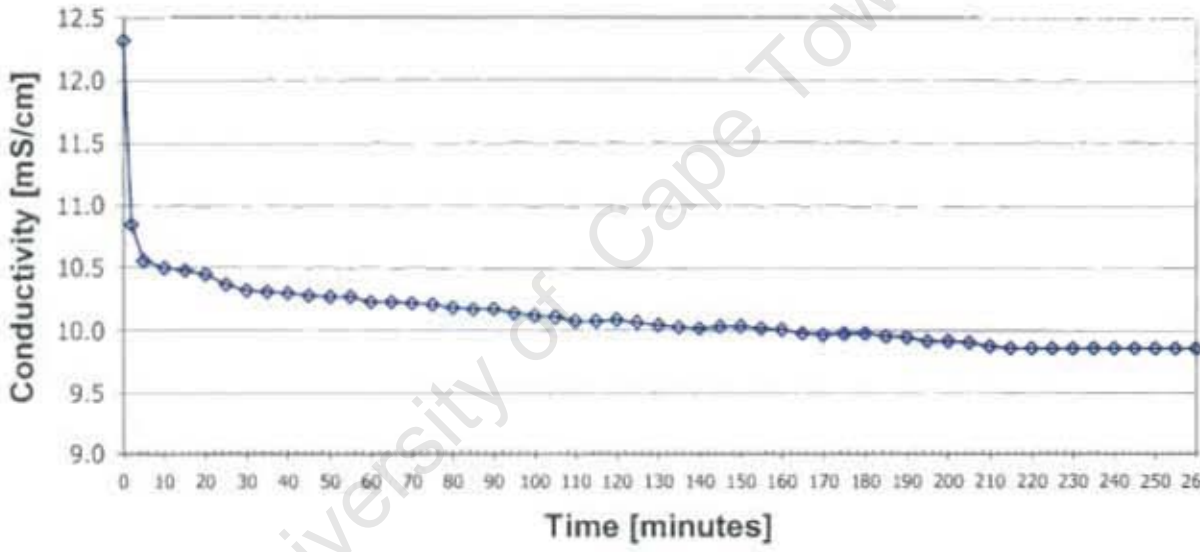

Figure 6.8: conductivity readings obtained from experiment A6

It was observed that when the sulphate to calcium ratio was higher than 1, the conductivity of the solutions initially increased for the time during which the sodium sulphate solution was pumped into the reactor and decreased after all the sodium sulphate had been transferred into the reactor. The initial increase in the conductivity meter readings suggests that the rate of addition of ions was higher than the reaction rate. Once all the sodium sulphate had been pumped into the reactor, the reaction of the ions was the only factor affecting the ion concentration and thus a decrease in the conductivity was observed until equilibrium was reached. Such a trend can be seen in Figure 6.9, the graph showing the conductivity meter readings obtained from experiment C1 where the sulphate to calcium ratio was 4.

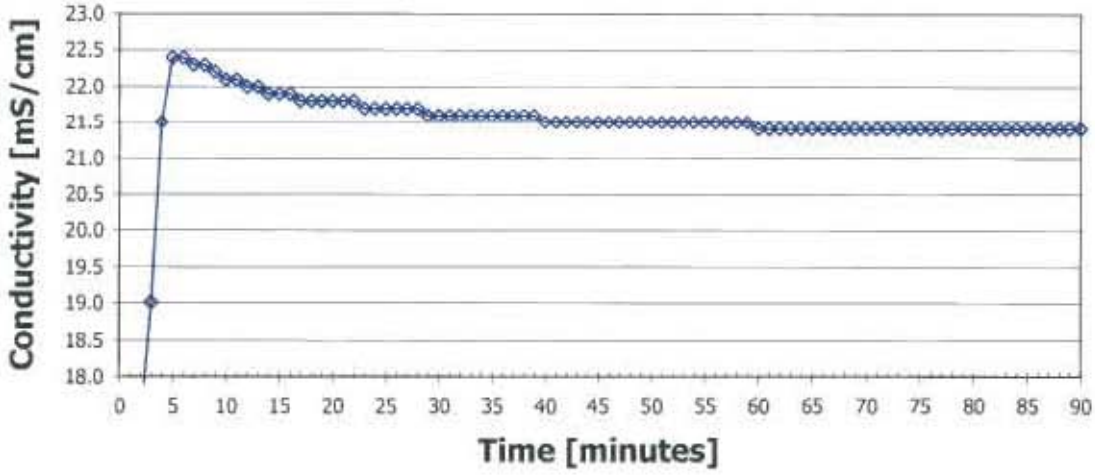

Figure 6.9: Conductivity readings obtained from experiment C1

6.2.2 Particle size distributions

Figure 6.10 shows the particle size distributions of the seed crystals and the crystals obtained from equilibrium solution in experiment B5. The mean particle size of the seed crystals in experiment B5 was 24.43 μm. After the experiment, the mean particle size of the gypsum crystals harvested from equilibrium solution was 28.94 μm. This increase in mean particle size distribution is represented by the shift of the particle size distributions in a left to right direction as shown in Figure 6.10. During the course of the experiment there was an increase of 18.05% in the mean particle size of crystals.

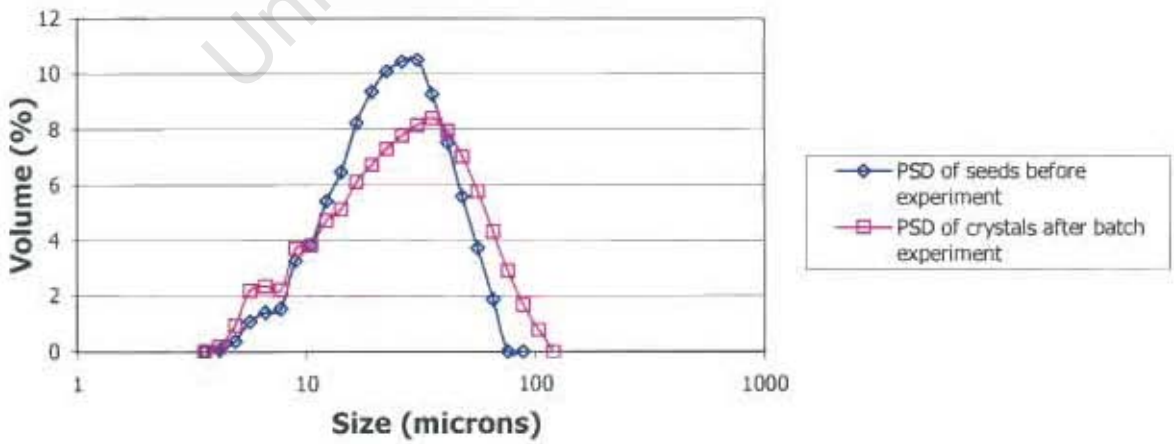

Figure 6.10: Particle size distributions obtained from experiment B5

The same trend was observed in all of the other experiments. An increase in particle size for all the experimental runs suggests that the gypsum formed from the reaction of sulphate

and calcium ions deposited on the seed crystals, causing them to grow. The positive percentage growth also suggests that there was no primary nucleation occurring. If primary nucleation were to occur, there would be primary and fine particles forming, causing the particle size distribution to shift to the left. The desupersaturation of the gypsum solution can be confidently attributed to a growth mechanism of the seed crystals. The reacting solutions were at a concentration of 0.03 M, which is a slightly supersaturated solution. According to the supersaturation theory, at this low supersaturation level, the primary nucleation rates are significantly lower than the growth rates (Sohnel and Garside, 1992).

These results confirm that seeding provides preferential sites for deposition of gypsum to take place. This is beneficial to the SPARRO process as blockages of membrane pores and scaling on equipment surfaces is highly undesirable. Operating conditions that would result in a minimum percentage crystal growth would be most desirable. As a seed crystal increases in size, the surface area to volume ratio available for precipitation decreases.

6.3 Results from system modeling (OLI Systems Inc., Stream Analyser v 1.2)

6.3.1 Effect of sulphate to calcium ratio

Figure 6.11 is a graph showing the effect of sulphate to calcium ratio on the solubility and supersaturation ratio of gypsum and obtained from OLI (version 1.2) modeling. The solubility of gypsum decreases when the sulphate to calcium increases from 1 to 4 and stabilises for sulphate to calcium ratios above 4. A decrease in the solubility will lead to an increase in the mass of gypsum precipitation from reagent solutions. Liu and Nancollas (1970) found that an excess of sulphate ions favoured the gypsum crystal growth. This was because the solubility decreased with an increase in the sulphate to calcium molar ratio.

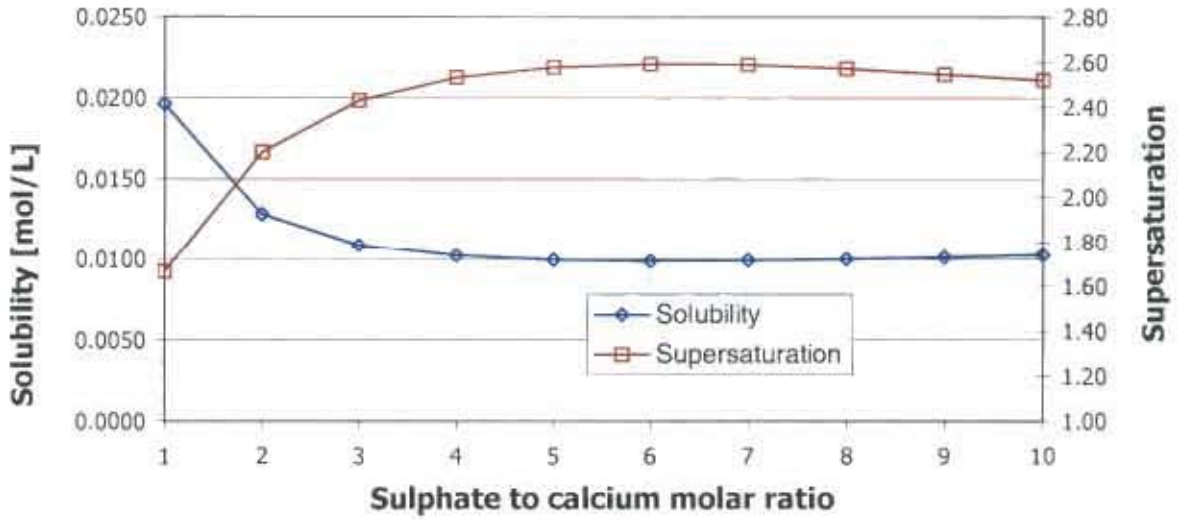

Figure 6.11: Effect of sulphate to calcium ratio on solubility limit of gypsum

As the solubility increases, the driving force of the precipitation reaction, the supersaturation ratio increases. In the experiments that were conducted the maximum supersaturation ratio reached was 2.6, which occurred at sulphate to calcium ion molar ratios of 6 and 7. An increase in the driving force for precipitation, can lead to faster gypsum precipitation kinetics. This was experimentally found by Zhang and Nancollas (1992).

6.3.2 Effect of pH

Figure 6.12 is the graph showing the effect of pH on the solubility of gypsum obtained from OLI (version 1.2) modeling. HCl and NaOH were used for the pH survey, as in the experiments. For a sulphate to calcium ratio of 1, the solubility decreases when pH is increased from 1 to 4. Between the pH 4 to 11, the solubility remains constant and for pH greater than 11 the solubility increases. The same trend is observed for the higher sulphate to calcium molar ratios of 4 and 7.

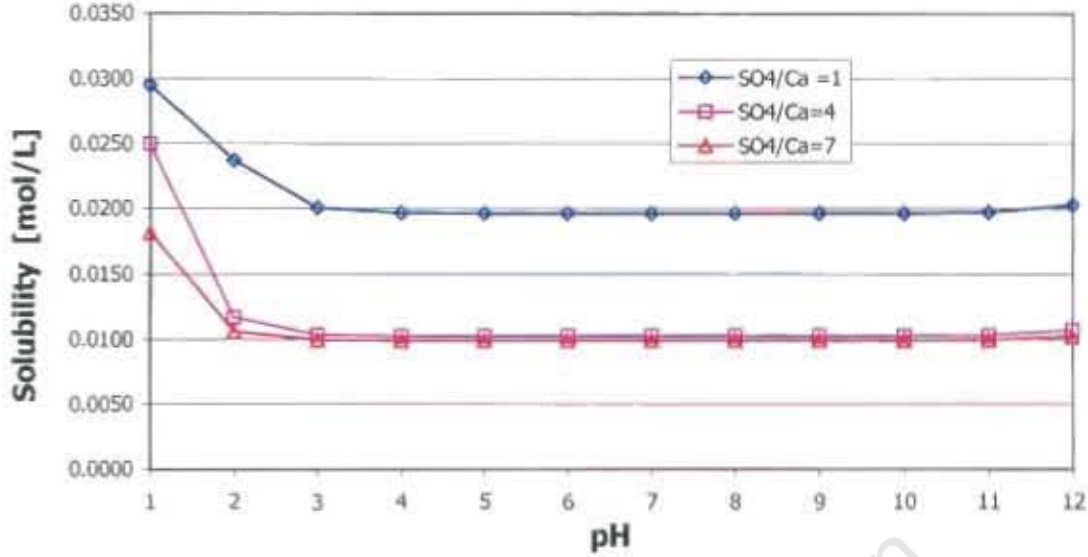

Figure 6.12: Effect of pH on the solubility of gypsum

The effect of pH on solubility can be explained by speciation of free sulphate and calcium ions. At low pH the concentration of H^+ ions is high and this favours the reaction 6-1 to proceed in the forward reaction.

$$H^+ + SO_4^{2-} \leftrightarrow HSO_4^- \qquad (6\text{-}1)$$

At low pH (1-4), the concentration of HSO_4^- is thus high, as shown in Figure 6.13. The more the reaction 6-1 is favoured, the lower is the concentration of free sulphate ions as more sulphate ions are consumed.

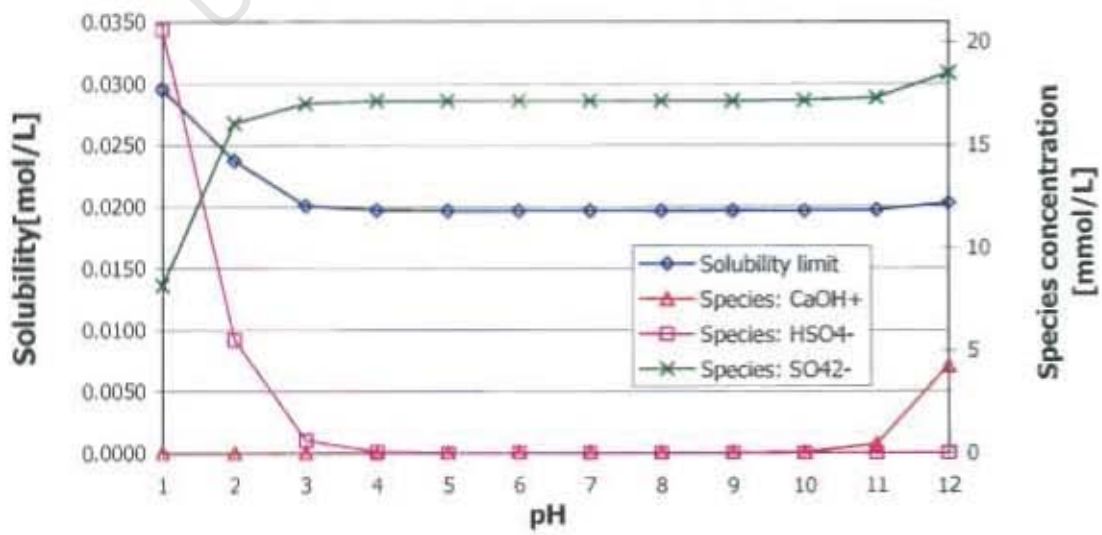

Figure 6.13: Effect of pH on speciation

At high pH the concentration of OH^- ions is high and this favours the reaction 6-2 to proceed in the forward direction.

$$OH^- + Ca^{2+} \leftrightarrow CaOH^+ \quad (6\text{-}2)$$

At high pH (10-12), the concentration of $CaOH^+$ is thus high, as shown in Figure 6.13. $CaOH^+$ reduces the free Ca^{2+} ions, which will increase the solubility resulting in more free sulphate ions remaining in solution.

Liu and Nancollas (1970) found that changing the pH of the gypsum solution between 7.6 and 11.6 did not have major influence on the gypsum crystal growth. Their result is valid because for the range of pH they investigated, there is no significant variation in the solubility limit of gypsum.

6.4 Effect of initial seed morphology

6.4.1 Effect of initial seed morphology on gypsum kinetics

Conductivity meter readings obtained from experiments A11 and B11 are compared in Figure 6.14. In both the runs the process parameters were the same but needle-like and plate-like seed crystals were used in experiment A11 and B11 respectively. Equilibrium was reached in 185 minutes when plate like seed crystals were used compared to 275 minutes when needle-like seed crystals were used. The kinetics of gypsum precipitation were much faster when plate-like seed crystals were used because the plate-like seed crystals provided larger specific surface area for deposition compared to the needle-like seed crystals.

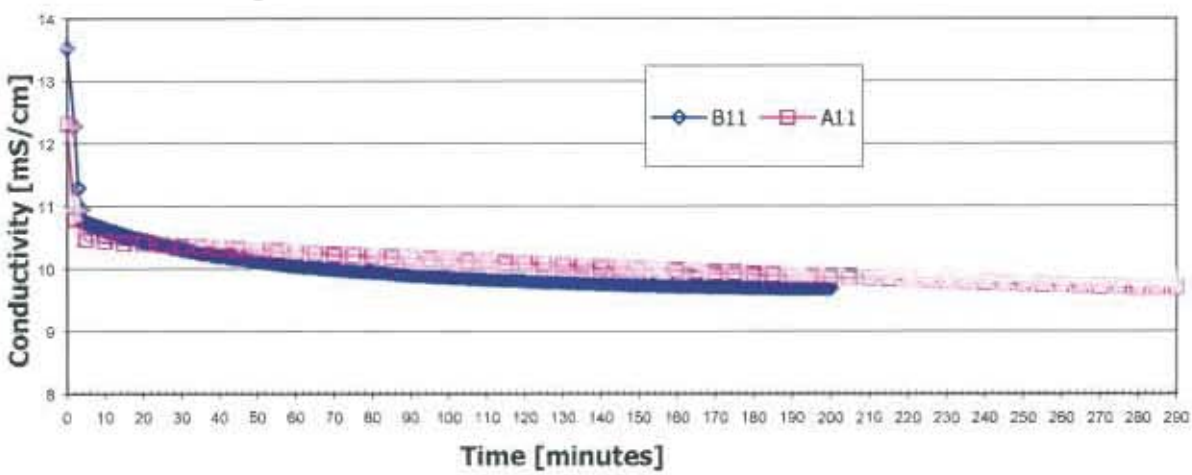

Figure 6.14: Conductivity meter readings obtained from experiments A11 and B11

6.4.2 Control of gypsum morphology by appropriate seeding technique

The initial morphology of the seed crystals affects the final morphology of the gypsum crystals after the precipitation reaction. Figures 6.15 and 6.16 show the images of gypsum crystals harvested from equilibrium solutions of experiments A1 and B1 respectively, obtained by scanning electron microscopy at a magnification of 1000x. The operating conditions in experiments A1 and B1 were identical. The only difference was the use of different seed crystal morphology. In experiment A1 needle-like seed crystals were used and in experiment B1 plate-like seed crystals were used.

Figure 6.15: Crystals from experiment A1 (scale-bar: 20 μm)

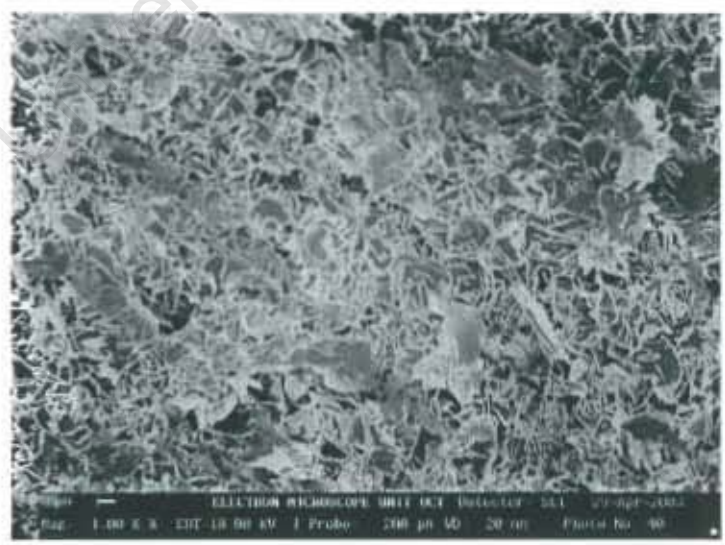

Figure 6.16: Crystals from experiment B1 (scale-bar: 10 μm)

Visual analysis of the Figures 6.15 and 6.16 illustrates that the initial morphology of the seed crystals influences the final crystal morphology. Under normal circumstances, in the absence

of seeds, a solution of a concentration of 0.03 M of sulphate and calcium ions will produce gypsum crystals of the needle-morphology. From Figures 6.15 and 6.16 it is evident that the final crystal morphology can be controlled by the addition of the appropriate seed crystals, namely, needle-like and plate-like seed crystals. In addition to the control of the gypsum crystals to plate-like morphology, through the addition of plate-like seed crystals, it can be observed that there are no needle-like crystals visible in Figure 6.13. The gypsum from the solution precipitates on the seed crystals, maintaining the morphology of the seed crystals used.

The picture from Figure 6.12 yielded a low percentage edge detected of 4.75 ± 1.02. The picture from Figure 6.13 generated a higher percentage edge detected of 15.16 ± 2.06. This quantitative analysis also shows that the final crystal morphology remains similar to that of the seed crystals used in the process.

Based on the comparison of results presented above, the choice of an appropriate seed crystal has implications for the kinetics of gypsum precipitation and the final morphology of the crystals. When Juby (1994) developed the SPARRO process, insufficient emphasis was put on the size and morphology of the seed crystals. An analysis of the seed particles showed that on average the particles were of similar shape and dimensions, roughly 100 μm in length and 20 μm wide. This description clearly fits the features of needle-like crystals. There was a lack of understanding of the precipitation aspect of gypsum. With precipitation occurring in the desupersaturation reactor, the needle-like morphology would have been maintained. Also, the use of needle-like seed crystals would have slowed the gypsum precipitation due to their lower specific surface area relative to plate-like crystals.

6.5 Effect of seed quantity

6.5.1 Effect of seed quantity on kinetics

Figure 6.17 shows the conductivity meter readings from experiments D1-D3. Different seed quantities were used in the experiments, while keeping the other factors constant. Seed quantity significantly affected the kinetics of gypsum precipitation in the desupersaturation reactor. Equilibrium was achieved in 152, 65 and 48 minutes in experiments D1, D2 and D3 respectively. The concentration of seed material in the system directly affects the total

surface area for precipitation to occur. The higher the amount of seed crystals the faster the kinetics of precipitation. Seeded precipitation of gypsum is thus surface controlled.

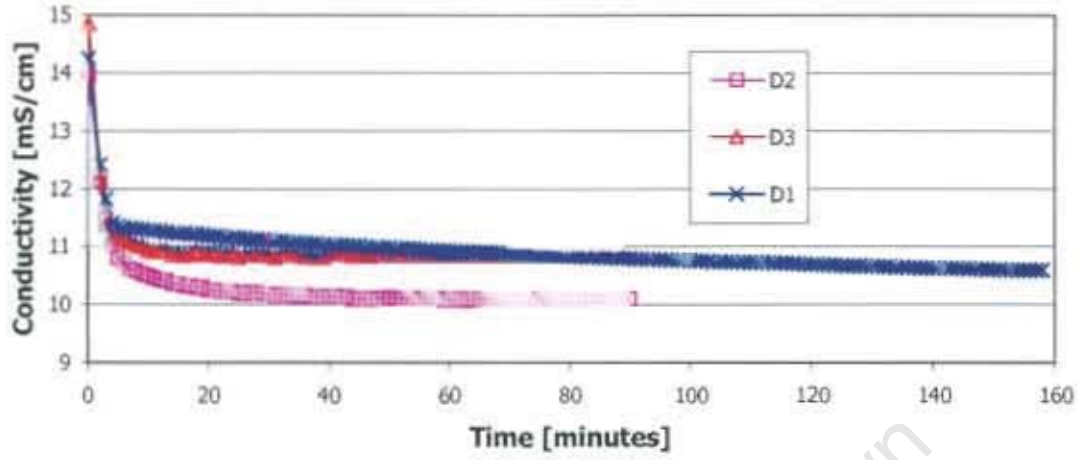

Figure 6.17: Conductivity meter readings from experiments D1-D3

To compare the rates quantitatively, equation 2-9 is modified to equation 6-3. This modification is relevant to the experiments carried out, where there were no varying concentrations of spectator ions (such as magnesium, magnesium and aluminium) which could affect the conductivity of the solution. The following considerations have been taken into account:

- Conductivity is a direct measure of concentration, so the concentration terms in equation 2-9 have been replaced with conductivity terms
- In the experiments D1-D3, the conductivity meter reading reflected the total ion concentration and not that of calcium or sulphate ions individually. Thus, the concentration terms of ion A have been replaced with conductivity of the total ions present in the system.

$$-\frac{d\kappa}{dt} = P'\left(\kappa - \kappa^*\right)^n \qquad (6\text{-}3)$$

Where,

κ is the conductivity of the total ions present in the solution at time t

κ^* is the conductivity of the total ions present in the solution at equilibrium conditions

P' is a kinetic rate constant [cm(mS min)$^{-1}$ if n=2]

n is the order of the growth

If n=2, then:

$$-\frac{d\kappa}{dt} = P'\left(\kappa - \kappa^*\right)^2 \qquad (6\text{-}4)$$

Linearising equation 6-2 and integrating:

$$-\int_{\kappa_0}^{\kappa} \frac{d\kappa}{\left(\kappa-\kappa^*\right)^2} = \int_0^t P' dt \tag{6-5}$$

$$\frac{1}{\left(\kappa-\kappa^*\right)} = P' t + \frac{1}{\left(\kappa_0-\kappa^*\right)} \tag{6-6}$$

A graph of $\frac{1}{\left(\kappa-\kappa^*\right)}$ versus t will have a slope of P'. Figure 6.18 shows the corresponding plots from experiments D1, D2 and D3. Table 6.1 gives the values of the rate constants obtained graphically.

Table 6.1: Rate constants obtained from experiments D1-D3

Experiment	Seed quantity [volume %]	Rate constant, P' [cm(mS min)$^{-1}$]
D1	1	0.039
D2	4	0.273
D3	7	0.704

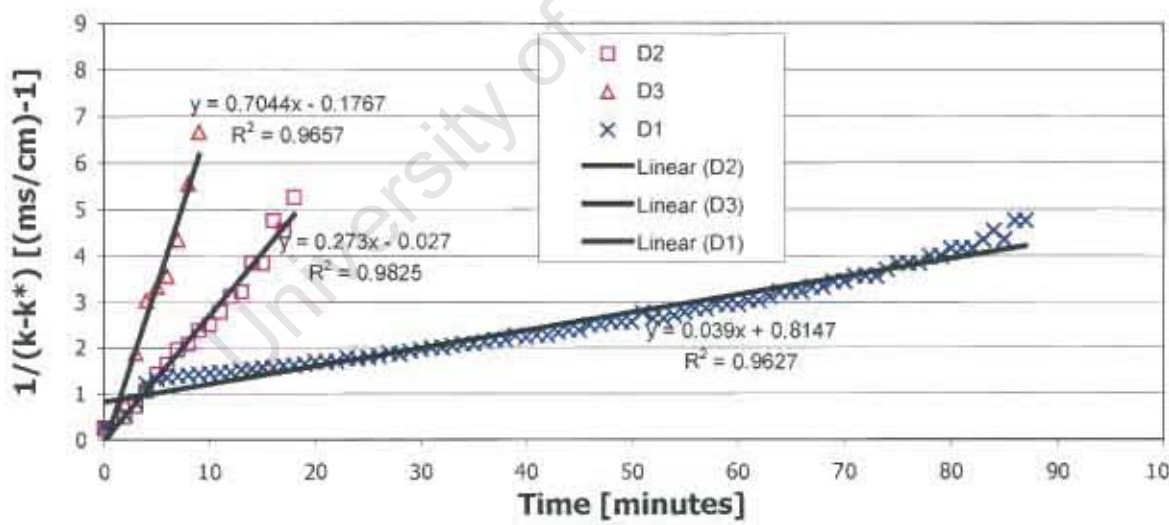

Figure 6.18: Determination of rate constants for experiments D1-D3

The straight-line graphs show that the precipitation of gypsum follows a second order growth process as described by equation 6-3. A second order growth process for gypsum was also experimentally determined by Liu and Nancollas (1970, 1973 and 1975), Christoffersen *et al.* (1982), Nancollas *et al.* (1973), Brandse et al. (1977) and Çetin *et al.* (2001).

From Table 6.1 it can be seen that the gypsum precipitation kinetics are directly related to the seed quantity present in the reactor, thus the surface area available. The higher the concentration of seed crystals in the reactor, the higher the growth rate constants. This result is consistent with the results obtained by Liu and Nancollas (1970), who found that the growth rate constant increased with an increase in the number of seed crystals and hence the number of active growth sites available.

The influence of the seed quantity on the crystal growth rate confirms the fact that seeded precipitation is surface controlled. Liu and Nancollas (1970) and Nancollas *et al.* (1973) also found that gypsum precipitation is surface controlled.

6.5.2 Effect of seed quantity on crystal morphology

Figures 6.19 - 6.22 show that the seed quantity greatly influences the degree of control of morphology of the gypsum crystals. Table 6.2 gives the percentage edges detected for each crystal sample obtained from the experiments under analysis.

Table 6.2: Effect of seed quantity on the final crystal morphology

Experiment	Seed quantity [volume %]	% Edge detected
B8	1	8.12 ± 1.97
B3	4	10.50 ± 1.07
B1	7	15.16 ± 2.06
C2	10	16.83 ± 0.98

These results illustrate that the seed quantity plays a major role in the control of the morphology of the gypsum crystals. The more seed crystals present, the less the growth per seed crystal. These results can be supported by mass balance. Table 6.3 gives the mass of gypsum precipitated from solution at different sulphate to calcium ion molar ratios that have been obtained from system modeling (OLI Stream analyzer v1.2). The mass of gypsum precipitated has been compared to the mass of the gypsum seed crystals (for different % by volume of seed crystals) added to the reactor.

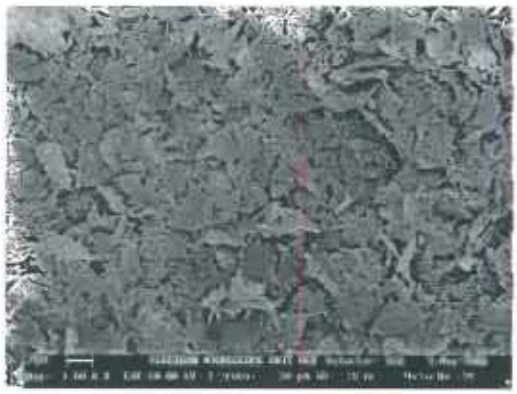

Figure 6 19: Crystals from experiment B8

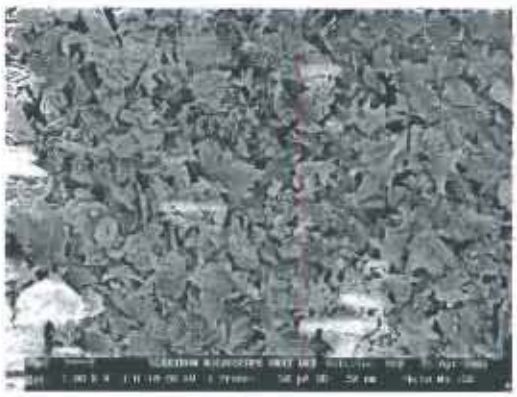

Figure 6.20: Crystals from experiment B3

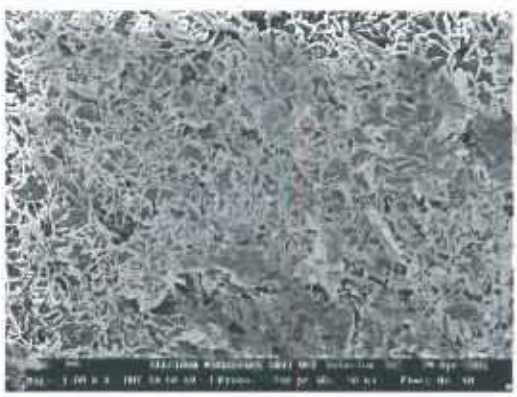

Figure 6.21: Crystals from experiment B1

Figure 6.22: Crystals from experiment C2

Increase in seed quantity

Increase in % edge detected

Enhanced control of plate-like morphology

Table 6.3: Comparison of mass of gypsum precipitated out of solution and mass of seed crystals

		1% by volume of seed crystals	4% by volume of seed crystals	7% by volume of seed crystals
Sulphate to calcium molar ratio	Mass of gypsum precipitated [g]	Mass of gypsum precipitated/Mass of seed crystals [%]	Mass of gypsum precipitated/Mass of seed crystals [%]	Mass of gypsum precipitated/Mass of seed crystals [%]
1	7.90	30.76	7.83	4.66
2	13.72	53.42	13.61	8.10
3	15.39	59.92	15.26	9.09
4	16.00	62.29	15.87	9.45
5	16.25	63.25	16.11	9.59
6	16.32	63.52	16.18	9.63
7	16.30	63.46	16.16	9.62
8	16.23	63.19	16.09	9.58
9	16.13	62.80	16.00	9.52
10	16	62.29	15.87	9.45

It can be seen that as the amount of seed crystals was increased, the ratio of mass of gypsum precipitated to mass of the seed crystals decreased. The percentage crystal growth calculations from the experiments were close to the ratio of mass of gypsum precipitated to the mass of the seed crystals added. In experiments B2, B4, B6 and B11 (where 1% by volume of seed crystals was used), the percentage growth in crystals was 40.03, 39.07, 47.8, and 68.2 % respectively. In experiments B3, B5, B7 and B10 (where 4% by volume of seed crystals were used), the percentage growth in crystal was 20.61, 17.73, 22.02 and 26.15 % respectively. In experiments B1, B8, B9 and B12 (where 7% by volume of seed crystals were used), the percentage growth in crystal was 11.33, 14.76, 13.27 and 18.77 % respectively. These analyses show that as the amount of seed crystals added to the reactor is increased, the percentage crystal growth decreases. Crystal growth takes place without change of the morphology of the plate like seed crystals. Low seed quantity corresponds to the largest percentage crystal growth.

In previous studies of the SPARRO process, only 1.76% of seed crystals were added to the reactor (Juby, 1994). This amount of seed crystals would cause preferential precipitation of gypsum from solution onto the seeds, however, the control of the gypsum morphology would be poor.

6.6 Effect of mixing

6.6.1 Macromixing time

Figure 6.23 shows the results obtained from the experiments E1-E5.

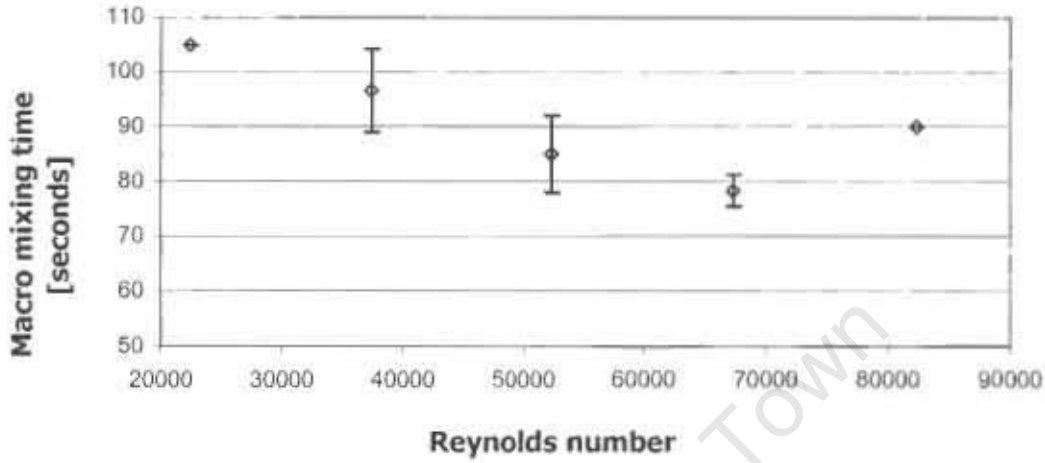

Figure 6.23: Macromixing time scale results from experiments E1-E5

Table 6.4 gives the values of the Reynolds number at the different impeller speeds used. The Reynolds numbers obtained suggest that at all the values of impeller speeds the operating conditions were turbulent. From Figure 6.23 it can be seen that with an increase in the Reynolds number from 2.2×10^4 (300 rpm) to 6.7×10^4 (900 rpm) the macromixing time decreased from 105 to 78 seconds. This is because as the Reynolds number increased, the turbulence in the reactor contents increased, circulation rate of bulk contents increased, thus the macromixing time decreased. Beyond the Reynolds number 6.7×10^4 (900 rpm), the macromixing time increased. This increase could have been the result of excessive turbulent conditions within the reactor. Entrainment of air into the reactor was observed at Reynolds number 8.2×10^4 (1100 rpm). The air bubbles, which got entrained in the reactor, could have interfered with the pH probe readings.

The experimentally recorded macromixing times were however much larger than theoretical ones (calculated using equation 2-17) as given in Table 6.4. The difference in the macromixing times can be explained by time delays such as the pH probe response time as well as the position of the pH probe and the point of injection of the sodium hydroxide into the reactor.

Table 6.4: Reynolds number, experimental and theoretical macromixing times at different impeller speeds

Impeller Speed [rpm]	Reynolds number	Experimental macromixing time [sec]	Theoretical macromixing time [sec]
300	22445	105	6.85
500	37408	96.7 ± 7.6	4.11
700	52372	85.0 ± 7.1	2.94
900	67335	78.3 ± 2.9	2.28
1100	82299	90	1.87

During the experimental runs it was visually observed that for all the experiments good solid/liquid suspension was achieved and satisfactory down-pumping motion was created.

6.6.2 Comparison of macro and micromixing time

Table 6.5 gives the values of the Reynolds number, micromixing and macromixing times for experiments C5, B3 and C6. Results from experiments C5, B3 and C6 have been used because in those experiments the seed quantity, pH and sulphate to calcium molar ratio were constant at 4% by volume, 7 and 4 respectively. The only factor varied in those experiments was the impeller speed. Equations 2-17 and 2-24 were used to calculate the macro and micromixing times respectively.

Table 6.5: Reynolds number and mixing times for experiments C5, B3 and C6

Experiment	Impeller speed [rpm]	Reynolds number	Macromixing time [seconds]	Micromixing time [seconds]
C5	300	22445	6.85	0.044
B3	500	37408	4.11	0.020
C6	900	67335	2.28	0.0084

Micromixing occurred significantly faster than macromixing at the different Reynolds number occurring in experiment C5, B3 and C6. Equilibrium was reached in 21, 18 and 16 minutes in experiments C5, B3 and C6 respectively. In these cases the micromixing times were significantly smaller than the reaction times. According to Sohnel and Garside (1992), since the micromixing time was much smaller than the reaction time, the reaction kinetics controlled the process, the reactor was essentially homogeneous and the reaction took place throughout the vessel.

6.6.3 *Effect of Reynolds number on gypsum precipitation*

As with all other precipitation processes, it is crucial to determine the controlling mixing factor in the gypsum precipitation process. This can be useful when considering a scale-up of the desupersaturation reactor. To do so, the effects of macro and micromixing times on the system responses in experiments C5, B3 and C6 have been compared. Figure 6.24 shows the effect of Reynolds number on the time for the gypsum solution to reach equilibrium and the percentage crystal growth. With an increase in the impeller speed, there was a decrease in both the time to reach equilibrium and percentage crystal growth.

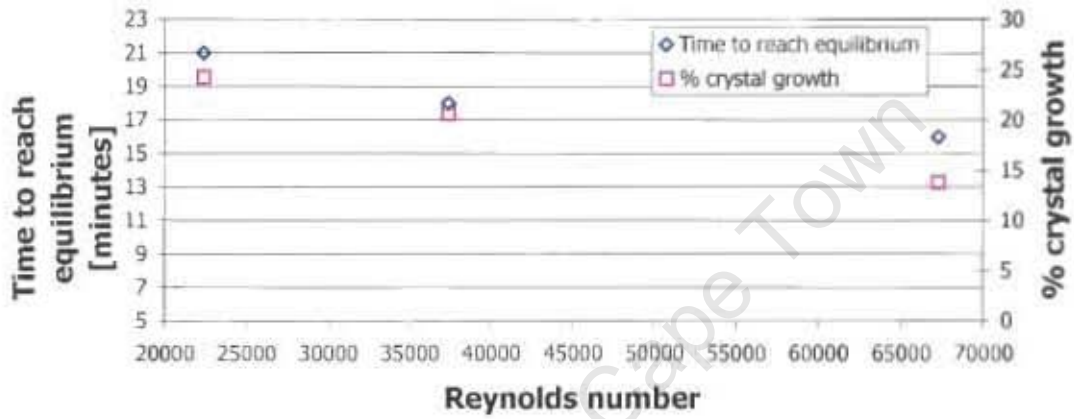

Figure 6.24: Effect of mixing on time to reach equilibrium and % crystal growth

These results can be discussed according to two arguments:

The first argument is that there are to two zones that can be present in the stirred tank reactor (Pohorecki and Baldyga, 1988 and Chen *et al.*, 1996):

Zone 1: regions in the reactor where high supersaturation prevails

Zone 2: regions in the reactor where low supersaturation prevails

Regions described by zone 1 are a result of micromixing and lead to high nucleation rates. Regions described by zone 2 dilute any supersaturation in the bulk regions of the reactor and as a result, crystals growth overtakes nucleation. In the experimental results, an increase in impeller speed reduced the crystal growth. This suggests that with an increase in impeller speed, the area of influence of zone 1 increases (Pohorecki and Baldyga, 1988 and Chen *et al.*, 1996). The reaction spreads in regions of zone 1. With higher supersaturation prevailing, the driving force for precipitation increases and equilibrium is reached faster. Also, with higher supersaturation profiles, primary nuclei are formed, which reduces the percentage crystal growth.

It should be questioned whether the model of the reactor presented by Chen *et al.* (1996) and Baldyga and Pohorecki (1988) can be applied to this case of gypsum precipitation. The following are key differences between the system studied by Pohorecki and Baldyga (1988) and Chen *et al.* (1996) and the system investigated in this research project:

- $BaSO_4$ was the precipitated product, which Pohorecki and Baldyga (1988) and Chen *et al.* (1996) studied. In this project gypsum is under investigation. The solubility product of $BaSO_4$ and gypsum are 1.1 E-10 and 2.4 E-5 respectively. This means that at the same concentration, the supersaturation of $BaSO_4$ would be significantly higher than that of gypsum
- Pohorecki and Baldyga (1988) and Chen *et al.* (1996) studied the spontaneous precipitation of $BaSO_4$. In the case with the system under investigation, seeding was used. Seeding preferentially induces precipitation by crystal growth (Bremere *et al.*, 1999).

Over and above the differences presented above, there following are points that provide evidence that nucleation was unimportant in the gypsum seeded system that was studied and that growth of seed crystals was the mechanism by which solutions precipitated:

- Nucleation processes in gypsum seeded precipitation were found to be unimportant by Christoffersent *et al.*, 1982. They investigated gypsum precipitation from solutions at supersaturation ratios of 1.03 to 2. In the current system, the maximum supersaturation ratio was 2.6.
- There exists a critical supersaturation ratio of 4, below which nucleation is significantly slow (Mullin, 2001). The system under investigation was studied under the critical supersaturation ratio.
- The mass of gypsum precipitated from solution in the experiments compared to the mass of the seed crystals corresponded to the percentage growth of crystals calculated.

The second argument is particle attrition. As the Reynolds number increased in experiments C5, B3 and C6, particle attrition could have occurred. This could have increased the number of particles as well as increasing the available surface area, therefore reducing the time to equilibrium, assuming a growth dominated system.

Weighing the arguments presented in an attempt to explain the effect of mixing suggests that there is more evidence that nucleation was not the cause of decrease in percentage crystal growth and time to reach equilibrium in experiments C5, B3 and C6. However, it cannot be confirmed that no nucleation was occurring. This presents a gap in this research and further work involving crystal number counting can be carried out. In order to prove the shear argument, further experiments can be carried out. These can involve investigating the effect of Reynolds number on the particle size of gypsum seed crystals. These experiments should be carried out in a saturated solution of gypsum to prevent crystal growth and to allow independent study of the influence of shear rate.

6.7 Statistical analysis of the experimental results

The aims of the statistical analysis of the experimental data were:

- To identify the factors that have the greatest impact on seeded gypsum precipitation,
- To locate the ideal operating conditions for the desupersaturation reactor.

The results database was analysed by the STATISTICA software package. Section 6.7.1 gives the first order models fitted for the responses when needle-like and plate seed crystals were used (experiments A1-A12 and B1-B12). Section 6.7.2 gives the second order models fitted for the responses when plate-like seed crystals were used (experiments C1-C8). Tables 6.6 and 6.7 show the notations and units of the responses and factors used in the models.

Table 6.6: Notations and units of responses used in models

Response	Notation	Unit
Time to reach equilibrium	T	Minutes
Percentage crystal growth	% growth	-
Percentage edge detected	% edge	-

Table 6.7: Notations and units of factors used in the models

Factor	Notation	Unit
Seed quantity	SQ	% volume
pH	pH	-
Stirrer speed	N	rpm
Sulphate to calcium ratio	SCR	-

6.7.1 First order models

Appendix F and G give the outputs obtained from the statistical analysis of results obtained from experiments A1-A12 and B1-B12 respectively.

6.7.1.1 Effect of process parameters on time to reach equilibrium

The effects of the process parameters on the time to reach equilibrium using needle-like and plate-like seed crystals are given by the best-fit models in Tables 6.8 and 6.9 respectively. The standard errors (SE) and the p-values are also given.

Table 6.8: 1st order model for time to reach equilibrium using needle-like seed crystals

T =	286.6250	-25.1667(SQ)	-0.66667(pH)	-0.06125(N)	-14.4167(SCR)
SE	64.33	5.38	5.38	0.08	5.38
P-values	0.0030	0.0023	0.90	0.47	0.031

Table 6.9: 1st order model time to reach equilibrium using plate-like seed crystals

T =	179.3750	-13.9167(SQ)	-1.0833(pH)	-0.03125(N)	-12.250(SCR)
SE	53.76	4.49	4.49	0.067	4.49
P-values	0.013	0.017	0.82	0.66	0.029

The models in Tables 6.8 and 6.9 account for 80.9% and 71.2 % of the variation in the time to reach equilibrium respectively. The p-values identify seed quantity and sulphate to calcium ratio as the most significant factors affecting the time required to reach equilibrium in both of the first order models.

6.7.1.2 Effect of process parameters on percentage crystal growth

The effects of the process parameters on the percentage crystal growth using needle-like and plate-like seed crystals are given by the best-fit models presented in Tables 6.10 and 6.11 respectively.

Table 6.10: 1st order model for % crystal growth using needle-like seed crystals

% growth =	38.0990	-6.3871(SQ)	-1.04958(pH)	-0.01497(N)	-1.46542(SCR)
SE	13.55	1.13	1.13	0.02	1.13
P-values	0.0261	0.0008	0.3849	0.41	0.24

Table 6.11: 1st order model % crystal growth using plate-like seed crystals

% growth =	72.1827	−5.7071(SQ)	−1.0579(pH)	−0.012056(N)	−1.9096(SQR)
SE	11.87	0.99	0.99	0.015	0.096
P-values	0.0005	0.0007	0.3215	0.4443	0.096

The models in Tables 6.10 and 6.11 account for 83.4 % and 84.7 % of the variation in the percentage crystal growth respectively. Seed quantity is the most significant factor affecting percentage crystal growth in both the models as can be seen by the corresponding p-values.

6.7.1.3 Effect of process parameters on gypsum crystal morphology

The effects of the process parameters on gypsum crystal morphology as measured by % edges detected using needle-like and plate-like seed crystals are given by the best-fit models presented in Tables 6.12 and 6.13 respectively.

Table 6.12: 1st order model for % edges detected using needle-like seed crystals

% edge =	2.99750	+ 0.11750(SQ)	− 0.00250(pH)	− 0.00390(N)	− 0.26500(SCR)
SE	13.55	1.13	1.13	0.02	1.13
P-values	0.0261	0.0008	0.3849	0.41	0.24

Table 6.13: 1st order model for % edges detected using plate-like seed crystals

% edge =	6.5388	+ 0.43750(SQ)	+ 0.04417(pH)	− 0.000538(N)	+ 0.4741(SCR)
SE	2.52	0.21	0.21	0.0032	0.21
P-values	0.036	0.077	0.84	0.87	0.06

The models in Tables 6.12 and 6.13 accounts for 64.7 % and 57.4% of the variation in the % edges detected respectively. The p-values show that seed quantity has the greatest influence on the % edges detected in both the models.

The R^2 values for all the first order models were relatively low. These gave grounds to fit second order models using plate-like seed crystals. The analysis of variance indicated that the responses of time to reach equilibrium, percentage growth and percentage edge detected were curvilinear within the experimental region. This meant that second order models could be fitted and the critical region where a minimum, maximum or saddle point occurred could be located.

6.7.1.4 Comparison of first order models using needle and plate-like crystals

A test was carried out to find whether a single first order model is appropriate for both needles and plate-like seed crystals (appendix I). The discrete factors (plate-like and needle-like seed crystals) were included in the model and given values 0 and 1 respectively. From the analyses of variances for each of the response variables, it was evident that different models needed to be fitted for plate and needle-like seed crystals. The p-values for the t-statistics were all less than 0.05, confirming that the responses obtained using plate and needle-like seed crystals were significantly different. These results consolidate the discussion in section 6.4. The seed crystal morphology affects both the kinetics of gypsum precipitation and the final crystal morphology. Kinetics are faster when plate-like seed crystals are used because they provide a larger surface area for gypsum precipitation as compared to when the needle-like seed crystals are used. Maintenance of the plate-like morphology is possible by seeding with plate-like seed crystals.

6.7.2 Second order models for plate-like seed crystals

Appendix H gives the output obtained from the statistical analysis of the results collected from central composite experiments, B1-B12 and C1-C8.

6.7.2.1 Second order model for time to reach equilibrium

Table 6.14 summarises the second order model fitted to the response of time to reach equilibrium.

Table 6.14: 2nd order model for T using plate-like seed crystals

Parameter	Parameter estimate	Standard error	p-value
Intercept	331.573820	31.934095	0
SQ	-47.375184	5.627490	0
SCR	-39.026347	3.635723	0
pH	-8.824160	4.503383	0.0857
N	-0.202148	0.085261	0.0452
$(SQ)^2$	2.218246	0.324207	0.0001
(SQ)(SCR)	2.388889	0.418687	0.0005
$(SCR)^2$	2.101967	0.324207	0.0002
(SQ)(pH)	0.666667	0.418687	0.15
$(pH)^2$	0.414628	0.324207	0.2368
(SQ)(N)	0.003333	0.006280	0.61
$(N)^2$	0.000152	0.000072947	0.0707

This best-fit model accounts for 97.84 % of the variation in the time to reach equilibrium. The critical point is a minimum, which occurs at a seed quantity of 6.33% by volume, a sulphate to calcium ratio of 5.68, a pH of 5.54 and a Reynolds number of 4.5×10^4 (595 rpm). According to the model, at the critical point, it takes −14 minutes for the reacting gypsum system to reach equilibrium. Even though this result is physically impossible, the model provides the operating region at which the time to reach equilibrium can be minimised. The seed quantity and sulphate to calcium ratios are the most significant contributors in the second order model. Keeping the least significant factors, pH and impeller speed, constant at 7 and 500 rpm (Reynolds number of 3.7×10^4), Figure 6.25 shows the 3-d surface of the model. The corresponding contour plot is shown in Figure 6.26 and the corresponding response values are shown on the contours.

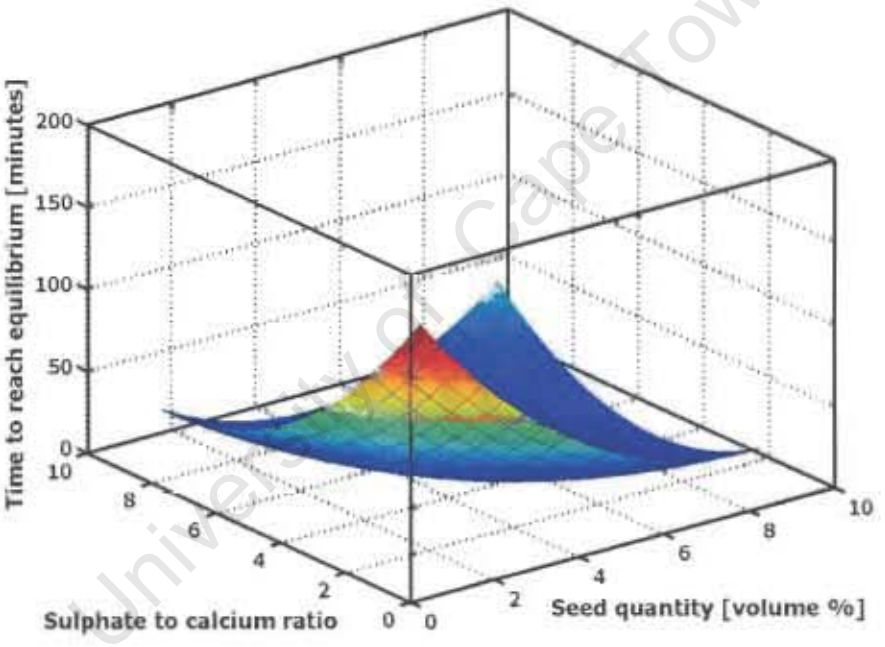

Figure 6.25: 3-D surface plot for time to reach equilibrium, factors pH and N constant

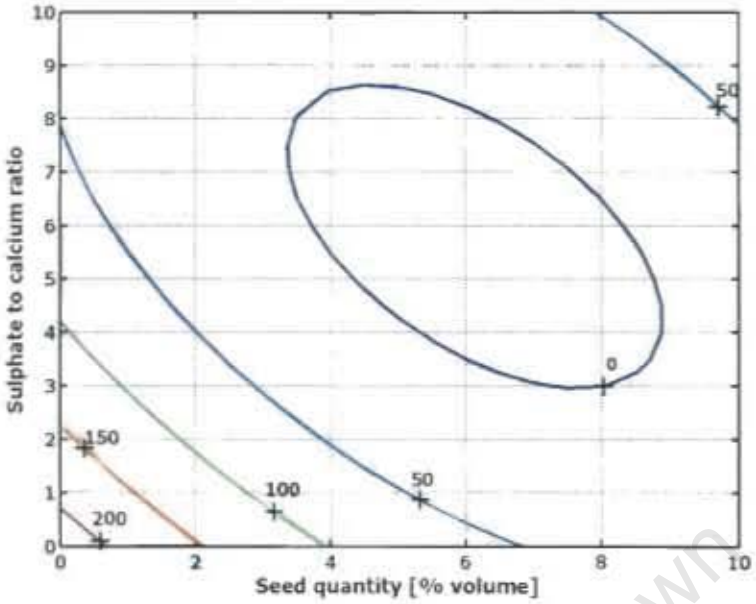

Figure 6.26: Contour plot for time to reach equilibrium, factors pH and N constant

6.7.2.2 Second order model for percentage crystal growth

Table 6.15 summarises the second order model fitted to the response of percentage crystal growth.

Table 6.15: 2nd order model for % growth using plate-like seed crystals

Parameter	Parameter estimate	Standard error	p-value
Intercept	102.006560	25.062063	0.0036
SQ	-14.763188	4.416486	0.0102
SCR	-6.189756	2.853336	0.0619
pH	-3.583593	3.534281	0.3403
N	-0.037686	0.066914	0.5887
$(SQ)^2$	0.558443	0.254440	0.0595
(SQ)(SCR)	0.388472	0.328588	0.2711
$(SCR)^2$	0.361350	0.254440	0.1933
(SQ)(pH)	0.187361	0.328588	0.5842
$(pH)^2$	0.195226	0.254440	0.4650
(SQ)(N)	0.004881	0.004929	0.3510
$(N)^2$	0.000003676	0.000057249	0.9504

This best-fit model accounts for 84.99 % of the variation in the percentage crystal growth. A critical point, a minimum, occurs at a seed quantity of 8.06 % by volume, a sulphate to

calcium ratio of 4.54, a pH of 5.39 and Reynolds number of 3.7 x 10^4 (496 rpm). A 9.08 % increase in crystal growth can be achieved at that critical minimum point. Seed quantity and sulphate to calcium ratio are the most significant contributors in the second order model. Keeping the least insignificant factors, pH and impeller speed, constant at 7 and 500 rpm (Reynolds number of 3.7 x 10^4), Figures 6.27 and 6.28 show the surface of the model and the corresponding contour plot respectively.

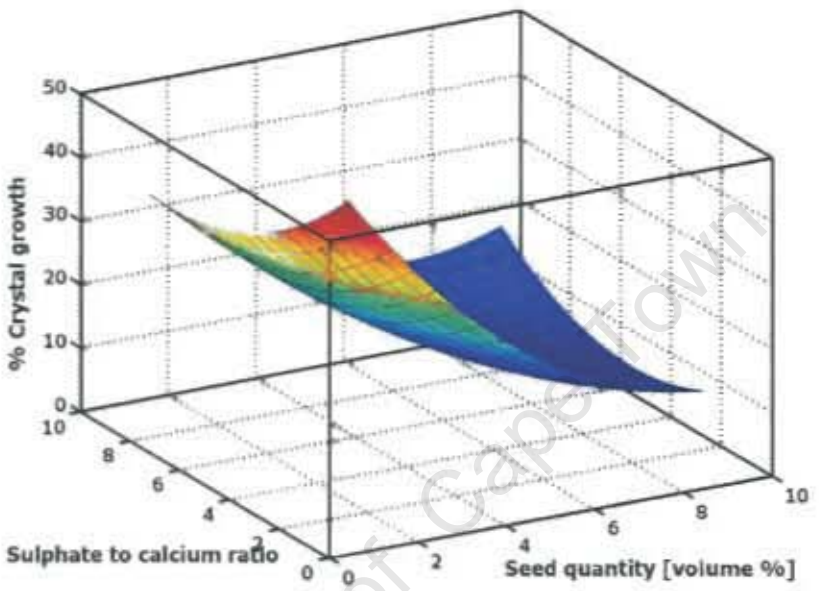

Figure 6.27: 3-D surface plot for % crystal growth, factors pH and N constant

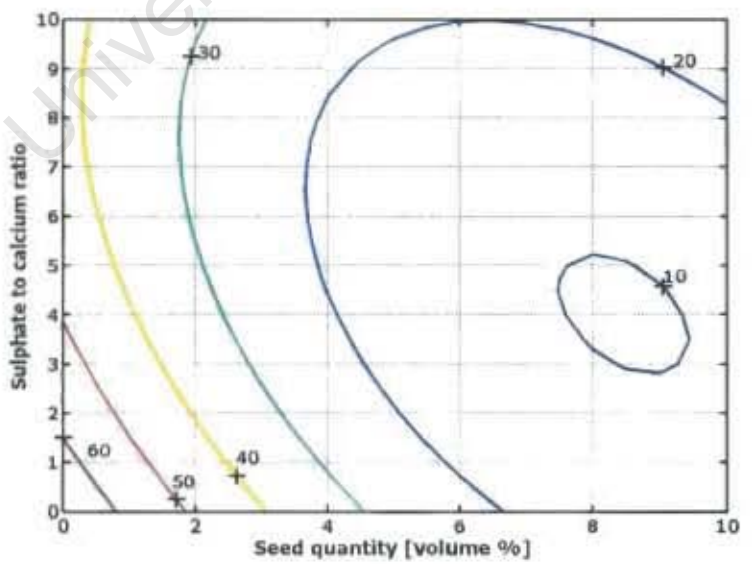

Figure 6.28: Contour plot for % crystal growth, factors pH and N constant

6.7.2.3 Second order model for percentage edges detected

Table 6.16 summarises the second order model fitted to the response of percentage edge detected.

Table 6.16: 2nd order model for % edge detected using plate-like seed crystals

Parameter	Parameter estimate	Standard error	p-value
Intercept	9.791481	4.30667	0.0526
SQ	-1.364805	0.0758930	0.1098
SCR	-0.536837	0.490318	0.3054
pH	0.2536860	0.607331	0.6871
N	-0.000184	0.011498	0.9877
$(SQ)^2$	0.085918	0.043723	0.0850
(SQ)(SCR)	0.169167	0.056465	0.0172
$(SCR)^2$	0.049975	0.043723	0.2861
(SQ)(pH)	0.001944	0.056465	0.9734
$(pH)^2$	-0.020064	0.043723	0.6585
(SQ)(N)	0.001137	0.000847	0.2161
$(N)^2$	-0.000002680	0.000009838	0.7922

This best fit model accounts for 89.06 % of the variation in the percentage edges detected. The interaction parameter between the seed quantity and the sulphate to calcium ratio, AD, affects the crystal morphology greatly. The higher the seed quantity and sulphate to calcium ratio, the higher is the percentage edges detected. The critical point for the percentage edges detected lies outside the experimental region. Figures 6.29 and 6.30 show the 3-d surface and corresponding contour plot at ph 7 and impeller speed of 500 rpm (Reynolds number of 3.7×10^4). A ridge analysis reveals that a percentage edge detected as high as 22% can be achieved by using 9% by volume of seed crystals, 8.23 sulphate to calcium ratio, a pH of 5.5 and a Reynolds number of 4.8×10^4 (644 rpm).

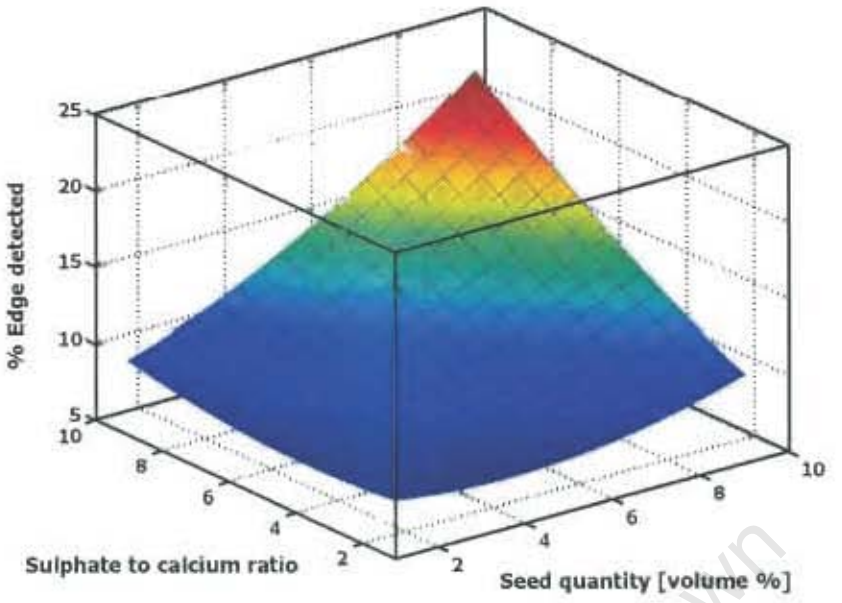

Figure 6.29: 3-D surface plot for % edges detected, factors pH and N constant

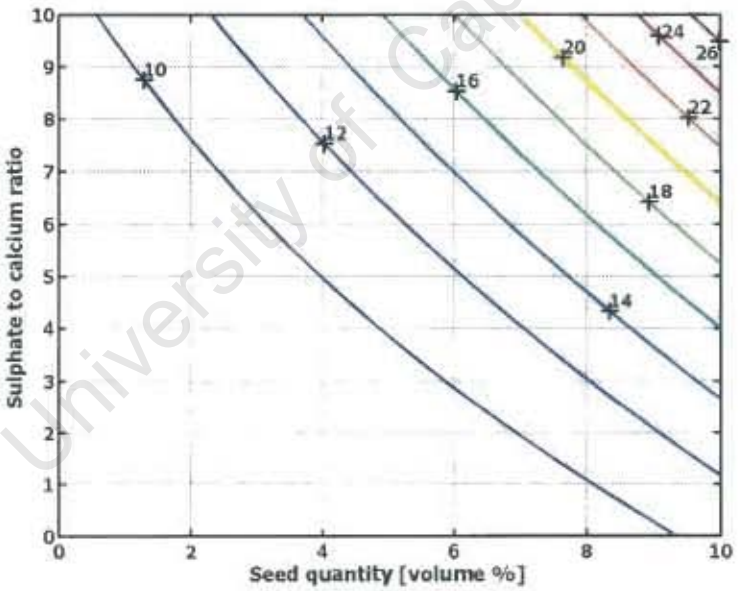

Figure 6.30: Contour plot for % edges detected, factors pH and N constant

6.8 Location of the ideal operating conditions for the desupersaturation reactor

It is one of the aims of the project to define the operating conditions for the operation of the desupersaturation reactor. The operating conditions need to achieve:

- A minimum time required for gypsum solution to reach equilibrium,
- A minimum crystal growth to occur,
- A maximum possible percentage edges detected - to maintain the morphology of the crystal to the plate-like morphology.

The second order models obtained when plate-like seed crystals were used show that regions of minimum for the time to reach equilibrium and percentage crystal growth were located. By fixing the pH and impeller speeds at 7 and a Reynolds number of 3.7×10^4 (500 rpm), the contour plots illustrated in Figures 6.26 and 6.28 were generated. Figure 6.31 shows the two contour plots superimposed. The region shaded in green is the region where the two responses are minimum. This area defines the operating region, which can simultaneously satisfy a minimum for time to reach equilibrium, and percentage crystal growth.

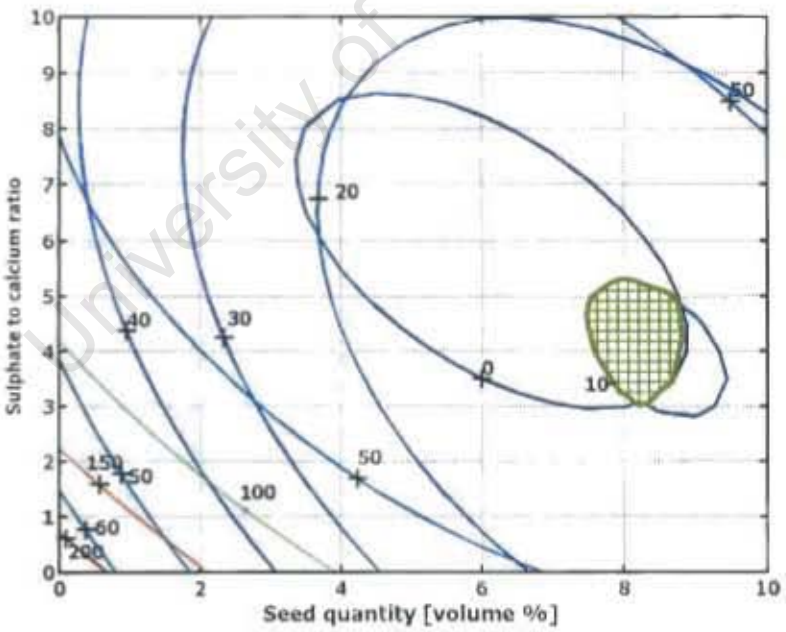

Figure 6.31: Contour plots of time to reach equilibrium and % crystal growth overlapped

The third criterion that needs to be achieved in the SPARRO desupersaturation reactor is the crystal morphology to be kept as plate-like as possible. The higher the percentage edges detected, the more plate-like the crystal is. It was beyond the scope of this project to carry out test on the membrane modules. An investigation into the effect of crystal morphology on

membrane damage in the SPARRO process can establish the size and morphology of gypsum crystals, which cause least damage to the membranes. The percentage edges detected for those particular crystals can then used to determine the ideal operating conditions for the desupersaturation reactor. The contour plot for the percentage edges detected is overlapped on the Figure 6.31 to give Figure 6.32.

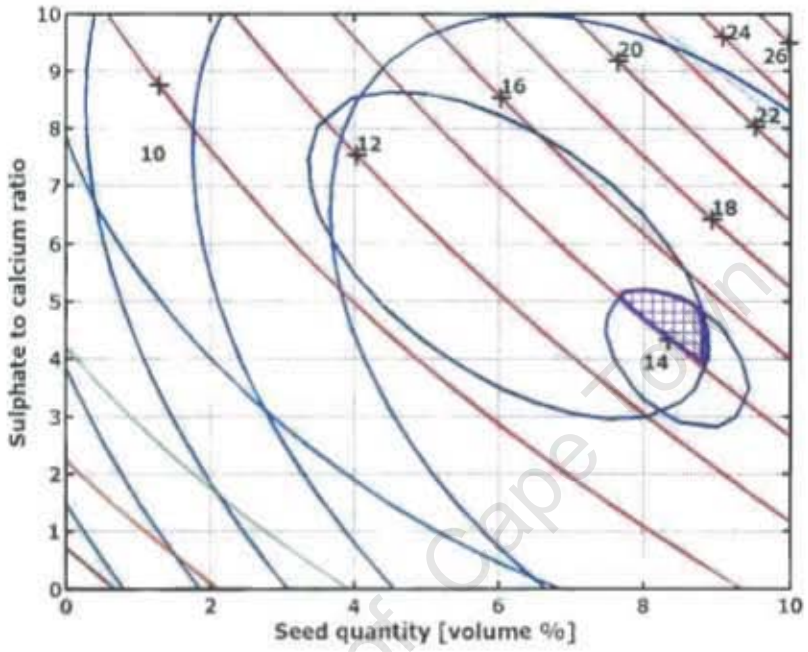

Figure 6.32: All three contour plots overlapped

The red lines represent the percentage edges detected and the corresponding values are shown on the contours. From Figure 6.32, it is possible to read off the required percentage edges detected and thus isolate the feasible operating region. For example, for operating conditions that yield a percentage edge detected of above 12%, the shaded green area on Figure 6.31 would meet all criteria required for the reactor. For 14% edges detected, then the area shaded in purple as shown in Figure 6.32 would define the operating conditions required to meet all the criteria of the reactor. For 16% edge detected, then all the criteria will not be met. In that case, a trade-off between the three responses and the levels of the factors would need to be carried out.

7. Conclusions

7.1 Gypsum seed crystals

The two extreme morphologies of gypsum crystals, the plate and needle-like crystals were used as seed crystals in the experiments. XRD results confirmed that both sets of crystal morphologies were gypsum. The needle-like seed crystals were formed using $CaCl_2$ and Na_2SO_4 solutions at concentration 0.04 M. The average particle size of the needle-like seed crystals was larger than 100 μm and the crystals had sharp edges. The plate-like seed crystals were formed from highly supersaturated solutions of $CaCl_2$ and Na_2SO_4, at a concentration 0.2 M. The average particle size of the plate-like seed crystals was approximately 25 μm and the crystals had smooth and rounded edges.

7.2 Quantifying gypsum morphology using Digital image processing

Analysis of images of the gypsum crystals acquired from Scanning Electron Microscopy at a magnification of 1000x using the edge detection approach was a successful, appropriate and novel method of classifying and quantifying the morphology of gypsum crystals. The Sobel edge operator was found to be a fast, relatively easy to use and automated algorithm to quantify the gypsum crystal morphology. Needle-like crystals exhibited % edges detected lower than 6 % and plate-like crystals exhibited % edges detected higher than 8%. The possibility of quantifying the crystal morphology allowed the relation of one of the main responses, final crystal morphology, to the operating conditions of the desupersaturation reactor.

7.3 Performance of 5 L lab-scale desupersaturation reactor

All the gypsum seeded precipitation experiments were carried out in the 5 L lab-scale desupersaturation reactor in batch mode. The schematics and dimensions of the reactor are given in Figures 5.2 and 5.3. Adequate solid/liquid suspension and satisfactory down-pumping motion was achieved in the reactor for all the experimental runs.

7.4 Modeling of the gypsum seeded precipitation system

7.4.1 Effect of sulphate to calcium molar ratio

Modeling the gypsum precipitating system in OLI System Inc. (Stream analyzer v 1.2) showed that the solubility of gypsum decreased when the molar ratio of sulphate to calcium ions increased from 1 to 4 and stayed almost constant for sulphate to calcium molar ion ratio range of 4 to 10. The decrease in the solubility resulted in an increase in the mass of gypsum precipitated from reagent solutions. As the solubility decreased, the driving force of precipitation, supersaturation ratio also increased. The maximum supersaturation ratio achieved in the experiments was 2.6.

7.4.2 Effect of pH

The pH survey carried out on the gypsum precipitating system using OLI System Inc. (Stream analyzer v 1.2) showed that the solubility of gypsum decreased when the pH of the solution increased from 1 to 4, stayed almost constant for the pH range of 4-10 and increased slightly for pH greater than 10. This trend was observed for sulphate to calcium molar ratios of 1, 4 and 7. At low pH (1-4), the H^+ ion concentration was high, and this led to the speciation of HSO_4^-. Since the concentration of HSO_4^- was high at low pH, the concentration of free SO_4^{2-} was also low. At high pH (10-12) the concentration of OH^- ions was high and this led to the speciation of $CaOH^+$. Since the concentration of $CaOH^+$ was high, the concentration of free Ca^{2+} ions decreased and this increased the solubility, resulting in more free sulphate ions remaining in solution.

7.5 Effect of initial seed morphology

7.5.1 Effect of initial seed morphology on gypsum precipitation kinetics

Experiments with all the conditions set to the same values showed that equilibrium was reached more rapidly when plate-like seed crystals were used as compared to when needle-like seed crystals were used. This can be attributed to the fact that plate-like seed crystals were much smaller in size and thus provided a larger specific surface area for precipitation to occur.

7.5.2 Effect of initial seed morphology on gypsum crystal morphology

The initial morphology of the seed crystals determined the final crystal morphology. Maintenance of the gypsum crystals of plate-like morphology was achieved by seeding using appropriate plate-like seed crystals. This was confirmed by visual analysis as well as the % edges detected of the images obtained from the experiments. Conductivity meter readings showed that there was a decrease in the conductivity of the reacting solution until equilibrium was reached and the conductivity meter readings stabilised. This was a result of solid gypsum precipitating, causing the concentration of ions in solution to decrease. The increase in the average particle size of the crystals during the course of the experiments showed that growth of the seed crystals occurred, maintaining the initial seed crystal morphology.

7.6 Effect of seed quantity

Results from the control experiments D1-D3 showed that the seed quantity significantly affected the kinetics of gypsum precipitation. An increase in the seed quantity decreased the time to reach equilibrium. It took 152, 65 and 48 minutes to reach equilibrium when 1 %, 4 % and 7% by volume of seed crystals were used. The higher the amount of seed crystals the greater the total surface area for precipitation. This showed that gypsum precipitation was surface controlled. The gypsum growth rate followed a second order law. It was found that the growth rate constant increased with an increase in the seed quantity added to the reactor. An increase in seed quantity decreased the growth per seed crystal and increased the percentage edges detected of the crystals. The ratio of the mass of gypsum precipitated from solution to the mass of the seed crystals matched the percentage crystal growth.

7.7 Effect of mixing

7.7.1 Macromixing time scale

Results obtained from experiments E1-E5 showed that the macromixing time decreased when Reynolds number increased from 2.2×10^4 to 6.7×10^4 and increased for Reynolds numbers larger than 6.7×10^4. The decrease in macromixing time occurred because there was an increase in the circulation rates in the reactor when the turbulence increased. For Reynolds number higher than 6.7×10^4 entrainment of air bubbles into the reactor occurred,

which could have interfered with the accuracy of the measurement. The experimentally determined macromixing times were found to be significantly higher than the theoretical ones. The difference could be a result of the pH probe response time. The micromixing times were significantly smaller than the macromixing times.

7.7.2 Effect of Reynolds number on gypsum precipitation

Results from experiments C5, B3 and C6 showed that an increase in the Reynolds number caused a decrease in the percentage crystal growth and time to reach equilibrium. Crystal attrition or nucleation could have been the reason behind this observation. Further research, in this area will help to confirm the real cause of this phenomenon and have been proposed in chapter 8.

7.8 Statistical analysis of experimental results

7.8.1 First order models

The result database was statistically analysed and the first order models obtained for each response, using needle and plate-like seed crystals, had relatively low R^2 values. This motivated the fitting of second order models using plate-like seed crystals.

7.8.1.1 Time to reach equilibrium

The second order model for time to reach equilibrium was given by:

$$T = 333.6 - 47.4(SQ) - 39(SCR) - 8.8(pH) - 0.2(N) + 2.2(SQ)^2 + 2.4(SQ)(SCR) + 2.1(SCR)^2 + 0.7(SQ)(pH) + 0.4(pH)^2 + 0.003(SQ)(N) + 0.0002(N)^2$$

The model accounted for 97.4 % of the variation in time to reach equilibrium. A minimum occurred at seed quantity (SQ) of 6.33 %, sulphate to calcium molar ratio of 5.68, pH of 5.54 and impeller speed (N) of 595 rpm (Reynolds number of 4.5×10^4).

7.8.1.2 Percentage crystal growth

The second order model for % crystal growth was given by:

$$\%\ Growth = 102.0 - 14.8(SQ) - 6.2(SCR) - 3.6(pH) - 0.04(N) + 0.6(SQ)^2 + 0.4(SQ)(SCR) + 0.4(SCR)^2 + 0.2(SQ)(pH) + 0.2(pH)^2 + 0.005(SQ)(N) + 0.000004(N)^2$$

The model accounted for 84.9 % of the variation in percentage crystal growth. A minimum occurred at seed quantity of 8.06 %, sulphate to calcium molar ratio of 4.54, pH of 5.39 and impeller speed of 496 rpm (Reynolds number of 3.7×10^4).

7.8.1.3 Percentage edges detected

The second order model for % edges detected was given by:

$$\%\,\text{Edges} = 9.8 - 1.4(SQ) - 0.5(SCR) + 0.3(pH) - 0.0002(N) + 0.09(SQ)^2 + 0.17(SQ)(SCR) + 0.05(SCR)^2 + 0.002(SQ)(pH) - 0.02(pH)^2 + 0.001(SQ)(N) + 0.000003(N)^2$$

The model accounted for 89.06 % of the variation in the percentage edges detected. A ridge analysis showed that percentage edges detected as high as 22% can be achieved by using a seed quantity of 9 %, sulphate to calcium molar ratio of 8.23, pH of 5.5 and impeller speed of 644 rpm (Reynolds number of 4.8×10^4).

In all the second order models the most significant factors were seed quantity and sulphate to calcium molar ratios.

7.8.2 Location of the ideal operating conditions for the desupersaturation reactor

Contour plots of the responses from the second order models were used to locate the operating conditions of the desupersaturation reactor required to achieve the fastest gypsum precipitation kinetics, the minimum crystal growth and the highest percentage edges detected. At a pH of 7 and a Reynolds number of 3.7×10^4, the criteria to achieve a minimum time to reach equilibrium and percentage crystal growth were satisfied simultaneously. However, as it was beyond the scope of this project to investigate the size and morphology of the gypsum crystals that cause least damage to the reverse osmosis membranes used in the SPARRO process, it was not possible to define the exact operating conditions at which all three criteria of the desupersaturation reactor can be met. The ideal operating conditions for the reactor can be found to meet all the three criteria if the required percentage edges detected lies between 12 and 14 %. If the percentage edges required is above 16% or below 12%, a trade off between the three responses and the levels of the factors will have to be carried out.

8. Recommendations

Some suggestions for further work are given below.

- The experiments carried out in this research can be repeated with the use of actual mine water instead of a synthetic solution of gypsum. This investigation can determine whether the presence of other elements in the mine water affects the physical aspects of the gypsum precipitation.

- Foreign seed particles with a regular spherical shape can be used instead of gypsum crystals. This can enhance the seeded gypsum precipitation and the membrane filtration can be carried out more easily and possibly with less damage.

- The effect of gypsum crystal size and morphology as well as presence of foreign ions (such as magnesium, sodium and manganese) on membrane damage must be carried out to determine the real cause of damage to the membrane modules.

- The scale up of the desupersaturation reactor should be implemented.

- To confirm the reason why crystal growth and time to reach equilibrium decrease with an increase in Reynolds number, crystal counting can be done to confirm if nucleation occurs at a supersaturation ratios studied in this project. To confirm the shear argument the influence of Reynolds number on gypsum seed crystals size in saturated gypsum solution can be investigated.

- The desupersaturation reactor should be run in a continuous mode with the membrane unit.

9. References

Alimi, F., Elfil, H. and Gadri, A. (2003) Kinetics of the precipitation of calcium sulphate dihydrate in a desalination unit. *Desalination*, **157**: 9-16.

Baldyga, J. and Bourne, J.R. (1989) Simplification of Micromixing Calculations. I. Derivation and Application of New Model. *The Chemical Engineering Journal*, **42**: 83-92.

Baldyga, J., Bourne, J.R. and Hearn, S.J. (1997) Interaction between chemical reactions and mixing on various scales. *Chemical Engineering Science*, **52**: 457-466.

Baldyga, J. and Bourne, J.R. (1999). *Turbulent Mixing and Chemical Reactions*. John Wiley and Sons, West Sussex.

Brandse, W.P., Van Rosmalen, G.M. and Brouwer, G. (1977) The influence of sodium chloride on the crystallisation rate of gypsum. *Journal of Inorganic and Nuclear Chemistry*, **39**: 2007-2010.

Bremere, I., Kennedy, M., Michel, P., van Emmerik, R., Witkamp, G. and Schippers, J. (1999) Controlling scaling in membrane filtration systems using a desalination unit. *Desalination*, **124**: 51-62.

Cairncross, L.R.C., Dustan, A.C. and Petrie, J.G. (1997) A structured approach to thermodynamic modelling of aqueous solutions for nickel processing. *Journal of the SAIMM*: 289-297.

Çetin, E., Eroglu, I. and Ozkar, S. (2001) Kinetics of gypsum formation and growth during the dissolution of colemanite in sulfuric acid. *Journal of Crystal Growth*, **231**: 559-567.

Chen, J., Zheng, C. and Chen, G. (1996) Interaction of macro- and micromixing on particle size distribustion in reactive precipitation. *Chemical Engineering Science*, **51**: 1957-1966.

Christoffersen, M.R., Christoffersen, J., Weijen, M.P.C. and Rosmalen, G.M.V. (1982) Crystal growth of calcium sulphate dihydrate at low supersaturation. *Journal of Crystal Growth*, **58**: 585-595.

Doran, P.M. (1995). *Bioprocess engineering principles*. Academic Press, London.

Franke, J. and Mersmann, A. (1995) The influence of the operational conditions on the precipitation process. *Chemical Engineering Science*, **50**: 1737-1753.

Gosele, W. and Kind, M. (1991) Study on the influence of mixing on the quality of continues precipitating products. *Chemie Ingenieur Technik*, **63**: 59-61.

Hall, E.I. (1979). *Computer image processing and recognition*. Academic Press, New York.

Green, W.B. (1983). *Digital Image Processing*. Van Nostrand Reinhold Company, New York.
Hall, E.I. (1979). *Computer image processing and recognition*. Academic Press, New York.

Harnby, M. and Nienow, A.W. (1992). *Mixing in the process industries*. Butterworth-Heinemann, Oxford.

Harries, R.C. (1985) A field trial of seeded reverse osmosis for the desalination of scaling-type mine water. *Desalination*, **56**: 227-236.

Hina, A., Nancollas, G.H. and Grynpas, M. (2001) Surface induced constant composition crystal growth kinetics studies. The brushite-gypsum system. *Journal of Crystal Growth*, **223**: 213-224.
Juby, G.H.G., Harries, R.C. and Greig, J.D. (1985). Improving the quality of mine service water in gold

mines in South Africa. *2nd International Mine Water Congress on Mine Water* (pp. 353-363). Grenada, Spain.

Juby, G.J.B. (1994). *Development of a novel membrane desalination technique for treating calcium sulphate scaling mine water: The SPARRO process.* University of Pretoria, Pretoria.

Juby, G.J.G. and Schutte, C.F. (2000) Membrane life in a seeded-slurry reverse osmosis system. *Water SA*, **26**: 239-248.

Lash, J.E. and Burns, G. (1984) Heats of crystallization of CaSO4.2H2O. *Bulletin des Societes Chimiques Belges*, **93**: 271-279.

Lewis, A., Nathoo, J., Seewoo, S. and Lacour, S. (2002). Prevention of scaling in mine waters using a slurry precipitation and recycle reverse osmosis (SPARRO). *15th International Symposium on Industrial Crystallisation* Sorrento, Italy.

Lewis, A.E. and Roberts, M. (2003) Using fractal structure and flow properties to describe morphology of nickel crystals. *Journal of the Minerals, Metals and Materials Society*, **55**: 59-61.

Liu, S. and Nancollas, G.H. (1970) The kinetics of crystal growth of calcium sulfate dihydrate. *Journal of Crystal Growth*, **6**: 281-289.

Liu, S. and Nancollas, G.H. (1973) Linear crystallization and induction-period studies of the growth of calcium sulphate dihydrate crystals. *Talanta*, **20**: 211-216.

Liu, S. and Nancollas, G.H. (1975) A kinetic and morphological study of the seeded growth of calcium sulfate dihudrate in the presence of additives. *Journal of Colloid and Interface Science*, **52**: 593-601.

Maree, J.P., Winter C.T. and Robertson, P. (1988) *Crystallisation kinetics of Calcium Sulphate.* Contract research task undertaken for the Chamber of Mines Research Organisation, CSIR, Division of Water Technology, Pretoria.

Miers, H.A. (1929). *An introduction to the scientific study of minerals.* Macmillan, London.

Mullin, J.W. (2001). *Crystallization.* Butterworth-Heinemann, Boston.

Myers, R.H. and Montgomery, D.C. (1995). *Response Surface Methodology.* John Wiley and Sons, New York.

Nagata, S. (1975). *Mixing: Principles and Applications.* John Wiley and sons, Tokyo.

Nancollas, G.H., Reddy, M.M. and Tsai, F. (1973) Calcium sulfate dihydrate crystal growth in aqueous solution at elevated temperatures. *Journal of Crystal Growth*, **20**: 125-134.

Nesse, W. (2000). *Introduction to Minerology.* Oxford University Press, Oxford.

Oldshue, J.Y. (1983). *Fluid mixing technology.* Chemical Engineering, New York.

Othmer, k. (1995). *Encyclopedia of Chemical Technology.* John Wiley and Sons, New York.

Pohorecki, R. and Baldyga, J. (1988) The effects of micromixing and the manner of reactor feeding on precipitation in stirred tank reactors. *Chemical Engineering Science*, **43**: 1949-1954.

Pulles, W., Juby, G.H.G. and Busby, R.W. (1992) Development of the slurry precipitation and recycle reverse osmosis (sparro) technology for desalinating scaling mine waters. *Water Science and Technology*, **25**: 177-192.

Roelands, C.P.M., Derksen, J.H., Kramer H J M.; Jansens, and Jansens, P.J. (2003) Analysis of mixing in a typical experimental set-up to measure nucleation rates of precipitation processes. *Chemical Engineering and Technology*, **26**: 296-303.

Seader, J.D. and Henley, E.J. (1998). *Separation Process Principles*. John Wiley and Sons, New York.

Sohnel, O. and Garside, J. (1992). *Precipitation*. Butterworth-Heinemann Ltd, Oxford.

Torbacke, M. and Rasmuson, A.C. (2001) Influence of different scales of mixing in reaction crystallisation. *Chemical Engineering Science.*, **56**: 2459-2473.

Uhl, V.W. and Gray, J.B. (1966). *Mixing*. Academic Press, New York.

Ulbrecht, J.J. and Patterson, G.K. (1985). *Mixing of liquids by mechanical agitation*. Gordon and Breach Science Publishers, New York.

Verdoes, D. and Hanemaaijer, J.H. (1996). Membrane-assisted crystallization: a new hybrid process exemplified by the softening of water. In J. Ulrich and K. Wangnick (Ed.), *Bremen International Workshop on Industrial Crystallization* (pp. 92-99).

Walpole, R.E. and Myers, R.E. (1985). *Probability and statistics for engineers*. Collier Macmillan, New York.

Zhang, J. and Nancollas, G.H. (1992) Influence of calcium/sulfate molar ratio on the growth of calcium sulfate dihydrate at constant supersaturation. *Journal of Crystal Growth*, **118**, 287-294.

Appendices

Appendix

A: Calculation of % by volume of seed material present in SPARRO reactor (Juby, 1994)

B1: Conductivity readings for experiments A1-A12

B2: Data from particle size distribution & Percentage crystal growth calculations: Experiments A1-A12

B3: Data from digital image processing & Percentage edge detection calculations: A1-A12

B4: Sample pictures of crystals from equilibrium solution: Experiments A1-A12

C1: Conductivity readings for experiments B1-B12

C2: Data from particle size distribution & Percentage crystal growth calculations: Experiments B1-B12

C3: Data from digital image processing & Percentage edge detection calculations: B1-B12

C4: Sample pictures of crystals from equilibrium solution: Experiments B1-B12

D1: Conductivity readings for experiments C1-C8

D2: Data from particle size distribution & Percentage crystal growth calculations: C1-C8

D3: Data from digital image processing & Percentage edge detection calculations: C1-C8

D4: Sample pictures of crystals from equilibrium solution: Experiments C1-C8

E: Conductivity readings from experiments D1, D2 and D3

F: Statistical analysis of results obtained from experiments A1-A12

G: Statistical analysis of the results collected from experiments B1-B12

H: Statistical analysis of the results collected from central composite experiments, B1-B12 and C1-C8.

I: Comparison of needle and plate data (1^{st} order data)

Appendix A:

Calculation of % by volume of seed material present in SPARRO reactor (Juby, 1994)

Suspended solid in desupersaturation reactor: 41g/L. (Juby, 1994)

Design volume of reactor: 3.5 m^3.

Amount of gypsum solid in reactor: (41g/L)*$(3.5m)^3$ = 143.5 kg

Density of gypsum: 2320 kg/m^3

Volume of gypsum in reactor: 143.5kg/(2320 kg/m^3) = 0.06185 m^3

% volume of solids in reactor: (0.06185/3.5)*100 = 1.77%

Appendix B1:Conductivity readings for experiments A1-A12

Time (Minutes)	A1	A2	A3	A4	A5	A6	A7	A8	A9	A10	A11	A12
0	12.19	12.1	12.3	12.25	12.24	12.32	12.20	12.28	12.1	12.39	12.01	12.19
1	12	20	11.87	27.6	11.07	10.85	11.21	11.62	12.6	17.4	10.95	10.76
2	27							10.8	10.5			
3	25.3											
4	11.6	11.6	11.4	11.5	11.6	11.56	11.4	9.57	11.6	11.5	10.47	9.9
5	10.1							9.9	11.46			9.76
6	10.1											
7	10.1											
8	10.2							9.84	11.4			9.88
9	10.45							9.78	11.6			9.5
10	10.6	33.1	11.4	11	11.6	10.5	11.1	9.77	11.4	11.1	10.44	9.65
11	10.4							9.68	11.4			9.61
12	10.4							9.59	11.4			9.7
13	10.4							9.67	11.4			9.44
14	10.4							9.65	11.4			9.48
15	10.4	32.9	11.1	32.8	11.4	11.44	11	9.64	11.4	11.1	10.43	9.44
16	10.4							9.6				9.4
17	10.4							9.49				9.41
18	10.4							9.49				9.29
19	10.4							9.46				9.36
20	10.4	33.9	11.2	32.8	11.2	10.42	10.9	9.45		11	10.4	9.39
21	10.4							9.46				9.38
22	10.4							9.42				9.37
23	10.4							9.47				9.35
24	10.4							9.4				9.35
25	10.4	32.9	11.1	32.7	11.2	10.37	10.8	9.39		11	10.38	9.31
26	10.4							9.36				9.33
27	10.4							9.35				9.33
28	10.4							9.34				9.33
29	10.4							9.34				9.33
30	10.4	32.7	11.2	32.7	11.1	10.32	10.8	9.32		11	10.36	9.32
31								9.33				9.33
32								9.3				9.33
33								9.31				9.32
34								9.3				9.33
35		32.9	11.2	32.7	11.1	10.31	10.8	9.31		25.9	10.35	9.3
36								9.29				9.3
37								9.29				9.3
38								9.29				9.3
39								9.28				9.3
40		32.8	11.1	32.8	11.1	10.3	10.8	9.24		25.8	10.33	9.3
41								9.26				9.3
42								9.24				9.3
43								9.23				9.3
44								9.24				9.3
45		32.5	11.2	32.7	[illegible]	10.29	[illegible]	9.21		25.8	10.32	9.3
46								9.21				9.3
47								9.2				9.3
48								9.21				9.3
49								9.2				9.3
50		32.5	[illegible]	32.7	11	10.27	10.8	9.2		[illegible]	10.3	9.29
51								9.2				9.29
52								9.2				9.29
53								9.2				9.29
54								9.2				9.29
55		32.5	11.1	32.7	11	10.27	10.8	9.2		25.9	10.34	[illegible]
56								9.2				9.28
57								9.2				9.28
58								9.2				9.28
59								9.19				9.28
60		32.5	11.1	32.8	11	10.23	10.8	9.19		25.8	10.27	9.28
61								9.19				9.28
62								9.19				9.28
63								9.19				9.28
64								9.19				9.28
65		32.5	11.1	32.8	11	10.23	10.8	9.19		25.8	10.33	9.28
66								9.19				
67								9.18				
68								9.18				
69								9.18				
70		32.5	11.1	32.8	11	10.23		9.15		25.8	10.22	
71								9.18				
72								9.18				
73								9.16				
74								9.16				
75		32.4	11.1	33.5		10.21		9.19		30.8	10.32	
76								9.18				
77								9.18				
78								9.18				
79								9.18				
80		32.3	11.1	32.8		10.18		9.18		32.8	10.3	
81								9.17				
82								9.17				
83								9.17				
84								9.17				
85		32.3	11.1	32.8		10.17		9.17			10.19	
86								9.17				
87								9.17				
88								9.17				
89								9.17				
90		32.3		33.5		10.17		9.17			10.16	
91								[illegible]				
92								9.16				
93								9.16				
94								9.16				
95		32.3		33.5		10.14		9.16			10.16	
96								9.16				
97								9.16				
98								9.16				
99								9.16				
100		32.4		33.5		10.12		9.16			10.16	
101								9.16				
102								9.16				
103								9.15				
104								9.16				
105		32.3		33.5		10.11		9.16			10.13	
106								9.16				
107								9.15				
108								9.16				
109								9.16				
110		32.3		33.5		10.09		9.16			10.12	
111												
112												
113												
114												
115		32.3		33.5		10.08					10.1	
116												
117												
118												
119												
120		32.2		33.5		10.03					10.09	
121												
122												
123												
124												
125		32.1		[illegible]		10.01					10.08	
126												
127												
128												
129												
130		32.1		32.4		09.95					10.06	
131												
132												
133												
134												
135		32.1		32.4		10.03					10.04	
136												
137												
138												
139												
140		[illegible]		32.4		10.02					10.03	
141												
142												
143												
144												
145		32.2		32.4		10.04					10.02	
146												

Time (minutes)	A1	A2	A3	A4	A5	A6	A7	A8	A9	A10	A11	A12
147												
148												
149												
150		32.3		12.4		10.04					10	
151												
152												
153												
154												
155		32.2				10.02					9.99	
156												
157												
158												
159												
160		32.2				10.01					9.97	
161												
162												
163												
164												
165		32.2				9.99					9.96	
166												
167												
168												
169												
170						9.97					9.93	
171												
172												
173												
174												
175						9.96					9.94	
176												
177												
178												
179												
180						9.94					9.92	
181												
182												
183												
184												
185						9.93					9.91	
186												
187												
188												
189												
190						9.93					9.90	
191												
192												
193												
194												
195						9.92					9.89	
196												
197												
198												
199												
200						9.92					9.87	
201												
202												
203												
204												
205						9.91					9.88	
206												
207												
208												
209												
210						9.88					9.86	
211												
212												
213												
214												
215						9.86					9.84	
216												
217												
218												
219												
220						9.85					9.82	
221												
222												
223												
224												
225						9.84					9.82	
226												
227												
228												
229												
230						9.83					9.8	
231												
232												
233												
234												
235						9.81					9.78	
236												
237												
238												
239												
240						9.80					9.78	
241												
242												
243												
244												
245											9.77	
246												
247												
248												
249												
250											9.76	
251												
252												
253												
254												
255											9.75	
256												
257												
258												
259												
260											9.74	
261												
262												
263												
264												
265											9.73	
266												
267												
268												
269												
270											9.72	
271												
272												
273												
274												
275											9.71	
276												
277												
278												
279												
280											9.7	
281												
282												
283												
284												
285											9.7	
286												
287												
288												
289												
290											9.7	

Time at which equilibrium has reached

Appendix B2

Data from particle size distribution & Percentage crystal growth calculations: Experiments A1-A12

Seed crystals analyis	A1	A2	A3	A4	A5	A6	A7	A8	A9	A10	A11	A12
D[4,3] -1st measurement	103.92	80.08	90.09	71.33	107.03	109.68	106.46	103.55	109.24	104.05	108.43	98.12
D[4,3]-2nd measurement	105.42	80.15	101.64	74.02	107.49	102.68	107.47	102.95	105.82	102.76	107.51	98.95
D[4,3]-3rd measurement	104.03	83.98	100.43	73.5	107.92	95.03	109.59	104.67	102.57	102.6	107.05	105.61
D[4,3] average	***104.46***	***81.40***	***97.39***	***72.95***	***107.48***	***102.46***	***107.84***	***103.72***	***105.88***	***103.14***	***107.66***	***100.89***
Standard deviation	***0.64***	***2.23***	***6.35***	***1.43***	***0.45***	***7.33***	***1.60***	***0.87***	***3.34***	***0.80***	***0.70***	***4.11***
Analysis of crystals from equilibrium solution												
D[4,3]-1st measurement	105.3	129.08	111.2	89.59	122.47	141.35	117.62	110.61	110	112.27	141.35	104.73
D[4,3]-2nd measurement	100.47	132.82	117.26	00106	118.74	132.54	121.98	108.72	106.35	116.81	144.95	101.33
D[4,3]-3rd measurement	114.83		92	111.86	114.13	136.3	117.74	108.78	112.7	111.38	138.52	101.07
D[4,3] average	***106.87***	***130.95***	***106.82***	***102.33***	***118.45***	***136.73***	***119.11***	***109.37***	***109.68***	***113.49***	***141.61***	***102.38***
Standard deviation	***7.31***	***2.64***	***13.19***	***11.48***	***4.18***	***4.42***	***2.48***	***1.07***	***3.19***	***2.91***	***3.22***	***2.04***
% Crystal growth (equation 5-1)	***2.31***	***60.87***	***9.69***	***40.27***	***10.20***	***33.44***	***10.45***	***5.44***	***3.60***	***10.04***	***31.53***	***1.47***
Error in crystal growth measurement	***0.18***	***2.90***	***1.83***	***5.30***	***0.40***	***3.47***	***0.37***	***0.10***	***0.22***	***0.04***	***0.04***	***0.06***

Appendix B3

Data from digital image processing & Percentage edge detection calculations: A1-A12

Analysis of crystals from equilibrium solution

	% Edge detected →											
	A1	A2	A3	A4	A5	A6	A7	A8	A9	A10	A11	A12
Picture 1	6.4341	3.4673	2.9409	2.6551	5.1956	7.4673	5.1226	3.9703	3.1137	5.5419	3.6811	6.4314
Picture 2	2.9361	3.4079	3.2853	1.6804	5.1033	6.357	4.4421	5.1031	3.3191	5.3509	4.5337	4.8446
Picture 3	5.0603	1.5389	3.1809	2.0257	4.007	5.0231	5.6203	3.2227	3.3609	5.3471	3.4526	6.8169
Picture 4	3.5127	4.6764	3.809	1.0299	4.4787	5.8279	6.3239	3.3726	3.0031	5.926	4.431	6.6394
Picture 5	5.2437	4.8827	2.573	4.664	4.6354	2.9756	4.834	3.6163		6.3136	3.7359	10.0236
Picture 6	5.0986	3.3741	1.9654	4.311	3.7531	6.2103	5.6051			5.0191	3.767	8.6241
Picture 7	4.1271	2.303	2.8471	2.8924	4.1697	5.9311	4.6307			4.0564	3.8531	6.0007
Picture 8	5.2983	2.8719	3.0087	3.9804	4.3437	6.319	5.2509			5.7047	4.1231	7.363
Picture 9	5.3511	1.8547	3.0549	4.0327	3.9664	4.1291	5.4501			6.6386	4.5233	6.4187
Picture 10	4.424	2.0163	3.5061	3.8636	3.129	6.357	5.2516			4.9884	4.5149	5.5979
Average % Edge detected	*4.75*	*3.04*	*3.02*	*3.11*	*4.28*	*5.66*	*5.15*	*3.86*	*3.20*	*5.49*	*4.06*	*6.88*
Standard deviation	*1.02*	*1.14*	*0.51*	*1.24*	*0.62*	*1.29*	*0.40*	*0.75*	*0.17*	*0.73*	*0.41*	*1.50*

Appendix B4: Sample pictures of crystals from equilibrium solution: Experiments A1-A12

A1

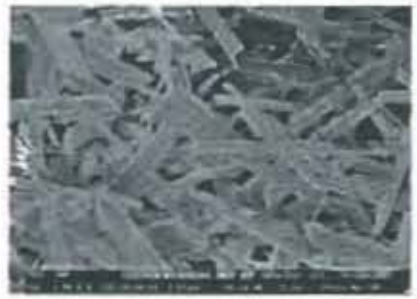

A4

A7

A10

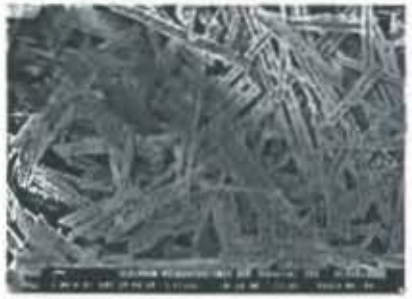

A2

A5

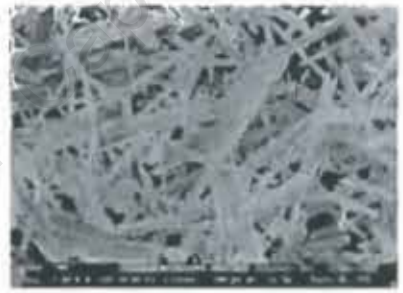

A8

A11

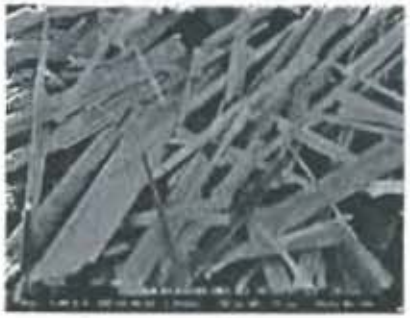

A3

A6

A9

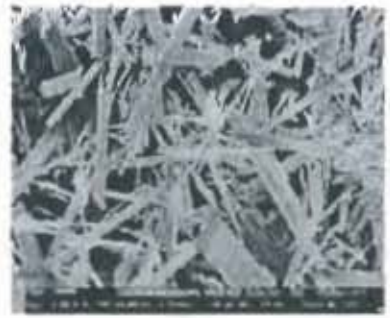

A12

Appendix C1:Conductivity readings for experiments B1-B12

Time [minutes]	B1	B2	B3	B4	B5	B6	B7	B8	B9	B10	B11	B12
0	14.62	13.54	14.01	13.25	14.04	13.27	14.1	14.88	15.01	13.27	13.52	14.73
1	16.33							12.92	18.03			12.78
2	21.2	23.8	16.54	24.8	16.25	11.67	17.17	12.18	22.5	11.67	12.28	11.81
3	25.2	28.9	16.56	33.6	18.51	11.16	19	11.4	25.5	11.16		11.45
4	29.4	32.9	20.4	33.1	20.3	10.83	21	11.15	30	10.83		11.21
5	31.6	33.7	21.6	32.8	21.7	10.72	21.8	11.15	31.5	10.72	10.74	11.08
6	31.5	33.4	21.5	32.8	21.7	10.7	21.8	11.13	31.6	10.7		11.07
7	31.3	33	21.5	32.7	21.7	10.62	21.8	11.08	31.5	10.62		11.01
8	31.5	32.9	21.5	32.7	21.7	10.63	21.8	11.03	31.5	10.63		10.97
9	31.6	32.9	21.5	32.7	21.5	10.59	21.7	11	31.5	10.59		10.96
10	31.6	32.9	21.5	32.7	21.5	10.58	21.7	10.94	31.5	10.58	10.64	10.95
11	31.6	32.8	21.5	32.7	21.5	10.55	21.7	10.91	31.5	10.55		10.9
12	31.6	32.8	21.5	32.7	21.5	10.53	21.7	10.93	31.4	10.53		10.88
13	31.6	32.8	21.5	32.7	21.5	10.5	21.7	10.93	31.4	10.5		10.9
14	31.6	32.8	21.4	32.7	21.5	10.47	21.7	10.86	31.4	10.47		10.85
15	31.6	32.8	21.4	32.6	21.5	10.44	21.7	10.87	31.4	10.44	10.45	10.84
16	31.6	32.7	21.4	32.6	21.5	10.42	21.6	10.85	31.4	10.42		10.84
17	31.6	32.7	21.4	32.6	21.5	10.35	21.6	10.88	31.4	10.35		10.83
18	31.6	32.7	21.3	32.6	21.5	10.36	21.6	10.91	31.4	10.36		10.83
19	31.6	32.7	21.3	32.6	21.4	10.32	21.6	10.86	31.4	10.32		10.82
20	31.6	32.7	21.3	32.6	21.4	10.3	21.5	10.87	31.4	10.3	10.38	10.81
21	31.6	32.7	21.3	32.5	21.4	10.3	21.5	10.89	31.4	10.3		10.82
22	31.6	32.7	21.3	32.6	21.4	10.29	21.5	10.84	31.4	10.29		10.82
23	31.6	32.7	21.3	32.6	21.4	10.25	21.5	10.86	31.4	10.25		10.8
24	31.6	32.7	21.3	32.6	21.4	10.25	21.5	10.86	31.4	10.25		10.83
25	31.6	32.7	21.3	32.6	21.4	10.24	21.5	10.81	31.4	10.24	10.31	10.85
26	31.6	32.7	21.3	32.6	21.4	10.23	21.5	10.85	31.4	10.23		10.85
27	31.6	32.7	21.3	32.6	21.4	10.2	21.5	10.85	31.4	10.2		10.86
28	31.6	32.7	21.3	32.6	21.4	10.19	21.5	10.87	31.4	10.19		10.83
29	31.6	32.7	21.3	32.6	21.4	10.16	21.5	10.87	31.4	10.16		10.86
30	31.6	32.7	21.3	32.6	21.4	10.15	21.5	10.86	31.4	10.15	10.25	10.84
31		32.7		32.6		10.14		10.82		10.14		10.81
32		32.7		32.5		10.13		10.86		10.13		10.83
33		32.7		32.6		10.13		10.87		10.13		10.84
34		32.7		32.6		10.12		10.87		10.12		10.85
35		32.7		32.6		10.08		10.85		10.08	10.2	10.85
36		32.7		32.6		10.09		10.83		10.09		10.85
37		32.7		32.6		10.09		10.84		10.09		10.85
38		32.7		32.6		10.09		10.81		10.09		10.85
39		32.7		32.6		10.06		10.82		10.06		10.85
40		32.7		32.6		10.07		10.87		10.07	10.16	10.85
41		32.7		32.6		10.06		10.88		10.06		10.85
42		32.7		32.6		10.06		10.87		10.06		10.85
43		32.7		32.6		10.06		10.86		10.06		10.85
44		32.7		32.6		10.05		10.84		10.05		10.85
45		32.7		32.6		10.05		10.85		10.05	10.12	10.85
46		32.7		32.6		10.05		10.86		10.05		10.85
47		32.7		32.6		10.04		10.84		10.04		10.85
48		32.7		32.6		10.04		10.85		10.04		10.85
49		32.7		32.6		10.02		10.85		10.02		10.85
50		32.8		32.6		10.01		10.86		10.01	10.09	10.85
51		32.8		32.6		10		10.86		10		10.85
52		32.8		32.5		9.99		10.85		9.99		10.85
53		32.8		32.5		9.98		10.85		9.98		10.85
54		32.8		32.5		9.97		10.85		9.97		10.85
55		32.8		32.5		9.96		10.85		9.96	10.05	10.85
56		32.8		32.5		9.94		10.85		9.94		10.85
57		32.8		32.5		9.93		10.85		9.93		10.85
58		32.8		32.5		9.94		10.85		9.94		10.86
59		32.8		32.5		9.91		10.85		9.91		10.85
60		32.8		32.5		9.92		10.85		9.92	10.02	10.85
61						9.92		10.85		9.92		
62						9.92		10.85		9.92		
63						9.91		10.85		9.91		
64						9.91		10.85		9.91		
65						9.9		10.85		9.9	9.99	
66						9.9		10.85		9.9		
67						9.89		10.85		9.89		
68						9.89		10.85		9.89		
69						9.88		10.85		9.88		
70						9.88		10.85		9.88	9.97	
71						9.85		10.85		9.85		
72						9.86		10.85		9.86		
73						9.86		10.85		9.86		
74						9.85		10.85		9.86		
75						9.83		10.85		9.85	9.95	
76						9.84		10.85		9.83		
77						9.84		10.85		9.84		
78						9.84		10.85		9.84		
79						9.84		10.85		9.84		
80						9.84		10.85		9.84	9.92	
81						9.83		10.85		9.83		
82						9.82		10.85		9.82		
83						9.82		10.85		9.82		
84						9.82		10.85		9.82		
85						9.81		10.85		9.81	9.9	
86						9.8		10.85		9.81		
87						9.8		10.85		9.8		
88						9.8		10.85		9.8		
89						9.8		10.85		9.8		
90						9.8		10.85		9.8	9.88	
91						9.79				9.79		
92						9.79				9.79		
93						9.79				9.79		
94						9.79				9.79		
95						9.76				9.78	9.86	
96						9.78				9.78		
97						9.76				9.78		

Time (minutes)	B1	B2	B3	B4	B5	B6	B7	B8	B9	B10	B11	B12
98						9.78				9.78		
99						9.77				9.77		
100						9.77				9.77	9.85	
101						9.76				9.76		
102						9.76				9.76		
103						9.75				9.75		
104						9.74				9.74		
105						9.74				9.74	9.83	
106						9.74				9.74		
107						9.74				9.74		
108						9.73				9.73		
109						9.73				9.73		
110						9.73				9.73	9.82	
111						9.73				9.73		
112						9.73				9.73		
113						9.72				9.72		
114						9.72				9.72		
115						9.72				9.72	9.81	
116						9.71				9.71		
117						9.71				9.71		
118						9.71				9.71		
119						9.7				9.7		
120						9.7				9.7	9.79	
121						9.69				9.69		
122						9.69				9.69		
123						9.69				9.69		
124						9.69				9.68		
125						9.67				9.67	9.78	
126						9.67				9.67		
127						9.67				9.67		
128						9.66				9.66		
129						9.66				9.66		
130						9.66				9.66	9.77	
131						9.65				9.65		
132						9.65				9.65		
133						9.65				9.65		
134						9.65				9.65		
135						9.65				9.65	9.76	
136						9.64				9.64		
137						9.64				9.64		
138						9.64				9.64		
139						9.64				9.64		
140						9.64				9.64	9.75	
141						9.64				9.64		
142						9.64				9.64		
143						9.63				9.63		
144						9.63				9.63		
145						9.63				9.63	9.74	
146						9.63				9.63		
147						9.63				9.63		
148						9.63				9.63		
149						9.63				9.63		
150						9.62				9.62	9.73	
151						9.62				9.62		
152						9.62				9.62		
153						9.62				9.62		
154						9.62				9.62		
155						9.62				9.62	9.72	
156						9.62				9.62		
157						9.62				9.62		
158						9.62				9.62		
159						9.62				9.62		
160						9.62				9.62	9.72	
161						9.62						
162						9.62						
163						9.62						
164						9.62						
165						9.62					9.71	
166						9.62						
167						9.62						
168						9.62						
169						9.62						
170						9.62					9.71	
171						9.62						
172						9.62						
173						9.62						
174						9.62						
175						9.62					9.71	
176						9.62						
177						9.62						
178						9.62						
179						9.62						
180						9.62					9.7	
181												
182												
183												
184												
185											9.69	
186												
187												
188												
189												
190											9.69	
191												
192												
193												
194												
195											9.69	

Time at which equilibrium has reached

Appendix C2

Data from particle size distribution & Percentage crystal growth calculations: Experiments B1-B12

Seed crystals analyis	B1	B2	B3	B4	B5	B6	B7	B8	B9	B10	B11	B12
D[4,3] -1st measurement	27.11	26.18	22.83	31.86	24.43	28.22	25.75	25.34	27.21	22.6	24.71	24.45
D[4,3]-2nd measurement	26.05	25.05	23.27	25.33	24.61	26.22	25.44	25.07	27.05		24.18	24.49
D[4,3]-3rd measurement	25.51	24.36	22.93	25.26	24.51	25.71	25.5	24.94	26.92		23.69	24.35
D[4,3] average	***26.22***	***25.20***	***23.01***	***27.48***	***24.52***	***26.72***	***25.56***	***25.12***	***27.06***	***22.60***	***24.19***	***24.43***
Standard deviation	***0.81***	***0,92***	***0.23***	***3.79***	***0.09***	***1.33***	***0.16***	***0.20***	***0.15***	***0.00***	***0.51***	***0.07***

Analysis of crystals from equilibrium solution

D[4,3]-1st measurement	28.04	35.13	27.19	37.95	28.94	39.54	31.03	29.69	31.62	28.51	41.3	28.43
D[4,3]-2nd measurement	29.7	35.64	27.31	00038	28.68	39.59	31.19	28.77	30.48		41.33	28.8
D[4,3]-3rd measurement	29.84	35.08	28.76	38.35	28.97	39.33	31.36	28.01	29.85		39.45	29.82
D[4,3] average	***29.19***	***35.28***	***27.75***	***38.22***	***28.86***	***39.49***	***31.19***	***28.82***	***30.65***	***28.51***	***40.69***	***29.02***
Standard deviation	***1.00***	***0.31***	***0.87***	***0.23***	***0.16***	***0.14***	***0.17***	***0.84***	***0.90***	***0.00***	***1.08***	***0.72***

% Crystal growth (equation 5-1)	***11.33***	***40.03***	***20.61***	***39.07***	***17.73***	***47.80***	***22.02***	***14.76***	***13.27***	***26.15***	***68.20***	***18.77***
Error in crystal growth measurement	***0.74***	***1.81***	***0.86***	***5.63***	***0.16***	***2.54***	***0.26***	***0.04***	***0.04***	***0.00***	***0.08***	***0.03***

Appendix C3

Data from digital image processing & Percentage edge detection calculations: B1-B12

Analysis of crystals from equilibrium solution

	% Edge detected											
	B1	B2	B3	B4	B5	B6	B7	B8	B9	B10	B11	B12
Picture 1	13.1664	8.009	10.33359	7.6761	10.6316	8.6541	10.1367	8.2774	13.8381	10.4176	8.9174	9.0311
Picture 2	12.5853	7.5031	9.5667	8.0576	10.5541	7.3719	10.2826	12.9737	12.5094	11.2199	9.5689	13.7234
Picture 3	12.954	8.7224	10.1227	7.5529	9.1754	8.3289	9.3723	9.5941	13.8604	11.707	9.7886	6.2656
Picture 4	14.9367	11.0439	10.0496	6.415	10.1144	9.031	10.138	7.3189	13.0623	10.1757	9.3816	10.118
Picture 5	13.8964	12.7363	9.8171	8.1959	10.3773	9.3001	9.9861	6.3973	13.837	9.8474	8.6396	5.7036
Picture 6	14.6376	8.6879	10.373	7.7011	8.5947	8.6769	9.4861	7.8327	16.884	10.2879	10.2266	
Picture 7	16.8229		9.7567	8.1024	10.9211	8.1526	9.7434	8.3884	14.4133	11.0279	11.166	
Picture 8	17.4897		10.0466	7.7703	11.2154	7.2063	10.9566	7.1966	12.691	8.9741	9.7039	
Picture 9	18.3573	10.6079	12.6636	7.7081	10.0771	8.1091	10.7923	6.8506	12.5047	9.7136	10.637	
Picture 10	16.7379	10.0821	12.2444	9.3983		8.0261	11.5179	6.384	13.7419	10.3017	10.452	
Average % Edge detected	***15.15***	***9.67***	***10.50***	***7.86***	***10.18***	***8.29***	***10.24***	***8.12***	***13.71***	***10.37***	***9.65***	***8.97***
Standard deviation	***2.06***	***1.76***	***1.07***	***0.73***	***0.83***	***0.67***	***0.68***	***1.97***	***1.29***	***0.79***	***1.24***	***3.24***

Appendix C4: Sample pictures of crystals from equilibrium solution: Experiments B1-B12

B1

B4

B7

B10

B2

B5

B8

B11

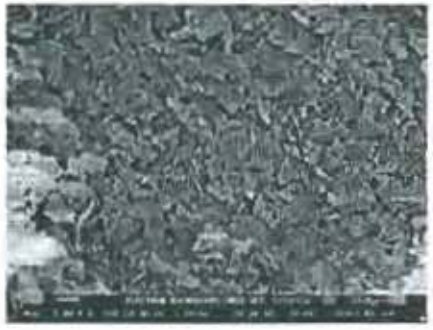

B3

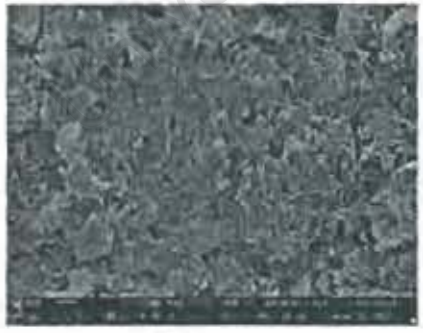

B6

B9

B12

Appendix D1:Conductivity readings for experiments C1-C8

Time (minutes)	C1	C2	C3	C4	C5	C6	C7	C8
0	13.07	15.84	14.32	13.58	14.5	14.37	13.97	14.44
1	15.19	16.15	15.42	14.79	15.05	15.13	12.93	19.51
2	17.31	17.1	17.24	16.3	16.62	16.75	12.11	26.8
3	19.01	19.36	18.79	18.86	18.71	18.63	11.48	33.2
4	21.5	20.8	20.7	21	20.7	20.8	11.04	38.7
5	22.4	21.8	21.8	21.7	21.9	21.6	10.8	42.6
6	22.4	21.7	21.6	21.6	21.9	21.6	10.71	42
7	22.3	21.7	21.5	21.5	21.9	21.5	10.61	42
8	22.3	21.7	21.5	21.4	21.8	21.7	10.56	42
9	22.2	21.7	21.5	21.4	21.8	21.5	10.52	42
10	22.1	21.7	21.5	21.4	21.8	21.4	10.5	42
11	22.1	21.7	21.5	21.3	21.8	21.3	10.46	42
12	22	21.7	21.5	21.3	21.8	21.1	10.42	42
13	22	21.7	21.5	21.3	21.8	21.2	10.41	42
14	21.9	21.7	21.4	21.3	21.8	21.1	10.36	42
15	21.9	21.7	21.4	21.3	21.8	21.2	10.36	42
16	21.9	21.7	21.4	21.2	21.7	21.3	10.31	
17	21.8	21.7	21.4	21.2	21.7	21.3	10.32	
18	21.8	21.7	21.4	21.2	21.7	21.3	10.29	
19	21.8	21.7	21.4	21.2	21.7	21.3	10.3	
20	21.8	21.7	21.4	21.2	21.7	21.3	10.25	
21	21.8		21.4	21.2	21.6	21.3	10.25	
22	21.8		21.3	21.2	21.6	21.3	10.22	
23	21.7		21.3	21.2	21.6	21.3	10.23	
24	21.7		21.3	21.2	21.6	21.3	10.23	
25	21.7		21.3	21.2	21.6	21.3	10.19	
26	21.7		21.3	21.2	21.6	21.3	10.18	
27	21.7		21.3	21.2	21.6	21.3	10.21	
28	21.7		21.3	21.2	21.6	21.3	10.2	
29	21.6		21.3	21.2	21.6	21.3	10.18	
30	21.6		21.3	21.2	21.6	21.3	10.18	
31	21.6		21.3				10.16	
32	21.6		21.3				10.17	
33	21.6		21.3				10.16	
34	21.6		21.3				10.16	
35	21.6		21.3				10.15	
36	21.6		21.3				10.16	
37	21.6		21.3				10.13	
38	21.6		21.3				10.14	
39	21.6		21.3				10.14	
40	21.5		21.3				10.15	
41	21.5						10.15	
42	21.5						10.12	
43	21.5						10.14	
44	21.5						10.09	
45	21.5						10.1	
46	21.5						10.1	
47	21.5						10.09	
48	21.5						10.11	
49	21.5						10.1	
50	21.5						10.12	
51	21.5						10.1	
52	21.5						10.11	
53	21.5						10.11	
54	21.5						10.1	
55	21.5						10.11	
56	21.5						10.1	
57	21.5						10.11	
58	21.5						10.11	
59	21.5						10.08	
60	21.4						10.09	
61	21.4						10.08	
62	21.4						10.1	
63	21.4						10.07	
64	21.4						10.09	
65	21.4						10.1	
66	21.4						10.1	
67	21.4						10.1	
68	21.4						10.1	
69	21.4						10.1	
70	21.4						10.1	
71	21.4						10.1	
72	21.4						10.1	
73	21.4						10.1	
74	21.4						10.1	
75	21.4						10.1	
76	21.4						10.1	
77	21.4						10.1	
78	21.4						10.1	
79	21.4						10.1	
80	21.4						10.1	
81	21.4						10.1	
82	21.4						10.1	
83	21.4						10.1	
84	21.4						10.1	
85	21.4						10.1	
86	21.4						10.1	
87	21.4						10.1	
88	21.4						10.1	
89	21.4						10.1	
90	21.4						10.1	

Appendix D2

Data from particle size distribution & Percentage crystal growth calculations: C1-C8

Seed crystals analyis	C1	C2	C3	C4	C5	C6	C7	C8
D[4,3] -1st measurement	21.89	25.73	27.27	21.39	22.83	28.6	24.93	27.56
D[4,3]-2nd measurement	21.87	25.64	25.9	21.3	22.75	28.5	24.92	26.77
D[4,3]-3rd measurement	21.78	25.46	25.21	21.19	22.58	28.31	25.03	26.38
D[4,3] average	***21.85***	***25.61***	***26.13***	***21.29***	***22.72***	***28.47***	***24.96***	***26.90***
Standard deviation	***0.06***	***0.14***	***1.05***	***0.10***	***0.13***	***0.15***	***0.06***	***0.60***
Analysis of crystals from equilibrium solution								
D[4,3]-1st measurement	27.69	28.8	33.36	29.01	28.7	32.66	30.4	33.23
D[4,3]-2nd measurement	27.8	28.85	32.05	00029	28.1	32.22	30.82	33.01
D[4,3]-3rd measurement	27.83	28.93	31.36	28.69	27.89	32.31	31.98	32.91
D[4,3] average	***27.77***	***28.86***	***32.26***	***28.83***	***28.23***	***32.40***	***31.07***	***33.05***
Standard deviation	***0.07***	***0.07***	***1.02***	***0.17***	***0.42***	***0.23***	***0.82***	***0.16***
% Crystal growth (equation 5-1)	***27.13***	***12.69***	***23.46***	***35.38***	***24.25***	***13.79***	***24.47***	***22.85***
Error in crystal growth measurement	***0.14***	***0.10***	***1.68***	***0.37***	***0.50***	***0.17***	***0.70***	***0.62***

Appendix D3

Data from digital image processing & Percentage edge detection calculations: C1-C8

Analysis of crystals from equilibrium solution

	% Edge detected →							
	C1	C2	C3	C4	C5	C6	C7	C8
Picture 1	6.8061	15.0786	8.453	8.1611	7.1441	8.0523	9.7571	14.4191
Picture 2	7.0527	17.5047	8.6704	8.1453	7.0046	9.4476	8.8921	15.4777
Picture 3	6.4949	17.6963	7.889	8.1153	7.041	9.8609	8.2584	14.3179
Picture 4	6.268	17.8097	8.2926	8.8327	7.9841	10.4333	8.3807	14.5651
Picture 5	6.5334	17.5917	9.6451	9.0393	7.5527	11.357	7.961	14.8226
Picture 6	5.9956	17.6736	10.1394	8.7571	6.6359	10.5156	7.1487	15.457
Picture 7	6.4364	16.689	10.5147	8.7926	7.008	10.7357	6.9401	15.6421
Picture 8	6.2381	15.9704	10.454	8.9144	6.7413	11.1023	6.0111	15.2719
Picture 9	6.7334	15.6677	10.1299	8.7594	5.8779	10.9994	6.014	14.8101
Picture 10	7.817	16.5751	8.9894	9.0396	7.8063	12.6284	7.577	14.8926
Average % Edge detected	*6.64*	*16.83*	*9.32*	*8.66*	*7.08*	*10.51*	*7.69*	*14.97*
Standard deviation	*0.51*	*0.98*	*0.97*	*0.37*	*0.61*	*1.22*	*1.21*	*0.47*

Appendix D4: Sample pictures of crystals from equilibrium solution: Experiments C1-C8

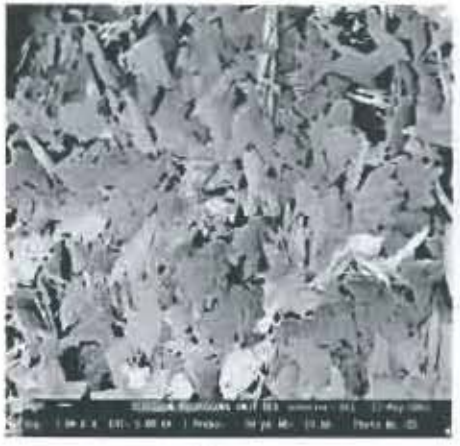

C1

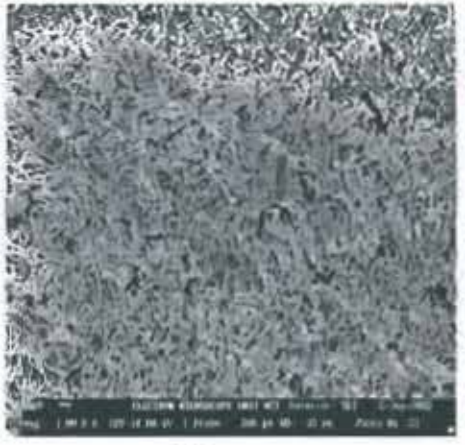

C2

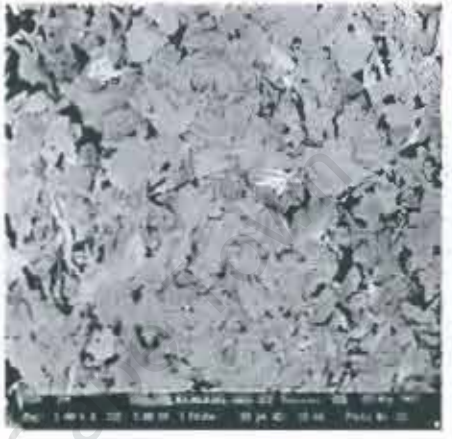

C3

C4

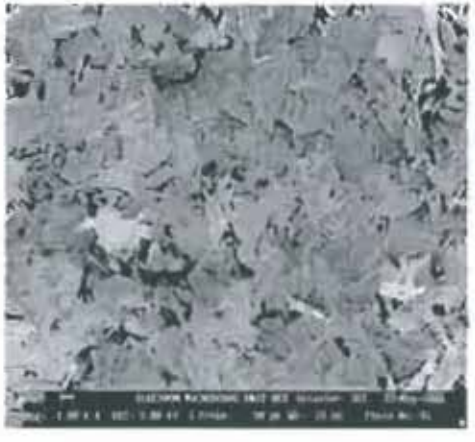

C5

C6

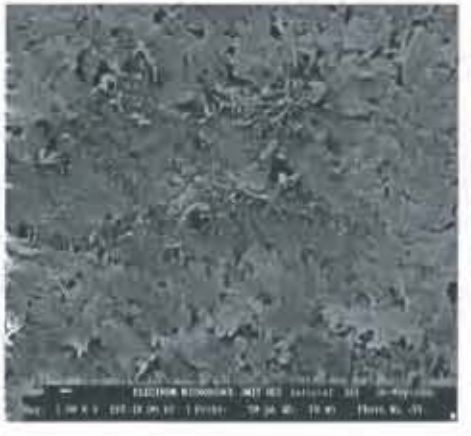

C7

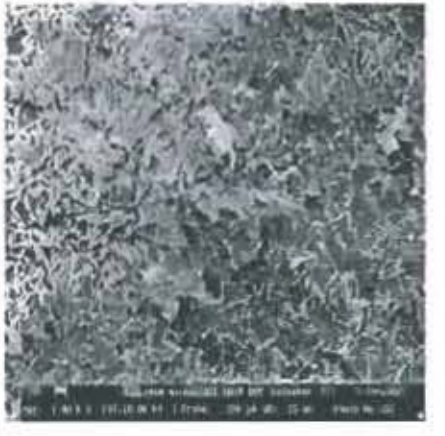

C8

Appendix E: Conductivity readings from experiments D1, D2 and D3

	D1 -1 0 0 -1	D 2 0 0 0 -1	D3 +1 0 0 -1
time (min)	cond (mS/cm)	cond (mS/cm)	cond (mS/cm)
0	14.24	13.97	14.66
2	12.41	12.11	12.16
3	11.82	11.48	11.36
4	11.41	11.04	11.18
5	11.35	10.8	11.15
6	11.33	10.71	11.13
7	11.31	10.61	11.08
8	11.3	10.58	11.03
9	11.29	10.52	11
10	11.28	10.5	10.94
11	11.27	10.46	10.91
12	11.27	10.42	10.93
13	11.25	10.41	10.93
14	11.24	10.36	10.86
15	11.23	10.36	10.87
16	11.23	10.31	10.85
17	11.21	10.32	10.88
18	11.21	10.29	10.91
19	11.2	10.3	10.86
20	11.18	10.25	10.87
21	11.18	10.25	10.89
22	11.18	10.22	10.84
23	11.15	10.23	10.86
24	11.16	10.23	10.88
25	11.15	10.19	10.81
26	11.14	10.18	10.85
27	11.12	10.21	10.85
28	11.13	10.2	10.87
29	11.11	10.18	10.87
30	11.1	10.18	10.85
31	11.09	10.18	10.82
32	11.09	10.17	10.86
33	11.08	10.16	10.87
34	11.07	10.16	10.87
35	11.07	10.15	10.85
36	11.06	10.16	10.83
37	11.05	10.13	10.84
38	11.05	10.14	10.81
39	11.03	10.14	10.82
40	11.04	10.15	10.87
41	11.03	10.15	10.88
42	11.03	10.12	10.87
43	11.02	10.14	10.86
44	11.01	10.09	10.84
45	11.01	10.1	10.85
46	10.99	10.1	10.86
47	10.99	10.09	10.84
48	10.98	10.11	10.85
49	10.98	10.1	10.85
50	10.96	10.12	10.86
51	10.95	10.1	10.86
52	10.97	10.11	10.85
53	10.97	10.11	10.85
54	10.96	10.1	10.85
55	10.95	10.11	10.85
56	10.94	10.1	10.85
57	10.94	10.11	10.85
58	10.93	10.11	10.85
59	10.93	10.08	10.85
60	10.93	10.09	10.85
61	10.92	10.08	10.85
62	10.92	10.1	10.85
63	10.91	10.07	10.85
64	10.9	10.09	10.85
65	10.9	10.1	10.85
66	10.9	10.1	10.85
67	10.89	10.1	10.85
68	10.89	10.1	10.85
69	10.88	10.1	10.85
70	10.88	10.1	10.85
71	10.87	10.1	10.85
72	10.87	10.1	10.85
73	10.87	10.1	10.85
74	10.86	10.1	10.85
75	10.85	10.1	10.85
76	10.85	10.1	10.85
77	10.85	10.1	10.85
78	10.84	10.1	10.85
79	10.84	10.1	10.85
80	10.83	10.1	10.85
81	10.83	10.1	10.85

	D1 -1 0 0 -1	D 2 0 0 0 -1	D3 +1 0 0 -1
time (min)	cond (mS/cm)	cond (mS/cm)	cond (mS/cm)
82	10.83	10.1	10.85
83	10.82	10.1	10.85
84	10.81	10.1	10.85
85	10.82	10.1	10.85
86	10.8	10.1	10.85
87	10.8	10.1	10.85
88	10.79	10.1	10.85
89	10.79	10.1	10.85
90	10.79	10.1	10.85
91	10.78		
92	10.78		
93	10.78		
94	10.77		
95	10.77		
96	10.77		
97	10.76		
98	10.76		
99	10.76		
100	10.76		
101	10.75		
102	10.75		
103	10.75		
104	10.73		
105	10.74		
106	10.74		
107	10.74		
108	10.73		
109	10.73		
110	10.73		
111	10.72		
112	10.72		
113	10.72		
114	10.71		
115	10.71		
116	10.71		
117	10.7		
118	10.7		
119	10.69		
120	10.69		
121	10.69		
122	10.68		
123	10.68		
124	10.68		
125	10.67		
126	10.66		
127	10.67		
128	10.67		
129	10.66		
130	10.66		
131	10.66		
132	10.65		
133	10.65		
134	10.64		
135	10.65		
136	10.64		
137	10.64		
138	10.63		
139	10.63		
140	10.63		
141	10.63		
142	10.62		
143	10.62		
144	10.62		
145	10.61		
146	10.61		
147	10.61		
148	10.61		
149	10.6		
150	10.6		
151	10.6		
152	10.59		
153	10.59		
154	10.59		
155	10.59		
156	10.59		
157	10.59		
158	10.59		
159	10.59		
160	10.59		
161	10.59		
162	10.59		

Appendix F: Statistical analysis of results obtained from experiments A1-A12.

FIRST ORDER MODELS FOR NEEDLES

DESUPERSATURATION TIME (TIME)
Fitted first order model:

TIME =	286.6250	- 25.1667A	- 0.66667B	- 0.06125C	- 14.4167D	
	(64.3321)	(5.3750)	(5.37502)	(0.08063)	(5.3750)	
t-test	p=0.0030	p=0.0023	p=0.9048	p=0.4722	p=0.0314	

The factor labels are A : Seed quantity B : pH C : Impeller speed D : Sulphate to Calcium ratio

The analysis of variance is as follows:

Source of variation	DF	SS	Mean Square	F value	Prob>F
Model	4	61799.0			
Quadratic effects	1	12421.5	12421.5	1490.6	p<0.01
Other effects	3	2114.5	704.8	84.6	p<0.01
Pure error	3	25.0	8.333		
Total	11	76360.0			

The model accounts for 80.9% of the variation in Desupersaturation time.

% GROWTH OF CRYSTALS (GROWTH)
Fitted first order model:

GROWTH =	38.0990	- 6.3871A	+ 1.04958B	- 0.01497C	+ 1.46542D	
	(13.5547)	(1.1325)	(1.13251)	(0.01699)	(1.13251)	
t-test	p=0.0261	p=0.0008	p=0.3849	p=0.4075	p=0.2367	

The analysis of variance is as follows:

Source of variation	DF	SS	Mean Square	F value	Prob>F
Model	4	3242.86145			
Quadratic effects	1	401.71984	401.71984	3310.4	p<0.01
Other effects	3	244.34156	81.44719	671.2	p<0.01
Pure error	3	0.36405	0.12135		
Total	11	3889.28690			

The model accounts for 83.4% of the variation in % Growth of crystals. For both the variables Desupersaturation time and % Growth of crystals, the analysis of variance indicates that the response surface is curvilinear within the experimental region. Thus, there is either a minimum or a saddle point in the region.

% EDGE DETECTED (EDGE)
Fitted first order model:

EDGE =	2.99750	+ 0.11750A	+ 0.00250B	+ 0.00390C	- 0.26500D	
	(1.30212)	(0.10879)	(0.10879)	(0.00163)	(0.10879)	
t-test	p=0.0548	p=0.3159	p=0.9823	p=0.0482	p=0.0450	

The analysis of variance is as follows:

Source of variation	DF	SS	Mean Square	F value	Prob>F
Model	4	10.9179			
Quadratic effects	1	0.0726	0.0726	0.06	p>0.05
Other effects	3	2.2523	0.7508	0.62	p>0.05
Pure error	3	3.6405	1.2135		
Total	11	16.8833			

The model accounts for 64.7% of the variation in the % Edge detection.For this variable there is no evidence of curvilinearity within the experimental region. The procedure of Steepest ascent is required to move the experimental region to where there is curvilinearity and a maximum response.

Appendix G: Statistical analysis of the results collected from experiments B1-B12.

FIRST ORDER MODELS FOR PLATES

DESUPERSATURATION TIME (TIME)
Fitted first order model:

TIME =	179.3750	- 13.9167A	- 1.0833B	- 0.03125C	- 12.250D	
	(53.7562)	(4.4914)	(4.4914)	(0.06737)	(4.4914)	
t-test	p=0.0125	p=0.0174	p=0.8163	p=0.6568	p=0.0294	

The factor labels are A : Seed quantity B : pH C : Impeller speed D : Sulphate to Calcium ratio

The analysis of variance is as follows:

Source of variation	DF	SS	Mean Square	F value	Prob>F
Model	4	25146.0			
Quadratic effects	1	6144.0	6144.0	3686	p<0.01
Other effects	3	4018.0	1339.3	803	p<0.01
Pure error	3	5.0	1.667		
Total	11	35313.0			

The model accounts for 71.2% of the variation in Desupersaturation time.

% GROWTH
Fitted first order model:

TIME =	72.1827	- 5.7071A	- 1.0579B	- 0.012056C	- 1.9096D	
	(11.8696)	(0.9917)	(0.9917)	(0.014876)	(0.9917)	
t-test	p=0.0005	p=0.0007	p=0.3215	p=0.4443	p=0.0955	

The factor labels are
A : Seed quantity B : pH C : Impeller speed D : Sulphate to Calcium ratio

The analysis of variance is as follows:

Source of variation	DF	SS	Mean Square	F value	Prob>F
Model	4	2734.74075			
Quadratic effects	1	272.76784	272.76784	24.240	p=0.0161
Other effects	3	189.15824	63.0527	5.603	p=0.0988
Pure error	3	33.75900	11.253		
Total	11	3230.42583			

The model accounts for 84.7% of the variation in % Growth.

% EDGE DETECTED (EDGE)
Fitted first order model:

TIME =	6.5388	+ 0.43750A	+ 0.04417B	- 0.000538C	+ 0.47417D	
	(2.5227)	(0.21077)	(0.21077)	(0.003162)	(0.21077)	
t-test	p=0.0358	p=0.0766	p=0.8400	p=0.8698	p=0.0592	

The analysis of variance is as follows:

Source of variation	DF	SS	Mean Square	F value	Prob>F
Model	4	30.20220			
Quadratic effects	1	0.0560666	0.560666	2.763	p=0.0965
Other effects	3	22.272048	7.424316	365.88	p<0.0001
Pure error	3	0.060875	0.020292		
Total	11	52.59209			

The model accounts for 57.4% of the variation in % Edge Detected.

For all three responses, the analysis of variance indicates that the response surface is curvilinear within the experimental region. Thus, there is either a minimum or a saddle point in the region.

Appendix H: Statistical analysis of the results collected from central composite experiments, B1-B12 and C1-C8.

Coding Coefficients for the Independent Variables

Factor	Subtracted off	Divided by
SEEDQUAN	5.500000	4.500000
SC_RATIO	5.500000	4.500000
PH	5.500000	4.500000
IMPELLER	600.000000	300.000000

Response Surface for Variable TIME

Response Mean	41.500000
Root MSE	10.658019
R-Square	0.9784
Coef. of Variation	25.6820

Regression	Degrees of Freedom	Type I Sum of Squares	R-Square	F-Ratio	Prob > F
Linear	4	26150	0.6222	57.551	0.0000
Quadratic	4	10953	0.2606	24.105	0.0002
Crossproduct	3	4018.000000	0.0956	11.791	0.0026
Total Regress	11	41120	0.9784	32.909	0.0000

Residual	Degrees of Freedom	Sum of Squares	Mean Square	F-Ratio	Prob > F
Lack of Fit	5	903.746947	180.749389	108.4	0.0014
Pure Error	3	5.000000	1.666667		
Total Error	8	908.746947	113.593368		

Parameter	Degrees of Freedom	Parameter Estimate	Standard Error	T for H0: Parameter=0	Prob > |T|
INTERCEPT	1	331.573820	31.934095	10.383	0.0000
SEEDQUAN	1	-47.375184	5.627490	-8.419	0.0000
SC_RATIO	1	-39.026347	3.635723	-10.734	0.0000
PH	1	-8.824160	4.503383	-1.959	0.0857
IMPELLER	1	-0.202148	0.085261	-2.371	0.0452
SEEDQUAN*SEEDQUAN	1	2.218246	0.324207	6.842	0.0001
SC_RATIO*SEEDQUAN	1	2.388889	0.418687	5.706	0.0005
SC_RATIO*SC_RATIO	1	2.101967	0.324207	6.483	0.0002
PH*SEEDQUAN	1	0.666667	0.418687	1.592	0.1500
PH*SC_RATIO	0	0	.	.	.
PH*PH	1	0.414628	0.324207	1.279	0.2368
IMPELLER*SEEDQUAN	1	0.003333	0.006280	0.531	0.6100
IMPELLER*SC_RATIO	0	0	.	.	.
IMPELLER*PH	0	0	.	.	.
IMPELLER*IMPELLER	1	0.000152	0.000072947	2.084	0.0707

Parameter	Parameter Estimate from Coded Data
INTERCEPT	-12.072489
SEEDQUAN	-18.760155
SC_RATIO	-12.446201
PH	-2.684613
IMPELLER	-0.420038
SEEDQUAN*SEEDQUAN	44.919481
SC_RATIO*SEEDQUAN	48.375000
SC_RATIO*SC_RATIO	42.564830
PH*SEEDQUAN	13.500000
PH*SC_RATIO	0
PH*PH	8.396225
IMPELLER*SEEDQUAN	4.500000
IMPELLER*SC_RATIO	0
IMPELLER*PH	0
IMPELLER*IMPELLER	13.681109

Factor	Degrees of Freedom	Sum of Squares	Mean Square	F-Ratio	Prob > F

SEEDQUAN	5	22032	4406.428854	38.791	0.0000
SC_RATIO	3	19050	6349.950908	55.901	0.0000
PH	3	581.245822	193.748607	1.706	0.2426
IMPELLER	3	771.469825	257.156608	2.264	0.1582

Canonical Analysis of Response Surface (based on coded data)

	Critical Value	
Factor	Coded	Uncoded
SEEDQUAN	0.186385	6.338731
SC_RATIO	0.040290	5.681303
PH	0.010030	5.545133
IMPELLER	-0.015302	595.409444

Predicted value at stationary point -14.081766

	Eigenvectors			
Eigenvalues	SEEDQUAN	SC_RATIO	PH	IMPELLER
68.408589	0.727340	0.680727	0.081809	0.029903
21.414008	0.612991	-0.701000	0.317849	0.178359
13.433533	-0.107783	0.089492	-0.144430	0.979548
6.305514	-0.289137	0.192875	0.933498	0.088204

Stationary point is a minimum.
Coding Coefficients for the Independent Variables

Factor	Subtracted off	Divided by
SEEDQUAN	5.500000	4.500000
SC_RATIO	5.500000	4.500000
PH	5.500000	4.500000
IMPELLER	600.000000	300.000000

Response Surface for Variable GROWTH

Response Mean	26.171000
Root MSE	8.364475
R-Square	0.8499
Coef. of Variation	31.9609

Regression	Degrees of Freedom	Type I Sum of Squares	R-Square	F-Ratio	Prob > F
Linear	4	2453.397857	0.6579	8.767	0.0051
Quadratic	4	527.121917	0.1413	1.884	0.2068
Crossproduct	3	189.158237	0.0507	0.901	0.4818
Total Regress	11	3169.678012	0.8499	4.119	0.0273

Residual	Degrees of Freedom	Sum of Squares	Mean Square	F-Ratio	Prob > F
Lack of Fit	5	525.956568	105.191314	9.348	0.0476
Pure Error	3	33.759000	11.253000		
Total Error	8	559.715568	69.964446		

Parameter	Degrees of Freedom	Parameter Estimate	Standard Error	T for H0: Parameter=0	Prob > |T|
INTERCEPT	1	102.006560	25.062063	4.070	0.0036
SEEDQUAN	1	-14.763188	4.416486	-3.343	0.0102
SC_RATIO	1	-6.189756	2.853336	-2.169	0.0619
PH	1	-3.583593	3.534281	-1.014	0.3403
IMPELLER	1	-0.037686	0.066914	-0.563	0.5887
SEEDQUAN*SEEDQUAN	1	0.558443	0.254440	2.195	0.0595
SC_RATIO*SEEDQUAN	1	0.388472	0.328588	1.182	0.2711
SC_RATIO*SC_RATIO	1	0.361350	0.254440	1.420	0.1933
PH*SEEDQUAN	1	0.187361	0.328588	0.570	0.5842
PH*SC_RATIO	0	0	.	.	.
PH*PH	1	0.195226	0.254440	0.767	0.4650
IMPELLER*SEEDQUAN	1	0.004881	0.004929	0.990	0.3510
IMPELLER*SC_RATIO	0	0	.	.	.
IMPELLER*PH	0	0	.	.	.
IMPELLER*IMPELLER	1	0.000003676	0.000057249	0.0642	0.9504

Parameter	Parameter Estimate from Coded Data
INTERCEPT	13.023654
SEEDQUAN	-11.360152
SC_RATIO	-0.352376
PH	-1.825284
IMPELLER	-1.928466
SEEDQUAN*SEEDQUAN	11.308477
SC_RATIO*SEEDQUAN	7.866562
SC_RATIO*SC_RATIO	7.317343
PH*SEEDQUAN	3.794063
PH*SC_RATIO	0
PH*PH	3.953331
IMPELLER*SEEDQUAN	6.589687
IMPELLER*SC_RATIO	0
IMPELLER*PH	0
IMPELLER*IMPELLER	0.330831

Factor	Degrees of Freedom	Sum of Squares	Mean Square	F-Ratio	Prob > F
SEEDQUAN	5	2536.217620	507.243524	7.250	0.0076
SC_RATIO	3	409.166691	136.388897	1.949	0.2003
PH	3	81.413825	27.137942	0.388	0.7650
IMPELLER	3	171.547089	57.182363	0.817	0.5197

Canonical Analysis of Response Surface (based on coded data)

Factor	Critical Value Coded	Uncoded
SEEDQUAN	0.181638	6.317369
SC_RATIO	-0.073557	5.168992
PH	0.143694	6.146623
IMPELLER	1.105594	931.678307

Predicted value at stationary point 10.807707

Eigenvalues	Eigenvectors SEEDQUAN	SC_RATIO	PH	IMPELLER
14.550412	0.850811	0.462664	0.152308	0.197143
5.714708	0.341835	-0.838953	0.368162	0.209198
3.460685	-0.235858	0.240544	0.908219	-0.248291
-0.815823	-0.321932	0.155690	0.128055	0.925053

Stationary point is a saddle point.

Estimated Ridge of Minimum Response for Variable GROWTH

Coded Radius	Estimated Response	Standard Error
0.0	13.023654	3.981998
0.1	11.980480	4.141316
0.2	11.170192	4.321735
0.3	10.560283	4.499004
0.4	10.100897	4.639839
0.5	9.729870	4.747933
0.6	9.397407	4.876351
0.7	9.076970	5.073521
0.8	8.756165	5.370104
0.9	8.428874	5.785292
1.0	8.091778	6.329837

Coded Radius	Uncoded Factor Values SEEDQUAN	SC_RATIO	PH	IMPELLER
0.0	5.500000	5.500000	5.500000	600.000000
0.1	5.940523	5.482414	5.565322	604.143848
0.2	6.382777	5.392404	5.612927	605.322885
0.3	6.816036	5.227108	5.626807	600.021425
0.4	7.214857	5.019183	5.594700	583.791446
0.5	7.549432	4.825336	5.529566	557.506431
0.6	7.822768	4.666818	5.454964	527.015098
0.7	8.055966	4.535133	5.380992	495.769362

0.8	8.264699	4.420398	5.309541	464.769728
0.9	8.457936	4.316501	5.240466	434.201102
1.0	8.640808	4.219869	5.173313	404.042358

Note that in the analysis of variance for each variable there are three cross product terms, which are given zero values. This is the price paid for having a half fraction instead of a complete replication of the factorial. The price is small however because such terms are not likely to be large and in fact they are just aliased with other cross product terms. From the analysis of both variables it is apparent that SEEDQUAN and SC_RATIO are the major factors influencing the variables

Response Surface for Variable %EDGE

Response Mean	10.222000
Root MSE	1.437353
R-Square	0.8906
Coef. of Variation	14.0614

Regression	Degrees of Freedom	Type I Sum of Squares	R-Square	F-Ratio	Prob > F
Linear	4	101.004124	0.6686	12.222	0.0017
Quadratic	4	11.270977	0.0746	1.364	0.3276
Crossproduct	3	22.272950	0.1474	3.594	0.0657
Total Regress	11	134.548051	0.8906	5.920	0.0090

Residual	Degrees of Freedom	Sum of Squares	Mean Square	F-Ratio	Prob > F
Lack of Fit	5	16.466994	3.293399	162.3	0.0008
Pure Error	3	0.060875	0.020292		
Total Error	8	16.527869	2.065984		

Parameter	Degrees of Freedom	Parameter Estimate	Standard Error	T for H0: Parameter=0	Prob > |T|
INTERCEPT	1	9.791481	4.306670	2.274	0.0526
SEEDQUAN	1	-1.364805	0.758930	-1.798	0.1098
SC_RATIO	1	-0.536837	0.490318	-1.095	0.3054
PH	1	0.253686	0.607331	0.418	0.6871
IMPELLER	1	-0.000184	0.011498	-0.0160	0.9877
SEEDQUAN*SEEDQUAN	1	0.085918	0.043723	1.965	0.0850
SC_RATIO*SEEDQUAN	1	0.169167	0.056465	2.996	0.0172
SC_RATIO*SC_RATIO	1	0.049975	0.043723	1.143	0.2861
PH*SEEDQUAN	1	0.001944	0.056465	0.0344	0.9734
PH*SC_RATIO	0	0	.	.	.
PH*PH	1	-0.020064	0.043723	-0.459	0.6585
IMPELLER*SEEDQUAN	1	0.001137	0.000847	1.343	0.2161
IMPELLER*SC_RATIO	0	0	.	.	.
IMPELLER*PH	0	0	.	.	.
IMPELLER*IMPELLER	1	-0.000002680	0.000009838	-0.272	0.7922

Parameter	Parameter Estimate from Coded Data
INTERCEPT	12.086384
SEEDQUAN	5.417560
SC_RATIO	4.244656
PH	0.196539
IMPELLER	0.856949
SEEDQUAN*SEEDQUAN	1.739836
SC_RATIO*SEEDQUAN	3.425625
SC_RATIO*SC_RATIO	1.011987
PH*SEEDQUAN	0.039375
PH*SC_RATIO	0
PH*PH	-0.406298
IMPELLER*SEEDQUAN	1.535625
IMPELLER*SC_RATIO	0
IMPELLER*PH	0
IMPELLER*IMPELLER	-0.241210

Factor	Degrees of Freedom	Sum of Squares	Mean Square	F-Ratio	Prob > F
SEEDQUAN	5	88.297313	17.659463	8.548	0.0046
SC_RATIO	3	64.776311	21.592104	10.451	0.0038
PH	3	0.449367	0.149789	0.0725	0.9731
IMPELLER	3	4.921700	1.640567	0.794	0.5307

Factor	Critical Value Coded	Uncoded
SEEDQUAN	-0.377316	3.802077
SC_RATIO	-1.458671	-1.064018
PH	0.223583	6.506123
IMPELLER	0.575292	772.587517

Predicted value at stationary point 8.236863

Eigenvalues	Eigenvectors SEEDQUAN	SC_RATIO	PH	IMPELLER
3.231496	0.779812	0.601787	0.004220	0.172416
0.116072	0.328359	-0.627758	0.012375	0.705654
-0.406187	0.005629	-0.006799	0.999618	-0.026198
-0.837067	-0.532956	0.493686	0.024358	0.686760

Stationary point is a saddle point.

Estimated Ridge of Maximum Response for Variable %EDGE

Coded Radius	Estimated Response	Standard Error
0.0	12.086384	0.684267
0.1	12.812445	0.717149
0.2	13.602974	0.763451
0.3	14.458009	0.826385
0.4	15.377576	0.908403
0.5	16.361696	1.011004
0.6	17.410382	1.134826
0.7	18.523646	1.279882
0.8	19.701497	1.445630
0.9	20.943941	1.632172
1.0	22.250984	1.838382

Coded Radius	Uncoded Factor Values SEEDQUAN	SC_RATIO	PH	IMPELLER
0.0	5.500000	5.500000	5.500000	600.000000
0.1	5.851219	5.775118	5.511720	603.840078
0.2	6.202234	6.049853	5.521741	607.904035
0.3	6.553125	6.324222	5.530468	612.139405
0.4	6.903943	6.598254	5.538186	616.509026
0.5	7.254718	6.871984	5.545104	620.985811
0.6	7.605467	7.145446	5.551375	625.549538
0.7	7.956203	7.418671	5.557117	630.184792
0.8	8.306934	7.691687	5.562421	634.879613
0.9	8.657664	7.964517	5.567357	639.624579
1.0	9.008397	8.237183	5.571981	644.412159

From the above analysis it would appear that SEED QUANTITY and SC RATIO are the influential factors on %EDGE, and a maximum response may be achieved outside the experimental region with higher values of SEED QUANTITY and SC RATIO.

APPENDIX I: **COMPARISON OF NEEDLES AND PLATES (1st order data)**

The folowing are the outputs from analyses of variance of each of the response variables. The purpose of each analysis is to test whether the same first order model is appropriate for both Plates and Needles. The factor Crystal has been included in the model to test this null hypothesis. The factor has a value 0 for Plates and 1 for Needles. For each response variable it is clear that the hypothesis is to be rejected. The evidence is that different models should be fitted to Plates and Needles. The evidence being the p values for the t statistics, which are all less than 0.05.

Dependent Variable: TIME

Analysis of Variance

Source	DF	Sum of Squares	Mean Square	F Value	Prob>F
Model	5	92403.00000	18480.60000	11.237	0.0001
Error	18	29603.50000	1644.63889		
C Total	23	122006.50000			

Root MSE	40.55415	R-square	0.7574
Dep Mean	72.25000	Adj R-sq	0.6900
C.V.	56.13031		

Parameter Estimates

Variable	DF	Parameter Estimate	Standard Error	T for H0: Parameter=0	Prob > |T|
INTERCEP	1	212.250000	41.28679791	5.141	0.0001
SEEDQUAN	1	-19.541667	3.37951230	-5.782	0.0001
PH	1	-0.875000	3.37951230	-0.259	0.7986
IMPELLER	1	-0.046250	0.05069268	-0.912	0.3736
SC_RATIO	1	-13.333333	3.37951230	-3.945	0.0009
CRYSTAL	1	41.500000	16.55616144	2.507	0.0220

Dependent Variable: GROWTH

Analysis of Variance

Source	DF	Sum of Squares	Mean Square	F Value	Prob>F
Model	5	5990.54039	1198.10808	12.465	0.0001
Error	18	1730.07268	96.11515		
C Total	23	7720.61306			

Root MSE	9.80383	R-square	0.7759
Dep Mean	23.27875	Adj R-sq	0.7137
C.V.	42.11495		

Parameter Estimates

Variable	DF	Parameter Estimate	Standard Error	T for H0: Parameter=0	Prob > |T|
INTERCEP	1	60.144583	9.98094919	6.026	0.0001
SEEDQUAN	1	-6.047083	0.81698611	-7.402	0.0001
PH	1	-0.004167	0.81698611	-0.005	0.9960
IMPELLER	1	-0.013512	0.01225479	-1.103	0.2847
SC_RATIO	1	-0.222083	0.81698611	-0.272	0.7888
CRYSTAL	1	-10.007500	4.00239821	-2.500	0.0223

Dependent Variable: EDGE

Analysis of Variance

Source	DF	Sum of Squares	Mean Square	F Value	Prob>F
Model	5	219.94485	43.98897	14.416	0.0001
Error	18	54.92404	3.05134		
C Total	23	274.86890			

Root MSE	1.74681	R-square	0.8002
Dep Mean	7.30042	Adj R-sq	0.7447
C.V.	23.92750		

Parameter Estimates

Variable	DF	Parameter Estimate	Standard Error	T for H0: Parameter=0	Prob > |T|
INTERCEP	1	7.693542	1.77836505	4.326	0.0004
SEEDQUAN	1	0.277500	0.14556727	1.906	0.0727
PH	1	0.023333	0.14556727	0.160	0.8744
IMPELLER	1	0.001681	0.00218351	0.770	0.4513
SC_RATIO	1	0.104583	0.14556727	0.718	0.4817
CRYSTAL	1	-5.850833	0.71313108	-8.204	0.0001